Journal of Human Evolution 201 (2025) 103647

Contents lists available at ScienceDirect

Journal of Human Evolution

journal homepage: www.elsevier.com/locate/jhevol

First articulating os coxae, femur, and tibia of a small adult *Paranthropus robustus* from Member 1 (Hanging Remnant) of the Swartkrans Formation, South Africa

Travis Rayne Pickering [a, b, *], Marine Cazenave [c, d, e], R.J. Clarke [b], A.J. Heile [a], Matthew V. Caruana [b, f], Kathleen Kuman [g], Dominic Stratford [g, h], C.K. Brain [i, 1], Jason L. Heaton [b, j]

[a] *Department of Anthropology, University of Wisconsin-Madison, Madison, WI, 53706, USA*
[b] *Evolutionary Studies Institute, University of the Witwatersrand, Johannesburg, WITS 2050, South Africa*
[c] *Department of Human Origins, Max Planck Institute for Evolutionary Anthropology, Leipzig, 04103, Germany*
[d] *Division of Anthropology, American Museum of Natural History, New York, 10024, USA*
[e] *Department of Anatomy, Faculty of Health Sciences, University of Pretoria, 0084, Pretoria, South Africa*
[f] *Palaeo-Research Institute, University of Johannesburg, Auckland Park, 2006, South Africa*
[g] *School of Geography, Archaeology and Environmental Studies, University of the Witwatersrand, Johannesburg, WITS 2050, South Africa*
[h] *Department of Anthropology, Stony Brook University, Stony Brook, NY, 11794, USA*
[i] *Department of Vertebrates, Ditsong National Museum of Natural History (Transvaal Museum), Pretoria, 0001, South Africa*
[j] *Department of Biology, University of Alabama at Birmingham, Birmingham, AL, 35205, USA*

A R T I C L E I N F O

Article history:
Received 12 February 2024
Accepted 31 December 2024
Available online 4 March 2025

Handling Editor: Dr S Xing

Keywords:
Hominin lower limb
Locomotion
Body size

A B S T R A C T

Since paleontological work began there in 1948, Swartkrans (South Africa) has yielded hundreds of Early Pleistocene hominin fossils, currently attributed to (in ascending order of quantity) cf. *Australopithecus africanus*, *Homo* spp., and *Paranthropus robustus*. The bulk of that large sample comprises craniodental remains, with (mostly fragmentary) postcranial materials being much less abundant at the site. In that context, our announcement here of the first articulating partial os coxae, nearly complete femur, and complete tibia of a young adult hominin (SWT1/HR-2), excavated from the <2.3 to >1.7-million-year-old Hanging Remnant (Member 1) of the Swartkrans Formation, represents an important addition to the understanding of hominin postural and locomotor behavior in Early Pleistocene South Africa. We provide qualitative and quantitative descriptions and initial functional morphological interpretations of the fossils, based mostly on external bone morphology. Epiphyseal fusion data, element dimensions, the crural index, and live body stature and mass estimates that we provide all indicate that SWT1/HR-2 is one of the smallest known adult hominins in the fossil record. We discuss the paleobiological implications of these findings in relation to our taxonomic diagnosis of SWT1/HR-2 as representing *P. robustus*.

1. Introduction

Paranthropus robustus was an endemic South African species of Early Pleistocene hominin,[2] represented principally by its abundant craniodental fossils at the cave sites of Kromdraai, Drimolen, and especially Swartkrans (e.g., Broom, 1938, 1949; Keyser, 2000; Keyser et al., 2000), and to a lesser extent at Sterkfontein, Gondolin, and Coopers (Menter et al., 1999; Kuman and Clarke, 2000; Steininger et al., 2008) (Fig. 1). Hominin postcranial remains have also been recovered from some of these sites, but their taxonomic allocations are complicated by the fact that skull elements of species other than *P. robustus*, such as *Homo ergaster*, co-occur stratigraphically with those of the former taxon (e.g., Broom and Robinson, 1949; Keyser et al., 2000; Kuman and Clarke, 2000; Braga and Thackeray, 2003).

* Corresponding author.
E-mail address: tpickering@wisc.edu (T.R. Pickering).
[1] Deceased.
[2] Some coauthors prefer the use of the term 'hominid' over 'hominin' for the clade of primates who split from a most recent common ancestor shared uniquely with the genus *Pan* (e.g., Clarke et al., 2021).

https://doi.org/10.1016/j.jhevol.2024.103647

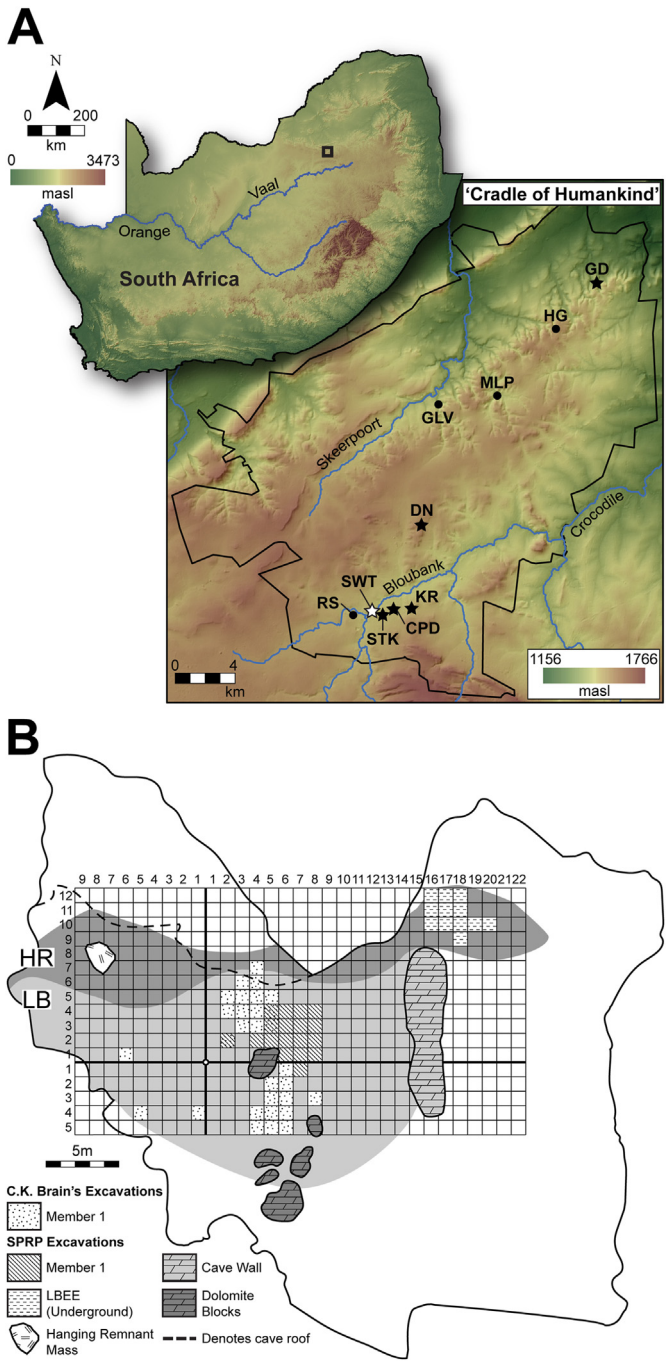

Figure 1. Maps showing the location of the UNESCO 'Cradle of Humankind' World Heritage Site (black-outlined box), South Africa (A, top left) and the position of Swartkrans Cave (SWT) in comparison to some other major Pliocene and Pleistocene paleontological sites within the boundaries of the 'Cradle of Humankind' (outlined in black) (stars indicate sites that have yielded *Paranthropus* fossils. Abbreviations: CPD = Coopers D; DN = Drimolen; GD = Gondolin; GLV = Gladysvale; HG = Haasgat; KR = Kromdraai; MLP = Malapa; RS = Rising Star; STK = Sterkfontein) (A, bottom right). Plan view of Swartkrans showing the extent of Member 1 of the Swartkrans Formation, which comprises two depositional subunits, the Lower Bank (LB) and the Hanging Remnant (HR) (B). The 'Hanging Remnant mass' (HRM), which yielded the SWT1/HR-2 hominin fossils discussed here, is indicated. For clarity, the HRM is superimposed on the HR in this image. However, the HRM actually reposes beneath the HR, a depositional residuum that adheres to the cave roof. Similarly, the LB underground excavation (Lower Bank East Extension, LBEE) is ~12 m below the cave surface; this means that it also rests below the HR, as well as beneath two other strata, the Early Pleistocene (but otherwise undated) 'Talus Cone Deposit' and a ≤110,000 ± 1980-year-old Middle Stone Age archaeological horizon. (For interpretation of the references to color in this figure, the reader is referred to the Web version of this article).

It is, in part, the uncertain taxonomy of isolated hominin postcranial bones from sites such as Swartkrans that engendered debate about, for instance, the toolmaking and tool-using capabilities of *P. robustus* (e.g., Susman, 1988 and, contra, Trinkaus and Long, 1990). Such doubt also undercuts the relevance of, for example, Susman and Brain's (1988) and, later, Komza and Skinner's (2019) functional assessments of a hominin first metatarsal from Swartkrans for characterizing the terrestrial locomotion of *P. robustus*. Indeed, in a comprehensive review of the genus *Paranthropus*, Wood and Schroer (2013: 470) conclude that the "position of the foramen magnum in *P. robustus* is consistent with that taxon being habitually upright, but there is otherwise frustratingly little fossil evidence relevant to interpreting its locomotor mode." Along with this important concern, debate also continues over other fundamental aspects of *P. robustus* paleobiology, including diet, foraging strategies, and social organization (e.g., Brain and Shipman, 1993, 1993; Backwell and d'Errico, 2001; Lockwood et al., 2007; Grine et al., 2012a; Pickering et al., 2012, 2016).

Relevant to these disputations, we describe here the first articulating partial os coxae, nearly complete femur, and complete tibia of a single, young adult hominin (cataloged as SWT1/HR-2[3]) from the Hanging Remnant (HR) subunit of Member 1 of the Swartkrans Formation, which we assign to *P. robustus*. In addition to providing justification for that taxonomic assignment, we also offer functional interpretations of the fossil-set's comparative anatomy. Moreover, we give estimates of the SWT1/HR-2 hominin's lower limb length and crural index, as well as of its live stature and body mass. Lastly, this contribution also includes discussion of SWT1/HR-2's relevance to C.K. Brain's (e.g., 1970, 1981) prominent taphonomic hypothesis that carnivores, including especially leopards (*Panthera pardus*), were responsible for accumulating some proportion of the hominin remains in Swartkrans Cave.

We also note that SWT1/HR-2 holds significant potential to inform us about other fundamental adaptations of *P. robustus*. To that end, detailed investigation of the internal bone structure, cross-sectional geometry, and cortical thicknesses of the SWT1/HR-2 fossil-set, and the relevance of each to understanding especially locomotor and positional behavior in *P. robustus*, are the subjects of the forthcoming doctoral thesis of A.J.H., under the direction of T.R.P. and M.C.

2. Materials and methods

2.1. Stratigraphy, geochronology, and field methods

Combined, Brain (1993a), Pickering et al. (2012, 2016), Gibbon et al. (2014), and Kuman et al. (2021) provide up-to-date stratigraphic and geochronological summaries of the Swartkrans Formation. Of most relevance to this study, Member 1 of that formation comprises two sedimentary subunits, the Lower Bank (LB) and the HR. As currently understood, this portion of Swartkrans lacks intrusive flowstones and is thus relatively uncomplicated geochronologically. To wit, the HR is capped by a flowstone that, using U-Pb techniques, has provided two dates of 1.71 ± 0.07 Ma

[3] Fossil specimens recovered by the Swartkrans Paleoanthropology Research Project are labeled sequentially from 1 with a SWT-prefix. 'SW' refers to Swartkrans, 'T' refers to the Transvaal Museum, the former (and rightful) repository of the fossils. A '1' added to the prefix refers to the fact that the fossil derives from Member 1 of the Swartkrans Formation. Within that designation, an HR prefix indicates that the fossil was recovered from the HR subunit of Member 1. The new system of designation was created to readily distinguish fossils recovered from Swartkrans by the Swartkrans Paleoanthropology Research Project from those recovered by earlier research projects at the site, which are designated by the prefixes SK, SKW, and SKX.

and 1.80 ± 0.005 Ma, which overlap in their error margins (Pickering et al., 2011). Another flowstone, which underlies the LB, yielded a U-Pb date of 2.249 ± 0.777 Ma (Pickering et al., 2011). Thus, the entire Member 1 sequence is <2.3 to >1.7 Ma.

The HR is renowned as the stratum from which Robert Broom and John Robinson (e.g., 1952) recovered most of the best-known hominin fossils (including the skull specimens SK 15, SK 46, SK 48, and SK 847) from the Swartkrans Formation (Fig. 1). For this reason, R.J.C. targeted a particularly highly fossiliferous mass for excavation that, based on its position and general appearance, we infer is a portion of the HR (Fig. 2). Subsequently, M.V.C. used a Nikon Nivo 5C™ total station to record the provenance of this HR mass (HRM) within a digital grid that was established for the site in 2017, with arbitrary coordinates of 500 (X), 300 (Y), 100 (Z). To maintain consistency in spatial recording used for previously excavated materials, the new survey points were then mapped onto Brain's (e.g., 1993a) original site survey grid (preserved today as metal framework that is positioned over the external portion of the site). In 2018 and 2019, M.V.C. and site senior technician, Andrew Phaswana, used handheld prying and digging tools to conduct controlled excavation of 12 blocks of varied sizes from the HRM (Fig. 2). To document the removal process and its associated loss of sedimentary volume, we constructed photogrammetric models of the HRM using a Canon 5D Mark III™ DSLR camera before and after its excavation. The excavated HRM breccia blocks were then transported to our field laboratory at the nearby Sterkfontein Caves for preparation.

2.2. Laboratory materials and methods

Preparatory methods All six excavated HRM breccia blocks were examined visually by various members of our team. The blocks were then reduced by R.J.C., Phaswana, and site technician, Abel Molepolle, using handheld air scribes to clean breccia away from fossils.

Comparative data sets For qualitative and quantitative anatomical and taxonomic analyses, the SWT1/HR-2 fossils were compared directly to hominin os coxae, femur, and tibia specimens from the Late Pliocene and Early Pleistocene paleontological levels of the South African sites of Swartkrans, Sterkfontein, Kromdraai,

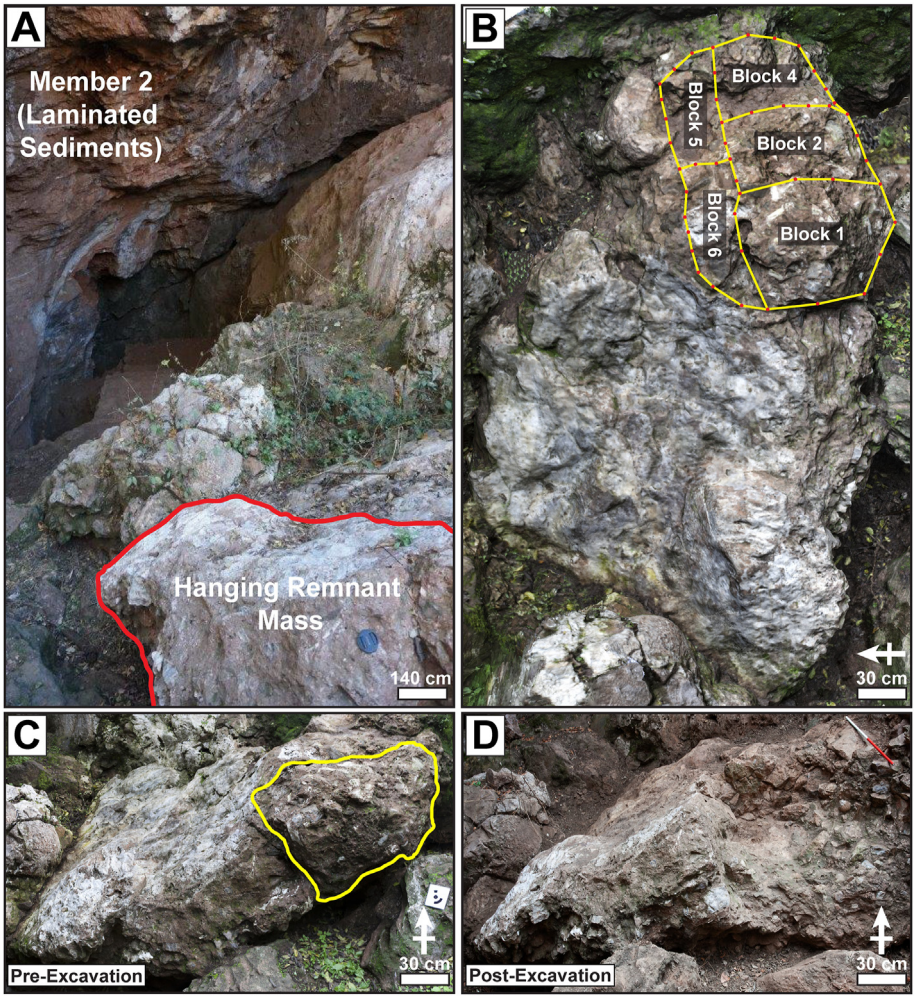

Figure 2. Excavation of the 'Hanging Remnant mass' (HRM). Informal view (i.e., unaligned to a cardinal direction) of the HRM from a position slightly above the mass, seen as it is naturally situated below the western portion of in situ Hanging Remnant main body (out of frame) (the laminated sediments of Member 2 of the Swartkrans Formation are seen in the background, north-northwest of the HRM, adhering to the western wall of Swartkrans Cave). The red outline indicates the extension of the HRM within the frame of the photograph (A). Orthophoto of the HRM prior to excavation of the six indicated blocks (outlined in yellow, with block 3 located under block 1); six more blocks, for a total of 12, were removed from underneath blocks 1–6 (the white arrow indicates North) (B). Informal, ground-level views of the HRM prior to (the yellow outline indicates portion targeted for removal; similar to B) (C) and after excavation (D) (white arrows indicate North). (For interpretation of the references to color in this figure legend, the reader is referred to the Web version of this article.)

Drimolen, Makapansgat, and Malapa (Table 1). Additional comparative data on other Miocene, Pliocene, and Pleistocene hominins were obtained from the literature, as were data on modern humans and modern nonhuman apes; we cite relevant studies and datasets throughout, below. The SWT1/HR-2 fossils are extremely small, so for body size analyses, they were not only compared to the bones of Western, industrialized modern humans ($n = 548$; Heaton et al., 2019, and others as cited below) but also to those of non-Western, 'traditional' modern human populations whose male mean statures are <150 cm and to whom we refer to as small-bodied modern humans. For taphonomic analyses, the SWT1/HR-2 fossils were compared to five distinct bone samples of modern baboons (*Papio* spp.), which were accumulated and modified under the various circumstances summarized in Table 2; one or more of the current authors personally analyzed and/or examined each of the listed samples. It is important to note that modern baboon carcasses are obviously not precise models of early hominin cadavers. However, in terms of general body size and structure, they are better matches for human ancestors than are, for instance, ungulates, which compose the majority of other potentially relevant neotaphonomic collections that are available for study.

Observations and data generation Overall macroscopic condition of each specimen was recorded, including completeness, degree of subaerial weathering (Behrensmeyer, 1978), and a qualitative assessment of staining by manganese dioxide (which is caused by dissolution of Swartkrans' dolomite parent rock). Each specimen was examined closely for bone surface modifications using 10× power magnification (e.g., Blumenschine et al., 1996).

We used Mitutoyo™ digital calipers, Paleotech™ spreading calipers, and field osteometric boards to collect standard osteometric linear measurements, and we collected standard osteometric angular measurements using SPI™ 0–180° protractors (e.g., Martin, 1928; Martin and Saller, 1957; McHenry and Corruccini, 1978; Buikstra and Ubelaker, 1994). All linear and angular measurements were generated by A.J.H. Each measurement was taken three times and averaged, and it is those mean values that appear in the text below and that are listed in the second column of Table 3.

Derivation of pelvic measurements, such as iliac pillar thickness and angle, acetabulosacral buttress thickness, and acetabulosacral load arm (ASLA), follows the methods of Kibii et al. (2011). Biomechanical lengths of the femur and tibia were calculated following the methods of Trinkaus et al. (1999), and femoral condyles were measured using landmarks described in the study by Lague (2002). The bicondylar angle of the femur was calculated using methods described by Preuschoft and Tardieu (1996). The medial, middle, and lateral trochlear groove angles were calculated using methods described by Tardieu et al. (2006). Tibial retroversion was calculated following methods described in the study by Wood (1920). The tibial arch angle was computed using the procedure outlined by DeSilva and Throckmorton (2010). Tibiotalar joint measurements were recorded as described by DeSilva (2009).

Femoral specimens are more common in the African Early Pleistocene hominin fossil record than are pelvic and tibial specimens. It is probably because of this bias that the hominin femur has received significantly more taxonomic consideration than have the os coxae and tibia (but see, e.g., Zihlman, 1971; Robinson, 1972; Lovejoy et al., 1973; Sigmon, 1986). Accordingly, of the three skeletal elements that the SWT1/HR-2 fossil-set comprises, it is the femur on which we base our taxonomic allocation of the fossil.

The crural index of SWT1/HR-2 was calculated by multiplying maximum tibia length by 100 and then dividing the result by the femoral bicondylar length (Schultz, 1937). Live body stature was estimated using the following equation, based on a reference sample of 19 African small-bodied humans, provided by Baab et al. (2016; Jungers et al., 2016): stature (cm) = [0.173 * (femoral bicondylar length (mm) + tibia maximum length (mm))] + 19.694; r = 0.93, s.e.e. = 2.9.

A voluminous body of research has demonstrated that the size of the femoral head is correlated with live body mass for various hominoids (e.g., Ruff, 1988, 1998, 2003, 2010; Ruff et al., 1988, 1991; Swartz, 1989; Jungers, 1991; McHenry, 1992; Rafferty and Ruff, 1994; Auerbach and Ruff, 2004). As described below, the head of the SWT1/HR-2b femur is incomplete. Thus, we derived an estimate of its femoral head maximum diameter (FHD) by modifying a technique used to estimate acetabula size of incomplete ossa coxae (Hammond et al., 2013). This method required us to first image the SWT1/HR-2b femur by X-ray microtomography (μXCT). Imaging was undertaken between 2022 and 2023 at the Microfocus X-ray Tomography Facility (MIXRAD) of the South African Nuclear Energy Corporation SOC Ltd. (Necsa), Pelindaba, using Nikon XTH 225 ST (Metris) equipment and according to the following parameters: 180–200-kV tube voltage; 80–128-mA tube current; and an angular increment of 0.36°–0.18° between each projection (for a total of 1000–2000 projections). The final volumes were reconstructed with an isotropic voxel size ranging from 28 μm to 51 μm.[4] From this X-ray microtomographic record of the femur, and consulting the original fossil, we then used Geomagic (3D Systems, 2023) to apply a best-fitted sphere to the preserved portion of the femoral head, which yielded a direct estimate of FHD.

The resulting FHD estimate was then entered into an equation for estimating hominin live body mass that is based on the FHD (Grabowski et al., 2015),[5] yielding a mass estimate for the SWT1/HR-2 hominin. The body mass index of the SWT1/HR-2 hominin was estimated using the method described by Keys et al. (1972).

Using Checkpoint (Stratovan Corporation, 2022), diaphyseal anteroposterior curvature of the SWT1/HR-2b femur was calculated based on digital methods presented by Macchiarelli et al. (2020). Specifically, virtual renderings of similarly oriented tomographic, microtomographic, and surface scan–based femur records were generated in Avizo (version 9.0.0; Visualization Sciences Group Inc.,

Table 1
Comparative South African hominin os coxae, femur, and tibia specimens.

Element	Site	Specimens
Os coxae	Swartkrans	SK 50, SK 1590, SK 3155b, SKW 8012
	Sterkfontein	Sts 14, Sts 65, StW 431, StW 573
	Kromdraai	TM 1605
	Drimolen	DNH 43B
	Makapansgat	MLD 7, MLD 8, MLD 25
	Malapa	UW 88-06+07+14+102, UW 88-10+52A and B+133
Femur	Swartkrans	SK 82, SK 97, SK 1896, SK 3121, SKW 19, SWT1/LB-2
	Sterkfontein	Sts 14, Sts 34, StW 25, StW 99, StW 121, StW 129, StW 311, StW 318, StW 361, StW 367, StW 392, StW 403, StW 448, StW 479, StW 501, StW 522, StW 527, StW 573, StW 598, StW 619, TM 1513
	Makapansgat	MLD 17, MLD 25, MLD 46
	Malapa	UW 88-04+05+39, UW 88-51+53+63
Tibia	Sterkfontein	StW 181, StW 389, StW 396, StW 514a, StW 515, StW 567, StW 573, StW 653
	Malapa	UW 88-89, UW 88-24+64+78+97, UW 88-21+40

[4] The same dates, facility, equipment, and parameters were used to image the SWT1/HR-2a os coxae and the SWT1/HR-2c tibia.

[5] Ln(mass) = 1.52765485 × Ln(femoral head maximum diameter) − 1.9161862 (Grabowski et al., 2015).

Table 2
Comparative neotaphonomic samples of baboon remains.

Locality	Type[a]	Agent/mechanism[b]	Baboon NISP/MNI[c]	Source
Mount Suswa (Kenya)	Naturalistic (shelter)	Leopard (inferred)	176/10	Brain (1981) [d]
Portsmut (Namibia)	Naturalistic (shelter)	Leopard (observed)	20/1	Brain (1981)
Vivo (South Africa)	Experimental (enclosure)	Leopard (observed)	454/8	Pickering (2001)
Mapungubwe (South Africa)	Naturalistic (mixed)	Leopard (inferred)	587/7	Pickering et al. (2011)
Misgrot (South Africa)	Naturalistic (shelter)	Natural death (inferred)	487/21[e]	Nel et al. (2021)

[a] Naturalistic = studies conducted among wild mammal populations in African landscapes; experimental = studies conducted among captive leopards with human-supplied baboon carcasses; shelter site = research collection area is a cave or rock overhang; mixed site = research collection area includes shelter sites and open spaces; enclosure site = research collection area is a human-constructed and human-maintained leopard enclosure.
[b] Agent = biological taphonomic actor; mechanism = process not directed by an extrinsic biological actor. Inferred = none or not all of taphonomic cause-and-effect behaviors observed by researchers; observed = taphonomic cause-and-effect behaviors observed by researchers.
[c] Abbreviations: NISP = the number of identified bone specimens; MNI = the minimum number individuals estimated to account for the observed NISP (see Lyman, 1994).
[d] The Mount Suswa Caves are in the form of multiple lava tubes. Many taphonomic agents and processes contributed to the accumulation of bones in the caves (Coryndon, 1964; Simons, 1966). However, the sample of baboon bones utilized in this study is from a closely circumscribed area of the caves, in which leopard activity is strongly inferred to have been the overwhelming, if not exclusive, mode of baboon bone deposition and modification (Brain, 1981).
[e] NISP and MNI are based only on completely skeletonized remains. In addition, nine mummified baboons, comprising a separate NISP of 1146, have also been recovered from the site.

Bordeaux). Lateral view images of renderings were then imported into ImageJ (Schneider et al., 2012), where a total of 20 points was placed manually along the anterior contour of the shaft, between 20% of the femoral biomechanical length and 1.3 cm inferior to the lesser trochanter, and used to extract a curve. By using the package Geomorph (version 4.0.4; Adams et al., 2021) for R (version 4.2.1; R Development Core Team, 2021), 12 equidistant two-dimensional semilandmarks were calculated along the curves between the two fixed landmarks, the most proximal and most distal points. We then performed generalized Procrustes analyses and a principal component analysis based on the Procrustes residuals using the extant taxa as groups. Table 4 summarizes the sources of the comparative femoral diaphysis anteroposterior curvature data that we used in this study. We followed the methods of Daver et al. (2022) and Cazenave et al. (2021) to derive values for femur diaphyseal antetorsion but with the slight modification that our proximal transverse section was not taken at the base of the lesser trochanter. Instead, it was taken at 1.3 cm inferior to the lesser trochanter, which is the most superior diaphyseal position for a well-preserved CT-slice on the SWT1/HR-2 femur. We calculated cross-sectional geometry properties of the femoral diaphysis using methods described by Ruff et al. (1999). It is important to note, however, that for the same reason as described earlier, we necessarily had to extract a section at 1.3 cm inferior to the lesser trochanter, rather than at 1.0 cm inferior to that feature, which is recommended by Ruff et al. (1999) and Domínguez-Rodrigo et al. (2013) as the reference position for estimated 80% of the femoral biomechanical length.

Age at death of the SWT1/HR-2 hominin was estimated via visual analysis of selected μXCT coronal slices of the proximal and distal metaphyses and epiphyses of the SWT1/HR-2b femur and SWT1/HR-2c tibia.

3. Results and interpretations

3.1. Stratigraphic and geological contexts

The inference that the HRM is a portion of the HR is confirmed by its spatial position directly below the main body of the HR (which adheres to the cave roof) and by sedimentological observations of the cleaned HRM breccia blocks. These blocks, like the main body of the HR (e.g., Robinson, 1952; Brain, 1981, 1993a), are composed of reddish-brown, strongly indurated, matrix-supported polymodal sediments. The matrix is a poorly sorted sand, the structure of which varies from massive and void-free to vesicular, with calcite-lined and calcite-filled voids that penetrate the breccia in the vicinity of speleothem formations. Larger voids (>30 mm) are frequently lined with coralloidal and crystal speleothem forms. Clasts are poorly sorted, vary in abundance locally (from 10% to 25% of clastic components), and range in size from 2 to 100 mm. Clasts are represented by rounded weathered dolomites; subangular to subrounded cherts, with orange weathering rinds; angular fresh cherts; speleothem fragments; small (<50 mm) rounded breccia and clay fragments; and occasional angular quartz chunks. Large clasts are generally dispersed and 'float' within the matrix. Occasionally, small, rounded clasts (<20 mm) occur in weak beds that also include complete and fragmentary microfaunal remains. Such bioclasts are relatively abundant (~10% of clastic components) and are represented by a poorly sorted mixture of craniodental and postcranial elements (2 to >100 mm) in complete and fragmentary states and with varying degrees of bone surface preservation. Larger (>30 mm), rounded fossil fragments with flaky cortical surfaces occur as isolated remains, whereas smaller (<30 mm), poorly preserved fragments are occasionally associated with weak pebble beds.

3.2. Laboratory discovery and extraction of the SWT1/HR-2 fossils

Site technician Lucas Sekowe observed a weathered section through a fossil on the outside of HRM breccia block 1. He recognized the bone as a possible hominin femur, with a neck that had been sectioned longitudinally by the extractive activities of lime miners who operated at Swartkrans in the early to mid-twentieth century. Sekowe brought this to the attention of R.J.C. and D.S. on March 20, 2019. R.J.C. then used an air scribe to clean around the fossil to confirm its identification (SWT1/HR-2b) and also to uncover its connected, more deeply buried, partial diaphysis. R.J.C. then recognized that the broken diaphysis contacted bone in the adjoining block 3. Further processing of blocks 1 and 3 by R.J.C., Phaswana, and Molepolle uncovered more of the femur and a complete hominin tibia (SWT1/HR-2c) beneath it. A partial hominin os coxae (SWT1/HR-2a) was then found jammed tightly against the posterior surface of the femoral head and neck (Fig. 3).

3.3. Preservation, taphonomy, and descriptions of the SWT1/HR-2 fossils

SWT1/HR-2a (Left os coxae)

Preservation The left os coxae is fragmentary. Its maximum anteroposterior length is ~126.0 mm; it measures a maximum of

Table 3
SWT1/HR-2b (femur) and SWT1/HR-2c (tibia) linear measurements (mm).[a]

Element	Measurement	Value	Reference
Femur	Maximum length	266.0	McHenry and Corruccini (1978)
	Bicondylar length	263.0	Buikstra and Ubelaker (1994)
	Biomechanical length	(244.0)	Trinkaus et al. (1999)
	Head diameter SI	(29.0)	McHenry and Corruccini (1978)
	Head diameter AP	(29.0)	McHenry and Corruccini (1978)
	Neck length	(42.4)	McHenry and Corruccini (1978)
	Neck SI	(23.3)	McHenry and Corruccini (1978)
	Lesser trochanter length	18.3	Harmon (2006)
	Lesser trochanter breadth	10.3	Harmon (2006)
	Subtrochanteric diameter AP	(19.2)	McHenry and Corruccini (1978)
	Subtrochanteric diameter ML	(26.6)	McHenry and Corruccini (1978)
	Diaphyseal diameter AP (MS)	17.9	McHenry and Corruccini (1978)
	Diaphyseal diameter ML (MS)	(22.6)	McHenry and Corruccini (1978)
	Diaphyseal circumference (MS)	(66.3)	Buikstra and Ubelaker (1994)
	Diaphyseal length	155.0	Buikstra and Ubelaker (1994)
	Epicondyle breadth	58.0	Buikstra and Ubelaker (1994)
	Intercondylar notch width	15.0	McHenry and Corruccini (1978)
	Lateral condyle width	16.4	McHenry and Corruccini (1978)
	Medial condyle width	(21.7)	McHenry and Corruccini (1978)
	Lateral condyle AP diameter	42.3	Tardieu et al. (2006)
	Medial condyle AP diameter	(37.1)	Tardieu et al. (2006)
	Lateral condyle height	23.1	Tardieu et al. (2006)
	Medial condyle height	33.2	Tardieu et al. (2006)
	Lateral condyle length	42.2	Tardieu et al. (2006)
	Total condyle width	52.9	Lague (2002)
	Projection of lateral lip	29.8	Lague (2002)
	Projection of medial lip	(21.3)	Lague (2002)
	Patellar width	(29.4)	Lague (2002)
Tibia	Maximum length	218.0	Buikstra and Ubelaker (1994)
	Biomechanical length	202.0	Trinkaus et al. (1999)
	Interspinal distance	8.1	DeSilva et al. (2018)
	Plateau depth AP	(34.4)	McHenry (1978)
	Plateau depth ML	55.4	McHenry (1978)
	Medial condyle depth AP	32.5	Buikstra and Ubelaker (1994)
	Medial condyle width ML	23.7	Buikstra and Ubelaker (1994)
	Lateral condyle depth AP	22.7	Buikstra and Ubelaker (1994)
	Lateral condyle width ML	24.5	Buikstra and Ubelaker (1994)
	Diaphyseal diameter AP[b]	(19.4)	Buikstra and Ubelaker (1994)
	Diaphyseal diameter ML[b]	(17.5)	Buikstra and Ubelaker (1994)
	Diaphyseal diameter AP (MS)	18.5	Martin (1928)
	Diaphyseal diameter ML (MS)	15.1	Martin (1928)
	Diaphyseal circumference[b]	64.3	Buikstra and Ubelaker (1994)
	Diaphyseal circumference (MS)	58.9	Martin (1928)
	Distal end depth AP (maximum)	(28.5)	Buikstra and Ubelaker (1994)
	Distal end breadth ML (maximum)	(34.2)	Buikstra and Ubelaker (1994)
	Lateral talar surface AP	(19.0)	DeSilva (2009)
	Midpoint talar surface AP	(21.0)	DeSilva (2009)
	Medial talar surface AP	20.0	DeSilva (2009)
	Anterior talar surface ML	19.2	DeSilva (2009)
	Midpoint talar surface ML	(20.7)	DeSilva (2009)
	Posterior talar surface ML	(19.0)	DeSilva (2009)
	Medial malleolus height SI (maximum)	11.8	DeSilva et al. (2010)
	Medial malleolus diameter AP	16.5	Zipfel et al. (2011)
	Medial malleolus diameter ML	10.1	Zipfel et al. (2011)

[a] Abbreviations: AP = anteroposterior; ML = mediolateral; MS = midshaft; SI = superoinferior. Each value is in mm and is a mean of three measurements. Values in brackets are estimates.
[b] It is directed that this measurement should be taken at the level of the nutrient foramen, which is not preserved. Thus, measurement was taken at a position one-third inferior to the proximal end of the bone, which serves as the approximate 'typical' position of the nutrient foramen on most modern human tibiae.

~93.0 mm superoinferiorly. It is truncated superiorly across much of the anteroposterior depth of the inferior ilium by a transverse line of ragged-edge chewing damage (see below) that begins anteriorly ~23.0 mm superior to the superior termination of the anterior inferior iliac spine. This damage continues posteriorly across the ilium and then curves inferiorly just anterior to the former position of the posterior inferior iliac spine, removing some of that feature (especially superiorly). The specimen is truncated inferiorly across the acetabulum, the only preserved portion of which is the roof of the lunate surface. There are four large fractures, each of which trends roughly superoinferiorly, that have slightly displaced adjoining sections of bone relative to one another. These fractures occur (1) starting along the medial surface of the curve between the anterior superior iliac spine and the anterior inferior iliac spine and carrying through the internal surface aspect of the anterior inferior iliac spine; (2) from the base of the superior ragged edge border inferiorly, down the iliac pillar; (3) from the base of the ragged edge border through the approximate midpoint of the greater sciatic notch; and (4) through the inferior arm of the auricular surface. Much of the greater sciatic notch is preserved, as is the inferior reach of the anterior gluteal line (Fig. 4).

Table 4
Origin, composition, and scanning information for the extant hominoid sample.

Catalog number[a]	Genus	Sex	Age	Ancestry/origin	Collection[b]	Modality	Scanned by
X155	*Homo*	M	51	European	PBC	μXCT	South African Nuclear Energy Corporation
5X67	*Homo*	F	32	African	PBC	μXCT	South African Nuclear Energy Corporation
58X8	*Homo*	F	32	African	PBC	μXCT	South African Nuclear Energy Corporation
595X	*Homo*	M	41	African	PBC	μXCT	South African Nuclear Energy Corporation
X957	*Homo*	F	29	African	PBC	μXCT	South African Nuclear Energy Corporation
6X68	*Homo*	F	42	European	PBC	μXCT	South African Nuclear Energy Corporation
63X8	*Homo*	F	21	European	PBC	μXCT	South African Nuclear Energy Corporation
650X	*Homo*	F	22	European	PBC	μXCT	South African Nuclear Energy Corporation
X028	*Homo*	M	26	African	PBC	μXCT	South African Nuclear Energy Corporation
AMNH-51393	*Pan*	M	Adult	Wild	AMNH	Surface scanning	Sergio Almécija, Angelique Aiello
AMNH-89406	*Pan*	M	Adult	Wild	AMNH	μCT	Sergio Almécija, Kelly Ostrofsky
CMNH-B-1718	*Pan*	M	Adult	Wild	CMNH	Surface scanning	Ashley Hammond, Susanna Israelsson
NMNH-176226	*Pan*	F	Adult	Wild	NMNH	Surface scanning	Elly Cordiner
NMNH-176227	*Pan*	M	Adult	Wild	NMNH	Surface scanning	Elly Cordiner
NMNH-220064	*Pan*	F	Adult	Wild	NMNH	Surface scanning	Louis Gorgone, Alisha Anaya
NMNH-220327	*Pan*	M	Adult	Wild	NMNH	Surface scanning	Elly Cordiner, Alisha Anaya
NMNH-395820	*Pan*	M	Adult	Wild	NMNH	Surface scanning	Elly Cordiner, Alisha Anaya
NMNH-481804	*Pan*	M	Adult	Wild	NMNH	Surface scanning	Elly Cordiner, Louis Gorgone
AMNH_167339	*Gorilla*	F	Adult	Wild	AMNH	Surface scanning	Alisha Anaya
AMNH_201460	*Gorilla*	M	Adult	Wild	AMNH	Surface scanning	Sergio Almécija
AMNH_2069	*Gorilla*	F	Adult	Wild	AMNH	Surface scanning	Ashley Hammond, Susanna Israelsson
AMNH_54356	*Gorilla*	M	Adult	Wild	AMNH	Surface scanning	Marine Cazenave
CMNH-2767	*Gorilla*	M	Adult	Wild	CMNH	Surface scanning	Sergio Almécija
CMNH-3393	*Gorilla*	F	Adult	Wild	CMNH	Surface scanning	Ashley Hammond, Susanna Israelsson
NMNH_174722	*Gorilla*	M	Adult	Wild	NMNH	Surface scanning	Elly Cordiner
AMNH-200898	*Pongo*	M	Adult	Wild	AMNH	Surface scanning	Marine Cazenave
NMNH-145301	*Pongo*	M	Adult	Wild	NMNH	Surface scanning	Elly Cordiner, Alisha Anaya
NMNH-145302	*Pongo*	F	Adult	Wild	NMNH	Surface scanning	Elly Cordiner, Alexander Prucha
NMNH-145305	*Pongo*	M	Adult	Wild	NMNH	Surface scanning	Elly Cordiner
NMNH-142169	*Pongo*	F	Adult	Wild	NMNH	Surface scanning	Elly Cordiner, Alisha Anaya
NMNH-153805	*Pongo*	F	Adult	Wild	NMNH	Surface scanning	Elly Cordiner
NMNH-153823	*Pongo*	M	Adult	Wild	NMNH	Surface scanning	Maryse Biernat

[a] Following South African stipulations, one digit within each individual label has been replaced by an 'X' to keep individual identity confidential.
[b] Abbreviations: PBC = Pretoria Bone Collection (University of Pretoria, South Africa); AMNH = American Museum of Natural History (New York, USA); CMNH = Cleveland Museum of Natural History (Cleveland, USA); NMNH = National Museum of Natural History (Washington, DC, USA).

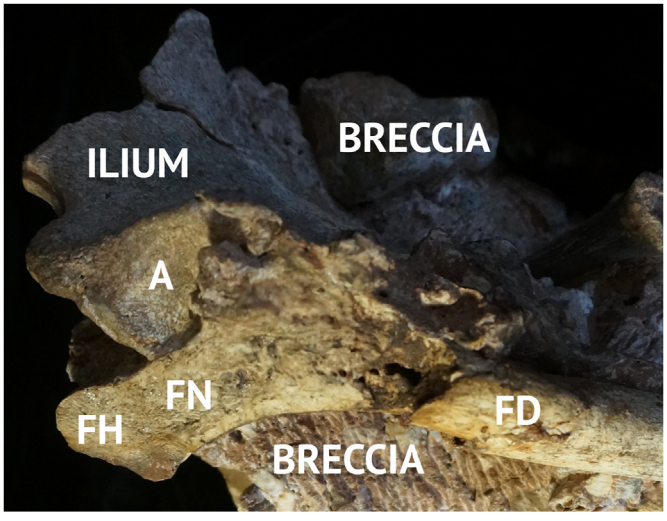

Figure 3. Informal laboratory view of the SWT1/HR-2a hominin os coxae (positioned approximately anterolaterally, superior up) and SWT1/HR-2b hominin femur (positioned approximately anteriorly, lateral up), part way through their mechanical preparation but still cemented together with adhering breccia. Abbreviations: A = acetabulum; FD = femur diaphysis; FH = femur head; FN = femur neck. (For interpretation of the references to color in this figure, the reader is referred to the Web version of this article).

Taphonomy SWT1/HR-2a displays good bone surface integrity, with light manganese dioxide staining and only moderate cracking (i.e., Behrensmeyer's (1978) weathering stage 1) across the entirety of its cortex. As mentioned earlier, the specimen's current form is due to extensive mammalian chewing activities that are now reflected in its ragged-edged superior border. This border is also split at its anterior end, and the internal surface portion is bent inferiorly out of natural position. Much of the ragged edge appears smoothed over and polished, perhaps as a result of the fossil's subsequent movement in and/or across cave sediments during the diagenetic phase. In addition, the terminal edges of the lunate surface and acetabulosacral buttress are also consistent in appearance with damage imparted by the teeth of mammalian actors. All edges of the fossil are coated with tightly adhering, calcified, poorly sorted clastic red sediments, which attest to the great antiquity and taphonomic integrity of the damage described earlier. Lastly, there is a prominent depression located just inferior to the specimen's superior ragged-edge border, on the posterior shoulder of the iliac pillar. The depression is ~4.3 mm (superoinferiorly) × ~3.0 mm (anteroposteriorly) and is mostly filled with calcified red sediment, again, attesting to the fact that it was created prehistorically. However, the rim of the depression is relatively smooth-edged and lacks any microfracturing and crushing, such as would characterize a typical tooth pit created by the masticatory actions of a feeding mammal (e.g., Domínguez-Rodrigo and Piqueras, 2003).

Anatomy The specimen is robust. It includes a completely fused, extremely well-developed anterior inferior iliac spine, the total superoinferior span of which is ~21.2 mm and with a cortical plate maximum thickness at its superior portion, or extremity (sensu Gommery and Thackeray, 2008), of ~8.8 mm. The spine's extremity is large and blunt and projects markedly over its lower portion and the adjoining acetabulum. A series of significant superoinferior fractures of SWT1/HR-2a is described earlier. The first-mentioned

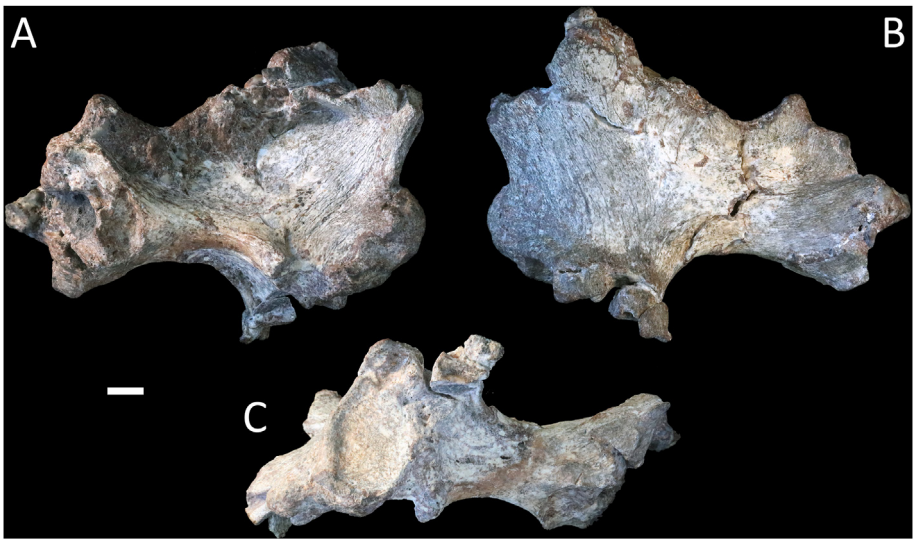

Figure 4. The SWT1/HR-2a hominin left os coxae shown in medial (superior up; anterior right) (A), lateral (superior up; anterior left) (B), and inferior (lateral up; anterior left) (C) views. Bar scale = 1 cm. (For interpretation of the references to color in this figure, the reader is referred to the Web version of this article).

travels through the spine's extremity, separating a nodule of that feature's internal surface away from its main, otherwise intact body.[6] The spine's extremity and lower portion are placed closely, and the latter adjoins to the superior rim of the acetabulum directly, with no intervening groove between those two features. The lower portion of the spine is convex and rugose and is broad from its internal to external surfaces. The superior rim of the acetabulum projects markedly and, posterior to its direct conjunction with the anterior inferior iliac spine, is bounded superiorly by a deep, slightly crescent-shaped supra-acetabular groove. The iliac pillar manifests as a subtle thickening of the ilium that starts at the superior rim of the acetabulum and appears to deflect anteriorly at its superior reach. Because the posterior inferior iliac spine is incomplete, we are only able to estimate the iliac pillar angle at ~57.0°. The approximate midpoint thickness of the iliac pillar is ~10.0 mm. The ilium thickens remarkably inferiorly as a result of its sharply raised acetabulosacral buttress, which projects markedly along its entire preserved length of ~39.5 mm. Its minimum thickness occurs at a point of some bone displacement (see above), but it is estimated at 20.0 mm. The buttress terminates posteriorly at the border of what appears to be an extremely tightly curved auricular surface. The ASLA is ~44.0 mm. The auricular surface is too incomplete to provide an accurate estimate of its surface area, but its preserved portion presents as a deeply cupped basin that is defined by well-demarcated edges. It is bounded inferiorly by an anteroposteriorly elongated arc of raised bone. The arc is broken through because of the damage described earlier, but, where preserved, it shows occasional slight negative relief within its boundaries. Those boundaries are clear superiorly and anteroinferiorly, taking the form, in both places, as a low cortical rim. The arc is open (i.e., rimless) anteriorly and posteroinferiorly. Overall, this mostly raised feature appears more like a paraglenoid groove than it does as a preauricular groove. The area lacks an associated piriform tubercle. The greater sciatic notch is nearly complete and is extremely wide and shallow, with a relatively inferiorly placed inflection point. The notch is also quite symmetrical, forming a near-semicircular shape.

[6] We are currently investigating the etiology of this feature, which may be taphonomic or pathological, such as a neoplastic growth.

SWT1/HR-2b (Left femur)

Preservation The left femur consists of several large pieces of bone glued together, most along good joins; there is, however, minor mediolateral displacement of adjoining bone fragments in the proximal diaphysis. In addition, SWT1/HR-2b is missing the anterior surfaces of its head, neck, proximal metaphysis, and extreme proximal diaphysis, along with the entirety of its greater trochanter. There is a large chip of cortex missing on the anterior aspect of the distal metaphysis, the base of which is ~13.5 mm superior to the superior projection of the patellar lip. The chip is ~7.7 mm in maximum superoinferior dimension and ~13.0 mm in maximum mediolateral dimension (Fig. 5).

Taphonomy SWT1/HR-2b is mostly unweathered but does show occasional stage 1–2 cracking on especially the anterior surface of its diaphysis. Larger cracks are filled with calcified red sediments. The specimen is lightly stained by patches of manganese dioxide across its entirety. There is minor exfoliation of the anterior periosteal surface of the distal diaphysis that is most likely the result of geochemical diagenesis. The most apparent damage to the fossil is the removal of the anterior surfaces of the proximal diaphysis, metaphysis, femoral neck, and head. The damaged surface has a sheared planar morphology that indicates strongly that this section of bone was removed through mining and/or paleontological excavation activities—typified by the use of explosives and handheld tools—conducted at Swartkrans in the early through mid-twentieth century. Indeed, it is not impossible that the missing portion of SWT1/HR-2b will someday be found in a curated breccia block from the site. Based on its sharp and right-angled fracture edge morphology, the large chip of missing cortex noted earlier was removed prehistorically by a nonbiotic, mechanical process(es), such as rockfall or sediment pressure, as was the posteroinferior corner of the lateral condyle. Other modifications to the fossil appear to be the result of the activities of prehistoric mammals that fed on the carcass of the SWT1/HR-2 individual. These modifications are in the form of ragged-edge chewing damage to the medial borders of the now-missing greater trochanter and intertrochanteric crest. Likewise, tooth furrowing damage is apparent on the posterior and inferior surfaces of the femoral head, the latter of which corresponds to the ragged-edge chewing damage on the lunate surface of the SWT1/HR-2a os coxae (described earlier). There is minor erosion of bone cortex along the medial margin of

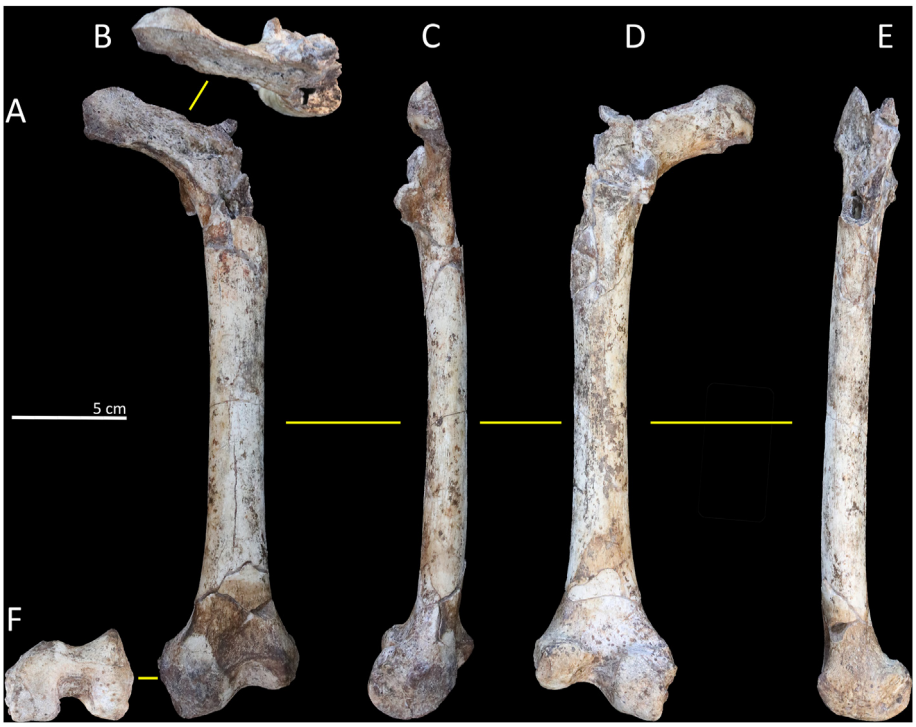

Figure 5. The SWT1/HR-2b hominin left femur shown in anterior (superior up) (A), superior (posterior up) (B), medial (superior up) (C), posterior (superior up) (D), lateral (superior up) (E), and inferior (anterior up) (F) views. (For interpretation of the references to color in this figure, the reader is referred to the Web version of this article).

the patellar surface. The exposed trabeculae in this area are filled with red sediments and are smoothed over and show the same patina and manganese dioxide staining as the fossil's intact cortical surfaces, attesting to the antiquity of the cortical removal. Erosion of the very thin cortical surface in this area is not uncommon on modern human femora in research collections and can result from even modest handling and movement of specimens in collection coffins. In this context, it is likely that the erosion of SWT1/HR-2b resulted from minor movements of the bone across and/or in cave sediments during the diagenetic phase, after the bone was defleshed.

Anatomy The femur is small. Its epiphyses are completely fused. As mentioned earlier, the anterior aspect of its proximal end is missing, so we begin our description with the posterior aspect of that end of the bone. The margin between the femoral head and neck is subtle. From examination of the posterior surface of the head, it appears that the complete head was relatively small. The femoral neck is long and connects to the proximal diaphysis at a low neck-shaft angle of 113°. The posterior aspect of the neck is flat, and it also lacks a marginal ridge. The obturator externus groove is not only palpable but also apparent visually. It is fairly wide mediolaterally and is set more toward the lesser trochanter than toward the femoral head. The intertrochanteric crest is incomplete due to damage described earlier, but its inferomedial portion is intact and unremarkable. The lesser trochanter is prominent and takes the form of a sharply raised flange that projects especially strongly posteriorly and much less so medially (it is barely visible when the femur is in standard anatomical position and viewed anteriorly). The spiral line is well developed, whereas the pectineal line is apparent superiorly, at the inferior root of the lesser trochanter, but then fades inferiorly. The gluteal tuberosity is moderately developed but slightly displaced medially from its natural, more lateral position by damage described earlier. Although this same damage obscures, to some extent, the posterolateral region of the femur, the inferior extent of a modestly developed hypotrochanteric fossa is still apparent. Anterolateral to this fossa, the femur swells slightly into a pilaster, but the robusticity of this feature is somewhat exaggerated, again, due to distortion of the fossil in this region. The moderately developed linea aspera terminates into very weakly expressed supracondylar lines that fade inferiorly into smooth bone surface so as to collectively demarcate an equally smooth and unremarkable popliteal surface. The posterior surface of the diaphysis does not bear a visible nutrient foramen. Overall, the diaphysis is fairly platymeric, especially proximally, and terminates in a pronounced bicondylar angle. In lateral view, the diaphysis shows a slight anterior convexity distally but is overall relatively rectilinear. The adductor tubercle is small but comes to a distinct peak, which is stacked superoanteriorly on an even more prominent tubercle that is the origin for the medial head of the gastrocnemius. The medial epicondyle is small but quite pronounced medially. The most distinctive feature of the medial condyle is its marked mediolateral expansion. Distally, the specimen does not show a well-developed, uniformly convex medial condylar boss, as is typical of modern human femora (Lovejoy, 2007). Instead, the medial condyle is more trochlear in form, with a relatively demarcated ridge that, starting at the base of the patellar surface and running posteriorly, follows the curve of the lateral margin of that structure's inferior surface. The medial meniscal groove is not preserved due to damage described earlier. The intercondylar fossa is unremarkable. The attachment sites for the cruciate ligaments are poorly developed, with that for the anterior one slightly more apparent than that for the posterior one. The popliteal groove and its contiguous impression for the popliteus are deeply excavated with well-defined, ridge-like boundaries. The impression for the lateral head of the gastrocnemius is an anteroinferiorly-posterosuperiorly elongated ridge that is positioned superior to a shallow trough for the attachment of the fibular collateral ligament. The lateral

Figure 6. The SWT1/HR-2c hominin left tibia shown in superior (posterior up) (A), anterior (superior up) (B), medial (superior up) (C), posterior (superior up) (D), lateral (superior up) (E), and inferior (anterior up) (F) views. (For interpretation of the references to color in this figure, the reader is referred to the Web version of this article).

condyle is capped by an unexceptional lateral epicondyle. The lateral meniscal groove is small but well defined. It is placed relatively anteriorly along the inferior border of the condyle. The lateral condyle, in lateral view, is more elliptical than is the medial condyle in medial view. The lateral patellar lip is very pronounced, projecting strongly anteriorly. The sustrochlear hollow is deep and mediolaterally expansive.

SWT1/HR-2c (Left tibia)

Preservation The left tibia is essentially complete, with only a few gaps of missing bone along the proximal metaphysis and diaphysis, where several small fragments of the fossil have been glued together along good joins (Fig. 6).

Taphonomy SWT1/HR-2c displays good bone surface integrity. The fossil is stained lightly in places by manganese dioxide and shows a maximum weathering of stage 1, with some sections completely unweathered. The specimen shows occasional minimal exfoliation of its periosteal cortical layers, mostly in the form of circular and oblong incidences, clustered mainly on the anterior aspect of the distal third of the specimen. These marks are miniscule, with the largest among them only ~2.0 mm (superoinferiorly) × ~1.5 mm (mediolaterally). They are most likely the result of geochemical diagenesis and should not be confused with biotically induced modification of the specimen. The only other major incidence of prehistoric damage on the specimen is the partial superolateral displacement fracture of the posterolateral corner of the distal epiphysis. This partial fracture is filled with calcified red sediments and an included clast.

Anatomy The tibia epiphyses are completely fused. The fossil is remarkably small but is defined by a mediolaterally expansive proximal metaphysis and epiphysis. The tibial plateau is rectangular with a mediolateral long axis in superior view. In that view, the medial condyle assumes a typical hominin, kidney-bean-shape that is more expansive anteroposteriorly than it is mediolaterally. Its anterior two-thirds is shallowly concave. In superior view, the lateral condyle is rhomboidal in outline and is more constricted anteroposteriorly than is the medial condyle. The ventral portion of the lateral condyle is flat, whereas its dorsal portion is gently convex. Those two portions of the lateral condyle are separated by a ventrodorsally narrow indentation that is set medially on the condyle, at the base of the lateral intercondylar tubercle. Both intercondylar tubercles rise markedly at the plateau midline to form a prominent intercondylar eminence. The attachment site for the anterior cruciate ligament is a clearly defined tubercle. It is more prominent than that for the posterior one, but neither is particularly expansive. The insertion for the semimembranosus is shallow and roughly wedge shaped, with its greatest anteroposterior dimension ~9.3 mm and its greatest superoinferior dimension (anteriorly placed) ~8.8 mm. Anteriorly, it caps a superoinferiorly elongated rugosity for the attachment of the medial collateral ligament that runs down the medial aspect of the proximal metaphysis and diaphysis. This enthesis is particularly distinct at its superior and inferior terminations, points at which it bulges strongly medially, with the former protrusion in the form of a tuberosity and the latter in the form of a dorsally concave flange. Just anterior to this long attachment site is an indistinct area for the attachment of the pes anserinus tendons. There is some damage and minor displacement of cortex in this area, but it does appear to have been naturally depressed. The superior fibular articular facet is expansive and slightly convex, with its maximum mediolateral measurement ~10.9 mm and its maximum superoinferior measurement ~11.0 mm. The insertion for the iliotibial tract is particularly robust, projecting strongly anterolaterally, and lies just superior to a small but very distinct, well-formed tuberosity for the origin of the extensor digitorum longus. Damage to the proximal end of the fossil, as described earlier, has only minimal effect on the assessment that its tibial plateau is only moderately retroverted. Anteriorly, the tibial tuberosity is weakly developed and, inferiorly, grades into a relatively sharp-peaked anterior crest, especially for the distal two-thirds of the diaphysis. The crest dissipates somewhat at the

distal metaphysis but does not flatten completely superior to the anterior rim of the talar facet. The interosseous surface of the proximal two-thirds of the diaphysis is slightly concave, whereas the medial surface of the same length of the diaphysis is slightly convex. Posteriorly, the popliteal surface is smooth and unremarkable, despite some small missing chips of cortex. The interosseous and medial crests are well developed. The former is particularly sharp and narrow superiorly and then broadens inferiorly. The latter is relatively thick and blunt superiorly and becomes more angular inferiorly. In addition, the specimen displays a slightly less developed vertical line that is most apparent on the middle third of the posterior surface of the diaphysis. Damage to the proximal posterior surface of the tibial diaphysis obscures visualization of the soleal line superiorly, but the line is palpable at its distal extent as a sharp, narrow ridge. The nutrient foramen is found on the posterior surface of the diaphysis, ~64 mm inferior to the most superior point of the proximal articular surface. Overall, the diaphysis of SWT1/HR-2c is roughly triangular in cross section for its extent and does not 'square off' distally but, instead, is slightly anteroposteriorly expanded in this inferior region. In general, the morphology of the distal epiphysis is modern humanlike. The anterior groove is very pronounced, with a sharp superior lip and is ~12.7 mm mediolaterally; there are no indications of superimposed squatting facets. The middle of the inferior border of the groove dips very slightly inferiorly but is not, by any means, a 'beak.' The medial malleolus is prominent, but the intercollicular groove lacks any appreciable depth, and there is only a subtle visible and palpable distinction between the anterior colliculus and posterior colliculus. The malleolar groove is mediolaterally broad and deep, with sharply raised medial and lateral borders. The entheses for attachment of the anterior and posterior tibiofibular ligaments are strongly developed; unfortunately, the intervening distal fibular articular surface is obscured by the damage and adhering sediments described earlier. The posterior ridge of the attachment site for the anterior tibiofibular ligament is contiguous with the distal reach of the interosseous crest. The talar facet is, in keeping with the overall appearance of the distal epiphysis, modern humanlike in its relatively substantial depth and squared inferior plan view.

3.4. Comparative anatomy of the SWT1/HR-2 fossils and inferences of postural and locomotor capabilities of the SWT1/HR-2 hominin

In this subsection, we provide inferences of the posture and locomotion of the SWT1/HR-2 hominin based on interpretations of implicating features found on its constituent fossils at the hip, on the thigh, at the knee, on the crus, and at the ankle. We focus on presenting interpretations of the primary and secondary actions of muscles, rather than on discussion of their functions.

The hip Experimental studies suggest that the relative degree of femoral neck anteversion relates functionally to differing patterns of hip biomechanics and especially to habitual hip postures in mammals (e.g., Wilkinson, 1962; Cibulka, 2004). Adult hominins that have been observed or reconstructed (using other criteria) as terrestrial bipeds show femoral neck anteversion angles[7] between <90° for 'typical' modern humans and a high range of 108.6°–118.9° ($\bar{x}$ = 115.2° ± 4.9) for four *Homo naledi* specimens, with australopiths (used here to include the genera *Ardipithecus*, *Australopithecus*, and *Paranthropus*, sensu Wood and Richmond, 2000) (n = 4; $\bar{x}$ = 108.7° ± 5.4, range = 104.0°–116.3°) falling closer to *H. naledi* than to modern humans (Marchi et al., 2017). Angles for extant quadrupedal apes are much lower; for instance, 56 chimpanzees (*Pan troglodytes*) show a mean angle of only 77.5° ± 11.9 (range = 39.0°–100.0°) (Marchi et al., 2017).

Because the anteroproximal portion of the SWT1/HR-2b femur is incomplete, we were not able to calculate directly its femoral neck anteversion. It is fortunate, however, that femoral neck anteversion is correlated with the antetorsion of the diaphyseal long axis (Ruff, 1995). Figure 7 shows that SWT1/HR-2b has a diaphyseal torsion angle of 26.5°, which is very near the modern human mean (Daver et al., 2002; Cazenave et al., 2021). That similarity is suggestive that SWT1/HR-2b, like modern human femora, possessed an angle of neck anteversion indicating bipedalism. However, we do note again that the proximal portion of SWT1/HR-2b is poorly preserved. This made it necessary to calculate its diaphyseal torsion angle at the nonstandard position of 1.3 cm inferior to its lesser trochanter. It is possible that its angle at the base of the lesser trochanter, where diaphyseal torsion angle is typically calculated, was different compared to 1.3 cm inferior to that position.

The os coxae of the SWT1/HR-2 hominin indicates less ambiguously than does its proximal femur that the individual engaged in terrestrial bipedalism. Even though the SWT1/HR-2a os coxae is very fragmentary, its apparent robusticity is striking in comparison to the pelves of other australopiths. Specifically, although the SWT1/HR-2a os coxae conforms to those of other *Australopithecus* and *Paranthropus* individuals in its subtle and apparently superoanteriorly directed iliac pillar (e.g., Lovejoy et al., 1973; Arsuaga, 1981; Gommery et al., 2002; Claxton et al., 2016) (Table 5), the minimum thickness of its acetabulosacral buttress greatly exceeds that predicted for a 'typical' australopith os coxae (reviewed in the study by Claxton et al., 2016). In this way, SWT1/HR-2a is most like the pelves of *Australopithecus sediba*, a species that also possesses a much thicker acetabulosacral buttress than do other australopiths (Kibii et al., 2011)—although the acetabulosacral buttress of SWT1/HR-2a is considerably thicker than even those of *A. sediba* ossa coxae (Table 5).

SWT1/HR-2a and *A. sediba* pelves also group together—and separate from those of other australopiths, of early *Homo*, and of modern humans—in having reduced ASLAs. In fact, SWT1/HR-2a's modern humanlike acetabulosacral buttress minimum thickness/ASLA ratio of 0.45 is identical to the mean acetabulosacral buttress minimum thickness/ASLA ratio of *A. sediba* (Kibii et al., 2011). The acetabulosacral region is the major load-bearing component of the ilium (e.g., Dalstra and Huiskes, 1995). In recognition of this fact, Kibii et al. (2011: 1410) suggested that the relatively elevated acetabulosacral buttress minimum thickness/ASLA ratio of *A. sediba* might reflect "increased force transduction through [that species'] pelves relative to earlier australopiths"; however, they then tempered that idea by noting that "the small sacroiliac and hip joints [of *A. sediba*] appear to contravene this idea." Because of its fragmentary nature, we are unable to provide precise estimates of the size of the sacroiliac and hip joints of the SWT1/HR-2 hominin. The incomplete auricular surface of SWT1/HR-2a is deep and well defined, but it does not appear particularly expansive in terms of surface area. Regardless, the rest of the ilium is also too incomplete to calculate the *relative* size of the specimen's sacroiliac joint. The same complication holds for the hip joint of SWT1/HR-2: although we provide estimates of the femoral head size for the purpose of a live body mass estimate (below) and could also estimate acetabulum size (from femoral head estimates; e.g., Plavcan et al., 2013), those values would still have to be compared to the incomplete iliac blade of SWT1/HR-2a.

Likewise, because the entire greater trochanter of the SWT1/HR-2b femur is missing, it is not possible to estimate the

[7] Measured as the angle between a transverse line that runs through the center of the femoral head and neck and that runs transversally through the knee joint (e.g., Fabry et al., 1973).

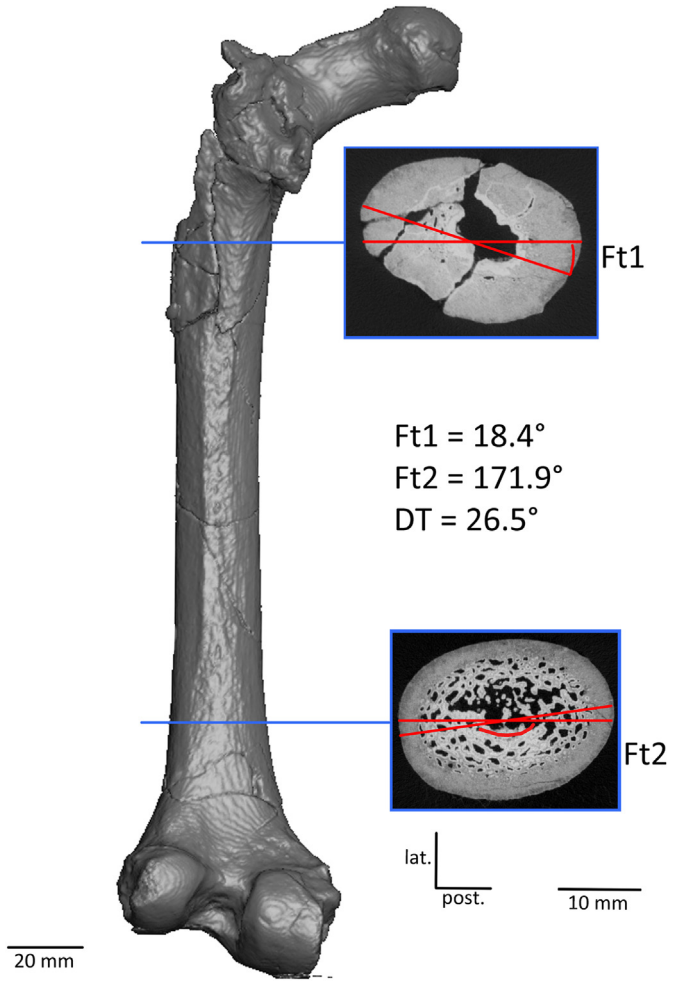

Figure 7. Diaphyseal torsion angle (DT) of the SWT1/HR-2b femur (shown in posterior view; superior up, medial to the right), calculated as the relative orientation of the proximal feret diameter measured in the transverse section extracted at 1.3 cm inferior to the lesser trochanter (Ft1; clockwise, relative to mediolateral axis) and the distal feret diameter measured in the transverse section extracted at 25% of the biomechanical length (Ft2; clockwise, relative to mediolateral axis), following the methods of Daver et al. (2022) and Cazenave et al. (2024). Abbreviations: lat. = lateral; post. = posterior. (For interpretation of the references to color in this figure, the reader is referred to the Web version of this article).

biomechanical length of its neck with any degree of accuracy. However, its neck-shaft angle is confidently measured at 113.0°, a relatively low figure that is typical for an australopith femur (e.g., Grine et al., 1995; Macchiarelli et al., 1999; Harmon, 2009a; Ruff and Higgins, 2013) (Table 6). Functionally, such a low neck-shaft angle increases the mechanical length of the neck. This, in turn, increases the moment arm of the gluteal abductors at the hip joint and, as such, seems to reflect the need to balance "the relatively large body weight moment arm that apparently characterized all early hominins [i.e., australopiths and early *Homo*]" (Ruff and Higgins, 2013: 520). Thus, to the degree that can be determined by analysis of its external characteristics, the hip of SWT1/HR-2 shows probable compensatory anatomy of the femoral neck that indicates the need to carry increased superoinferior bending loads across a proximal femur capped by a relatively small head (Ruff and Higgins, 2013). In this way, SWT1/HR-2b conforms to other known australopith femora in terms of inferred functional morphology.

If the large size of its anterior inferior iliac spine is an indication, the hip of the SWT1/HR-2 hominin also seems to have been reinforced by an extremely robust iliofemoral ligament. This ligament, which originates at the lower portion of the anterior inferior iliac spine, is the strongest ligament in the modern human body. Along with the pubofemoral and ischiofemoral ligaments, it functions to hold the femoral head in place within the acetabulum and to counteract gravity hyperextending the hip when the center of mass is located dorsal to the center of the hip joint. There are several significant differences in the pelves of modern humans and australopiths (reviewed in the study by Gruss and Schmitt, 2015) that suggest corresponding differences in terms of the center of mass in these distinct bipedal hominins. Regardless, the impressively broad and rugose lower portion of SWT1/HR-2a's anterior inferior iliac spine indicates a generally similar hip-stabilization morphocomplex as is observed in modern humans. Added to this is the remarkably pronounced enthesis for the iliotibial tract on the SWT1/HR-2c tibia, indicating the in vivo robusticity of that aponeurosis—which is a major lateral stabilizer of the bipedal hip and knee—on the SWT1/HR-2 hominin. In addition, the attachment site for the semimembranosus, a muscle that can act to resist deleterious anterior pelvic tilt (e.g., Reynolds et al., 1999; Lazennec et al., 2013; Zahn et al., 2017; Fukushima et al., 2018), is also quite prominent.

Likewise, the extremity of SWT1/HR-2a's anterior inferior iliac spine is also very strongly expressed. Given this morphology, it is

Table 5
Metric comparisons of the iliac pillar and acetabulosacral buttress of SWT1/HR-2a to those of other hominin ossa coxae.[a]

Hominin	Iliac pillar angle (°) mean (*n*, SD)	Acetabulosacral buttress		
		Minimum thickness (mm) mean (*n*, SD)	Load arm (mm) mean (*n*, SD)	Minimum thickness/load arm mean (*n*, SD)
SWT1/HR-2a	57.0	20.0	44.0	0.45
Australopithecus sediba[b]	49.0 (1)	17.9 (2, 0.1)	40.3 (2, 4.6)	0.45 (2, 0.05)
Other australopiths[c]	51.2 (5, 8.0)	15.8 (6, 1.7)	49.0 (6, 4.5)	0.32 (6, 0.02)
Early *Homo*[d]	66.3 (6, 3.9)	21.9 (8, 3.4)	49.6 (7, 6.2)	0.47 (6, 0.08)
Modern *Homo*[e]	76.6 (107, 4.3)	22.4 (107, 2.6)	48.8 (105, 5.5)	0.47 (105, 0.09)

[a] All comparative data are summarized in Kibii et al. (2011).
[b] UW 88-06+UW 88-07+UW 88-14+UW 88-102 and UW 88-10+UW 88-52A and B+UW 88-133 (Kibii et al., 2011).
[c] A.L. 288-1 (Johanson et al., 1982); KSD-VP-1/1 (Haile-Selassie et al., 2010); Sts 14, Sts 65, StW 431, SK 50, SK 3155b, TM 1605 (Kibii et al., 2011).
[d] KNM-ER 3228 (Rose, 1984); KNM-WT 15000 (Walker and Ruff, 1993); BSN 49/P27 (Simpson et al., 2008); Atapuerca Pelvis 1 (Arsuaga et al., 1999); OH 28, Arago XLIV, Kabwe E719, Kabwe E720, Kebara 2, Krapina 207 (all from casts; Kibii et al., 2011).
[e] Black South African (Raymond Dart Collection of the School of Anatomical Sciences, University of the Witwatersrand, South Africa), 52 males and 54 females (Kibii et al., 2011).

Table 6
Australopith femoral neck-shaft angles and meric index.[a,b]

Presumed taxon	Specimen	Angle (°)	Meric index	Source
Australopithecus afarensis	A.L. 152-2	125		Ward et al. (2012)
	A.L. 288-1	123	67.8	Johanson et al. (1982)
	A.L. 333-3	125	75.5	Lovejoy et al. (1982)
	A.L. 827-1	119		Ward et al. (2012)
	MAK-VP 1/1	117	71.6	Lovejoy et al. (2002)
Australopithecus africanus	Sts 14	118		Lovejoy (1975)
	StW 522	124	(79.3)	DeSilva et al. (2013)
	StW 598	121	90.6	Pickering et al. (2021)
Australopithecus sediba	UW 88-04+05+39	115	77.0	DeSilva et al. (2013)
Australopithecus prometheus	StW 573	125	77.9	Heaton et al. (2019)
Paranthropus robustus	MLD 46[c]	120		Reed et al. (1993)
	StW 99[c]	113	74.9	DeSilva et al. (2013)
	SK 82	120	81.7	Walker (1973)
	SK 97	118	73.8	Walker (1973)
	SWT1/HR-2b	**113**	**(72.2)**	**This study**
Paranthropus boisei	OH 80-12		75.0	Domínguez-Rodrigo et al. (2013)
	OH 84		81.3	Aramendi et al. (2024)

[a] Values in brackets are estimates.
[b] Meric index values calculated from measurements at the subtrochanteric level. Low meric index values indicate relatively platymeric femoral diaphyses.
[c] See discussion in text and in Partridge et al. (2003) and Pickering et al. (2021) for justification of taxonomic assignment.

not surprising that SWT1/HR-2a also shows a deeply developed sulcus superior to the superior rim of the acetabulum. These two features serve, respectively, as the origins for the straight and reflected heads of the rectus femoris. As with the iliofemoral ligament, the rectus femoris plays a role in modern human orthogrady and terrestrial bipedalism. Specifically, in addition to its actions as a hip flexor and knee extensor, the rectus femoris can be recruited as an antagonist of the gluteal muscles and hamstrings, and thus it can assist in balancing the upright trunk over the lower limb.

In summary, the hip of the SWT1/HR-2 hominin comprises a fairly typical australopith proximal femur and an os coxae that is unusually robust for that of an australopith. Specifically, the proximal portion of the SWT1/HR-2b femur is composed of a small head and a relatively long, low-angled, and load-bearing neck. The robusticity of the os coxae is expressed specifically in its acetabulosacral buttress. This is the region of the pelvis through which weight is transferred between the hip and sacroiliac joints when a subject is standing upright. Indeed, the minimum thickness of the acetabulosacral buttress of SWT1/HR-2a (Table 5) falls even closer to the mean minimum thicknesses of indisputably habitually bipedal early *Homo* and modern human pelves than it does to the mean value for six australopith ossa coxae (Kibii et al., 2011). Among australopiths, *A. sediba's* mean minimum thickness, although still lower, is the closest to that of SWT1/HR-2a. In the case of *A. sediba*, Kibii et al. (2011: 1410) argue that greater iliac robusticity (as compared to that of other australopith ossa coxae) was part of a general pelvic morphocomplex that can "most parsimoniously [be] attributed to altered biomechanical demands on the pelvis in locomotion"—the implication being that such 'altered biomechanical demands' relate to a *Homo*-like degree of bipedalism in *A. sediba* relative to its forebearers, and probably to its congeners, as well.

The solidly weight-bearing morphology of the acetabulosacral buttress of SWT1/HR-2a agrees with the largeness of its anterior inferior iliac spine. In relation to this, the proximal posterolateral region of the SWT1/HR-2b femur is also relatively robust, carrying both a lateral pilaster and a hypotrochanteric fossa. Both of these osteological features are relevant to assessing the nature of a primate's bipedal capabilities. This is because the hip-extending and hip-stabilizing gluteus maximus and the knee-extending vastus lateralis muscles, respectively, insert and originate (in part) in this general region of the femur. Moreover, a rugose insertion for the semimembranosus on the SWT1/HR-2c tibia indicates the in vivo presence of a large and capable, bipedal hip-extending muscle. Similarly, the prominent, posteriorly projecting lesser trochanter of SWT/HR-2b indicates that the SWT1/HR-2 hominin possessed a large psoas major muscle. Among its various actions, the psoas major acts in conjunction with the iliacus muscle to flex the trunk at the hip and to contribute to hip stability during orthograde posture and bipedal locomotion. Together, these observations and interpretations indicate that the SWT1/HR-2 hominin possessed a robustly built, stable hip—one well adapted for habitual extension and orthograde and bipedal load-bearing, as well as an overall lifestyle that included frequent and/or rigorous activities involving trunk and hip flexion.

The thigh The diaphysis of the SWT1/HR-2b femur is relatively platymeric, especially at the subtrochanteric level (Table 6), and less so distally. It is not fully understood why some hominin femoral shafts are flat anteroposteriorly. Most biomechanical explanations for the phenomenon reference the effects of both the vasti and gluteal musculature complexes on diaphysis cross-sectional geometry. More specifically, subtrochanteric platymeria in modern humans is correlated with high mediolateral loads at the hip (e.g., Ruff and Hayes, 1983a,b; Westcott, 2006). It is the large gluteal muscles of modern humans that counterbalance these bending movements; the extensively developed entheses and general rugosity of the modern human proximolateral femur reflects the importance of this and other functions of the gluteals for those obligate terrestrial bipeds. In this context, it is telling that in addition to its subtrochanteric platymeria, the proximolateral surface topography of SWT1/HR-2b is also complex and includes a distinct gluteal tuberosity.

Figure 8 shows the results of our comparative hominoid principal component analysis for anteroposterior curvature of the SWT1/HR-2b diaphysis. In that analysis, principal component 1 somewhat separates chimpanzees (negative values) from modern humans (positioned in central morphospace) and orangutans (*Pongo pygmaeus*) (positive values). The femoral diaphyseal outlines of chimpanzees are more anteroposteriorly curved than the slightly convex (and sometimes nearly flat) shape of the latter taxa. Along principal component 2, the relatively sinusoidal-shaped curvature of human femora somewhat separates them from the more concave femora of chimpanzees, with gorillas (*Gorilla* spp.) maximally variable and orangutans of intermediate shape. The SWT1/HR-2b femur is positioned in the same morphospace as are orangutans. An orangutan-like curvature also characterizes some

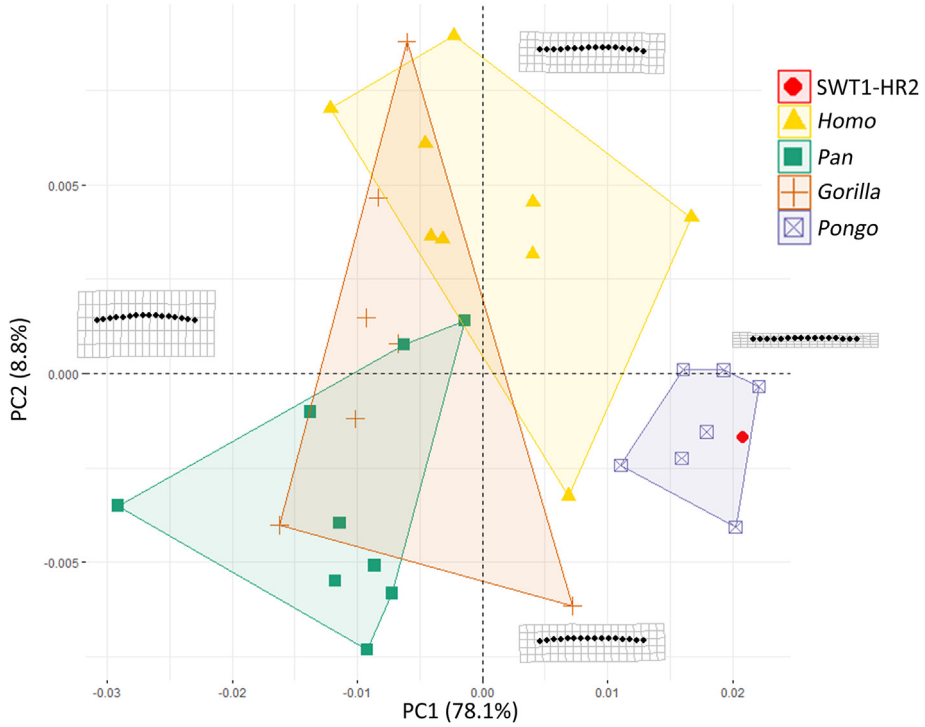

Figure 8. Principal component analysis (PCA) of the Procrustes shape coordinates of the anterior femoral diaphysis curvature of SWT1/HR-2b and in four comparative samples representing *Homo sapiens*, *Pan troglodytes*, *Gorilla gorilla*, and *Pongo pygmaeus*. Abbreviations: dist. = distal; post = posterior; PC1 = principal component 1; PC2 = principal component 2. (For interpretation of the references to color in this figure, the reader is referred to the Web version of this article).

femora assigned to early *Homo*, as well as the c. 6.0 Ma *Orrorin tugenensis* (BAR 1000′2) femur (Macchiarelli et al., 2020; Daver et al., 2022), while the c. 3.67 Ma StW 573m femur, attributed to *Australopithecus prometheus*, falls closest to chimpanzee femora in its curvature (Daver et al., 2022). The seemingly indiscriminate nature of these combined results leads us to conclude that more study is required to assess the functional, taxonomic, and phylogenetic usefulness of femoral anteroposterior curvature in paleoanthropology.

The knee Primates can have varus or, to varying degrees, valgus knee joints. As to the latter, bicondylar angulation of the femur appears to develop over the regular course of ontogeny in response to the mechanical stresses of bipedalism (e.g., Tardieu and Trinkaus, 1994; Shefelbine et al., 2002). Specifically, in a varus knee that is still developing, increasing bipedality places disproportionate compressive force on the femur's medial, rather than on its lateral, condyle; the metaphysis of the medial condyle responds accordingly and grows at a faster rate than does that of the lateral condyle (e.g., Tardieu, 1999; Preuschoft and Tardieu, 1996; Shefelbine et al., 2002; Tardieu et al., 2006). Thus, it is unsurprising that the knees of fully bipedal, modern human adults show relatively high bicondylar angles (e.g., a meta-analysis of 3225 individuals from 20 pooled-sex, protohistoric, historic, and recent global modern human populations calculated a mean angle of 9.4° [Hunt et al., 2021]). In comparison, modern human infants and most quadrupedal nonhuman primates show no or extremely low bicondylar angles. In this context, it is informative that the mean bicondylar angle of the femora of four (pooled-sex) dry-habitat chimpanzees from Semliki (Uganda), where the animals engage in frequent bipedal postures and locomotion, is 4.2° (standard deviation [SD] = 2.2) (Hunt et al., 2021). That value is intermediate to the bicondylar angle means of less frequently bipedal forest chimpanzees and of modern humans (Hunt et al., 2021). For fossil comparisons, measurable australopith knees ($n = 6$: Sts 34 and TM 1513 from Sterkfontein; U.W. 88-63 from Malapa; AL 129-1a, AL 333-4, and AL 333-140 from Hadar, Ethiopia) show a mean bicondylar angle of 11.4°, which is not statistically significantly different from the mean (pooled-sex) value of 10.9° for 76 modern humans (Hunt et al., 2021).

In this context, the 17.8° at which the SWT1/HR-2 distal femur and proximal tibia articulate is remarkably angled (Fig. 9). Based on studies of modern humans, such a hypervalgus knee is predicted to develop in bipedal individuals who possess short femora and/or relatively expansive biacetabular widths (e.g., Purkait and Chandra, 2004; Moffett, 2017). This prediction is, of course, harmonious with the observation that the SWT1/HR-2b femur is both extremely short and highly valgus. In turn, given that femoral obliquity and lateral condyle ellipticity are developmentally positively correlated in bipedal primates (Tardieu et al., 2006), the very low ratio between the height and length of the lateral condyle of SWT1/HR-2b (Table 4) was also expected. At 0.55, the SWT1/HR-2b index falls within the range of ratios (0.47–0.56) derived for the femora of 40 adult modern humans ($\bar{x} = 0.51$) and well outside the range of ratios (0.63–0.83) for the femora of 12 newborn modern humans ($\bar{x} = 0.72$) (Tardieu et al., 2006). Working from a 'two-pillar' model of the femoral diaphysis/distal metaphysis, Tardieu et al. (2006: 499) have suggested that this intrafemoral geometric relationship is "necessary to provide mediolateral and anteroposterior stability of the two femoral condyles on the two tibial condyles, under the influence of an increased practice of full-knee extension during childhood walking" and that the "increasing depth of the lateral pillar would contribute to the increasing radius of curvature of the lateral condyle in the femoro-tibial contact area, corresponding to full extension of the joint."

The extent to which genetics contributes to the development of the human bicondylar angle is still unresolved. As suggested in the preceding discussion, weight-bearing is a necessary requirement for the onset of modern human femoral obliquity (e.g., Tardieu,

1999), but other types of obligate bipedal vertebrates—bearing their own body weights—do not appear to develop valgus knees over the courses of their lifetimes (e.g., Tardieu et al., 2006). Thus, Tardieu and Trinkaus (1994) suggest that this human characteristic is currently best described as an 'epigenetic functional feature.'

Less ambiguous in the modern context are the significantly 'elevated' (i.e., anteriorly projecting) lateral patellar lips of human femora. This condition is present in the femora of modern human fetuses (e.g., Tardieu et al., 2006; Lovejoy, 2007), implying strongly that it is a bipedal adaptation to resisting lateral dislocation of the patella under load during stance phase (e.g., Heiple and Lovejoy, 1971; Tardieu, 1981). We infer the same reason for the presence of an extremely projecting lateral patellar lip on the SWT1/HR-2b femur. Among extant and extinct hominins, only the MH2 *A. sediba* femur shows a (slightly) higher lateral patellar lip (lateral trochlear groove angle = 31.3°) (DeSilva et al., 2013) than does that of SWT1/HR-2b (lateral trochlear groove angle = 30.0°). In this way, both fossil femora fall well above the means and outside the ranges of variation observed in lateral patellar lip height of other australopith, early *Homo*, and modern human femora (DeSilva et al., 2013).

However, unlike MH2, the high lateral patellar lipping of SWT1/HR-2b might also be, in part, related to a general anterior extension of its patellar surface. As indicated in Figure 10, in terms of patellar surface expanse, SWT1/HR-2b groups with femora of early *Homo* and stands apart from those of other australopiths. Overall anterior extension of the patellar area relates functionally to a greater mechanical advantage at the quadriceps femoris by increasing that muscle's moment arm, which characterizes the genus *Homo* and which is unlike those reconstructed for previously studied australopiths (e.g., Lovejoy, 2007; DeSilva et al., 2013).

In addition, SWT1/HR-2b displays other anatomical indications of a modern humanlike, 'tibial dominant' knee (sensu Lovejoy, 2007). Such knees lack complete patellofemoral congruity when in extreme flexion, and are, importantly, indicative of a hominin's inferred ability for terrestrial bipedal gait that incorporates/incorporated full knee extension (Lovejoy, 2007). First, as discussed earlier, the lateral condyle of SWT1/HR-2b is elliptical in lateral view. More specifically, the portion of it that contacts with the tibial lateral condyle is also elliptical, yielding a vertical-to-horizontal tangent lengths ratio of 47.7, as compared to means of 47.5 for 15 modern (bipedal) human lateral condyles (range = 41–53, SD = 3.9) and 65.9 for 15 modern (quadrupedal) chimpanzee lateral condyles (range = 55–82, SD = 8.2) (Lovejoy, 2007). Moreover, the inferior aspect of the medial condyle of SWT1/HR-2b is similar to those of some other South African australopith distal femora, such as the Sterkfontein fossils Sts 34, TM 1513, StW 573m and StW 573n, and StW 619. Each of these medial condyles has a mediolaterally narrow and anteroposteriorly elongated elevation along the length of its lateral edge (Heaton et al., 2019; Pickering et al., 2021). This morphology does not correspond precisely to that of the inferior aspects of the medial condyles of modern human femora, which, instead, typically present as more uniformly convex 'medial condylar bosses' (sensu Lovejoy, 2007). However, it is still closer to the bipedal form than to that of, for instance, the flat inferior aspects of medial condyles of quadrupedal chimpanzees. Second, SWT1/HR-2b also possesses a deep and capacious sustrochlear hollow, which would have received the patella at full knee extension during terrestrial walking (Tardieu, 2010).

In addition, as mentioned earlier, and as can be inferred from the robust iliotibial tract attachment site on the SWT1/HR-2c tibia, the

Figure 9. Articulation of the SWT1/HR-2b hominin femur (top) and SWT1/HR-2c hominin tibia (bottom) in anterior view (superior up). (For interpretation of the references to color in this figure, the reader is referred to the Web version of this article).

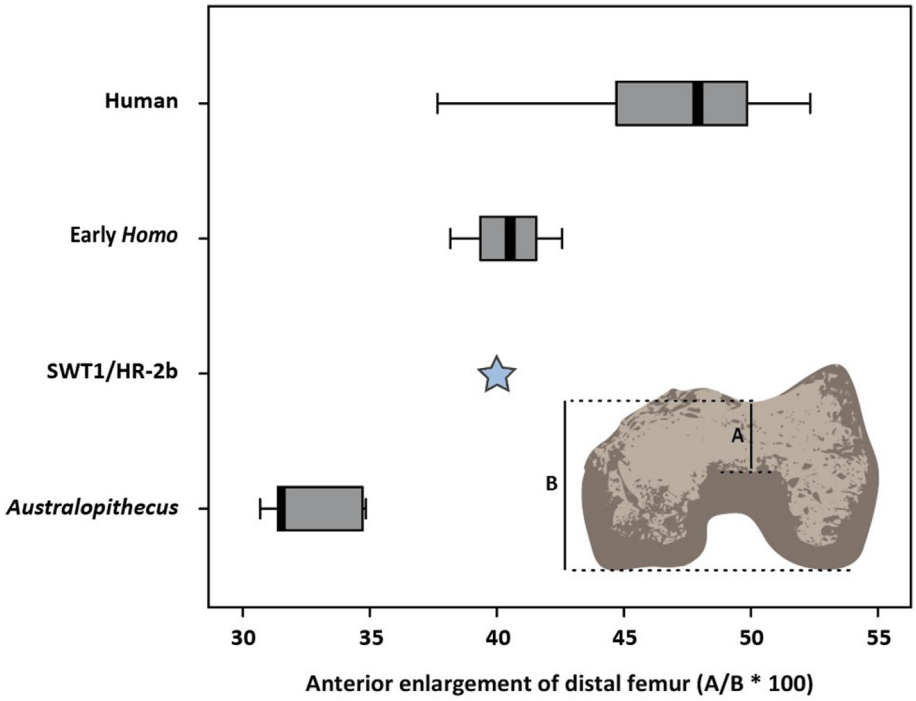

Figure 10. Comparison of the relative area of the patellar surface of the distal femur of *Australopithecus* spp. (A.L. 129-1, A.L. 333-4, A.L. 333w-56, Sts 34, TM 1513, MH2), early *Homo* (KNM-ER 1472, KNM-ER 1481, KNM-WT 15000), modern *Homo sapiens*, and SWT1/HR-2b (*Paranthropus robustus*). *Homo* spp. and *P. robustus* distal femora are distinct from measured *Australopithecus* distal femora in showing general anteriorward extension of the patellar surface, a condition that implies a greater mechanical advantage of the quadriceps femoris muscles. For SWT1/HR-2b: A = 12.0 mm; B = 30.0 mm. Comparative data and figure modified from DeSilva et al. (2013: Fig. S8). (For interpretation of the references to color in this figure, the reader is referred to the Web version of this article).

bipedal (hip and) knee of the SWT1/HR-2 hominin was further stabilized laterally by a well-developed iliotibial tract. Add to these observations the expansive femoral and tibial attachments for its medial and fibular collateral ligaments, and we infer that the SWT1/HR-2 hominin possessed a strongly reinforced bipedal knee joint.

As to the proximal portion of SWT1/HR-2c more generally, it also shows other morphological indications of belonging to a habitual terrestrial biped. On the grossest level, the proximal tibial metaphysis is expanded, especially in the mediolateral plane. Kunos and Latimer (2000) argued that enlargement of tibial metaphyses likely serves to increase trabecular bone volume, which would, theoretically, diffuse high peak loads transferred across the knee joint and associated with bipedal heel strike. Equally obvious, the tibial condyles of the fossil articulate conformably with the femoral condyles of SWT1/HR-2b, an element, which, as discussed earlier, reflects a 'tibial dominant,' modern humanlike knee—one with increased tibial cartilage contact and capable of full extension during normal bipedal gait.

Although the absence of evidence is not the evidence of absence, it is still the case that nothing about the external morphology of its proximal tibia indicates the SWT1/HR-2 hominin squatted habitually. Squatting hyperflexes the knee, which simultaneously compresses the femoral condyles into the superoposterior tibia as it also draws the patellar ligament to the superoanterior tibia; regular assumption of such repose results, in turn, in the dorsal inclination of the tibial plateau (Huard and Montagné, 1950). Angle of tibial retroversion in nonhabitually squatting modern human populations is not known to exceed about 11°, whereas habitually squatting populations range in inclination between 14° and 17° (e.g., Wood, 1920; Trinkaus, 1975; Boulle, 2001). At 12.7°, the angle

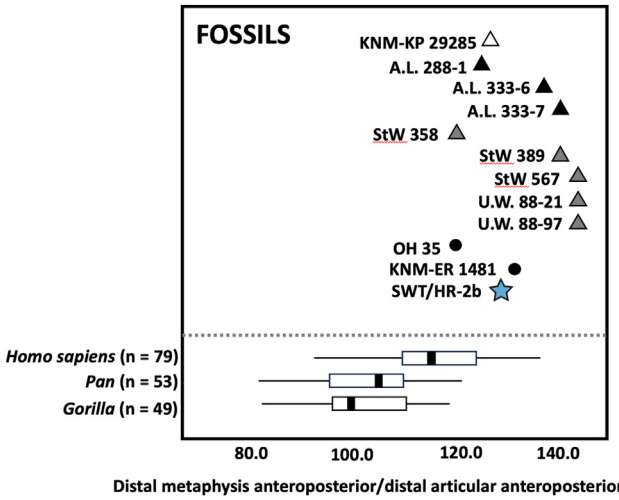

Figure 11. 'Inflation' of the tibia distal metaphysis relative to the distal articular surface anteroposterior diameter. Like the tibiae of all hominins, the SWT1/HR-2c tibia distal metaphysis is relatively expanded, a condition that might be related to strain dissipation during bipedalism (e.g., Zipfel et al., 2011). Catalog numbers of individual fossils appear next to the following symbols: open triangle = *Australopithecus anamensis*; black triangle = *Australopithecus afarensis*; gray triangle = South African *Australopithecus*; black circle = presumptive early *Homo*; blue star = *Paranthropus robustus*. All data from Zipfel et al. (2011), except for SWT1/HR-2c (this study), which equals 128.6; means indicated by dark lines, interquartile ranges by boxes, and range by whiskers. Figure modified from Zipfel et al. (2011, Fig. S1). (For interpretation of the references to color in this figure legend, the reader is referred to the Web version of this article.)

of SWT1/HR-2c's tibial retroversion is intermediate between the upper end of the range for nonhabitually squatting modern humans and the lower end of the range for habitually squatting modern humans. This result may imply that the SWT1/HR-2 hominin engaged in some amount of squatting but probably less than what is practiced by habitually squatting modern humans. That inference is not inconsistent with the lack of squatting facets on SWT1/HR-2c, as habitually squatting humans sometimes show the combination of relatively steeply dorsally inclined proximal tibiae and faceted distal tibiae (sometimes along with other features, such as Poirier's facets and Martin's facets on their femora) (e.g., Trinkaus, 1975).

In summary, all observations of the SWT1/HR-2 knee converge to conclude that it was an extremely stable joint. In this way, the SWT1/HR-2 knee is different from reconstructions of some other australopith knees, which are inferred to have been more mobile than are modern human knees (e.g., Berger and Tobias, 1996; DeSilva et al., 2013).

The crus The diaphysis of the SWT1/HR-2c tibia is remarkably eurycnemic, with a cnemic index of 90.2 and a midshaft index of 81.6. The latter value is well above the same index means for the tibiae of extant chimpanzees (68.3 ± 6.4), gorillas (75.2 ± 6.1), and humans (73.4 ± 6.1), and it is just barely contained within the range of values for gorillas (68.3–82.9, $n = 6$) and humans (64.3–86.9, $n = 23$), as well as for KNM-ER 741, KNM-ER 803b, KNM-WT 15000, and D3901, four purported early *Homo* tibiae from, Lake Turkana, Kenya (KNM-ER numbers), and Dmanisi, Georgia ($\bar{x} = 76.2 \pm 9.3$, range = 66.7–85.0) (Marchi et al., 2017). Compared to a platycnemic tibia, a eurycnemic tibia—with its hollow, triangular cross section and rounded corners (Lovejoy et al., 1976)—is better adapted to resist *both* bending *and* torsion strains from arbitrary directions (e.g., Frankel and Burstein, 1965).

SWT1/HR-2c's triangular diaphyseal form continues to its distal extent, where the fossil is thus slightly 'inflated' anteroposteriorly (Fig. 11). Carlson et al. (2020; see also Zipfel et al., 2011) argue that such geometry expands cortical and trabecular volume in the distal tibia, by which weight-bearing bipedal loads in that region are more efficiently dissipated. Indeed, such morphology also characterizes modern human and other australopith distal tibiae known/inferred to derive from terrestrial bipeds (e.g., Ward et al., 2001; Zipfel et al., 2011; Carlson et al., 2020).

Lastly, judging from the combined appearance of the SWT1/HR-2 fossil-set's preserved attachment sites for the triceps surae, the shank of the hominin was well adapted to resist torsional strain and to contribute significantly to the individual's bipedal propulsive abilities (see Myatt et al., 2011). Although the lateral supracondylar line of the femur (origin for the plantaris) is poorly expressed, the femoral-condylar origins for the two heads of the gastrocnemius are robust, as is the origin for the soleus, on the SWT1/HR-2c tibial diaphysis.

Overall, the tibial diaphysis of the SWT1/HR-2 hominin shows morphology that is consistent with that of its hip, thigh, and knee. Together, these parts of the lower limb indicate that SWT1/HR-2 was well adapted to terrestrial bipedalism, possessing stable joints and powerful muscles, presumably contributing to two-legged locomotor stabilization, flexion, extension, and propulsion.

The ankle The external morphology of the distal epiphysis of the SWT1/HR-2c tibia is, in several ways, like that of modern human tibiae. For instance, in the coronal plane, the ankle joint is directed nearly perpendicular relative to the tibial long axis, with a tibial angle of 85.9°. The perpendicularly directed ankle joints of modern humans minimize potentially damaging shear stress in the articular cartilage and are also reflective of the sagittal plane of motion of the lower limb during normal, terrestrial bipedal gait (Latimer et al., 1987). A perpendicularly directed ankle joint is thus a hallmark of modern human bipedalism (modern human tibial angle $\bar{x} = 91.1 \pm 2.4$, $n = 29$ [DeSilva, 2009]) and is also common to nearly all known early hominin distal tibiae (e.g., mean of four Sterkfontein Member 4 tibiae = 93.3 ± 2.2 [DeSilva, 2009]) (e.g., Latimer et al., 1987; Ward et al., 1999; DeSilva, 2009; Zipfel et al., 2011) (Fig. 12). Similarly, at 2.08°, the tibial arch angle (i.e., the angle that the plafond forms with the tibial diaphysis in the sagittal plane [DeSilva and Throckmorton, 2010]) of SWT1/HR-2c is modern humanlike and possibly indicates that the SWT1/HR-2 hominin possessed a rearfoot arch during life (Fig. 13). Rearfoot arching is not a necessary feature to be a primate habitual terrestrial biped; in fact, some modern humans possess perfectly functional, pain-free feet that lack longitudinal arches (e.g., Harris, 2010). However, the possible presence of longitudinal arches in the feet of the SWT1/HR-2 hominin is indicative that the individual, and its species, practiced an advanced form of terrestrial bipedalism, which included (at least in some individuals) a gait pattern that was characterized by the shock-absorbing and elastic-energy-creating benefits of a longitudinal arch (e.g., Ker et al., 1987).

In inferior view, the talar facet of SWT1/HR-2c is square shaped (maximum anteroposterior depth of the distal tibia/maximum mediolateral width of the distal tibia * 100 = 101.4), which is a modern humanlike form, and is distinct from the trapezoidal shape of the talar facets of extant African apes (e.g., DeSilva, 2009). It has been suggested that a square-shaped talar facet might be a bipedal adaptation for "more uniform distribution of forces across the joint surface and to maintain joint congruence throughout the range of [bipedal] motion" (DeSilva, 2009: 6568). More recently, DeSilva's (2009) study was reproduced but with an expanded comparative

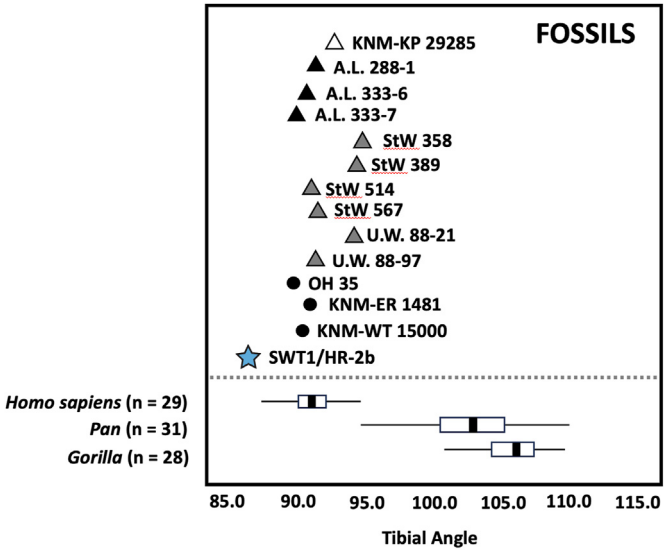

Figure 12. Angle (°) of the tibial plafond in the coronal plane relative to the tibial diaphysis (the 'tibial angle'). At 85.9°, the tibial angle of the SWT1/HR-2c tibia is slightly outside the normal range of variation of other hominin tibial angles. However, in the modern human clinical context, valgus deformity of the ankle is diagnosed at an angle of <85.0° (Kaya and Doral, 2012). In that sense, the ankle of the SWT1/HR-2 hominin should still be considered relatively perpendicularly directed, a condition that brings the ankles directly under the center of gravity during terrestrial bipedal orthogrady. Catalog numbers of individual fossils appear next to the following symbols: open triangle = *Australopithecus anamensis*; black triangle = *Australopithecus afarensis*; gray triangle = South African *Australopithecus*; black circle = presumptive early *Homo*; blue star = *Paranthropus robustus*. All data from Zipfel et al. (2011), except for SWT1/HR-2c (this study); means indicated by dark lines, interquartile range by boxes, and range by whiskers. Figure modified from Zipfel et al. (2011, Fig. S2). (For interpretation of the references to color in this figure legend, the reader is referred to the Web version of this article.)

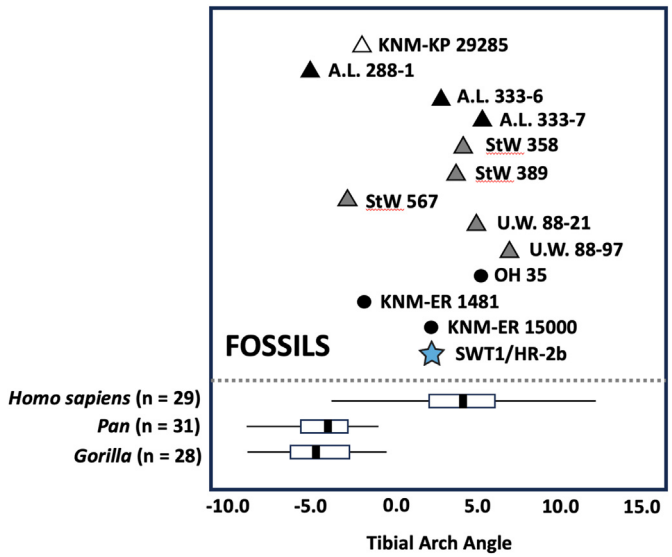

Figure 13. Angle (°) of the tibial plafond in the sagittal plane relative to the tibial diaphysis (the 'tibial arch angle'). It is suggested that tibiae with a more positive set, such as SWT1/HR-2c (2.08°), may reflect the in vivo presence of a rearfoot arch. Catalog numbers of individual fossils appear next to the following symbols: open triangle = *Australopithecus anamensis*; black triangle = *Australopithecus afarensis*; gray triangle = South African *Australopithecus*; black circle = presumptive early *Homo*; blue star = *Paranthropus robustus*. All data from Zipfel et al. (2011), except for SWT1/HR-2c (this study); means indicated by dark lines, interquartile range by boxes, and range by whiskers. Figure modified from Zipfel et al. (2011, Fig. S3). (For interpretation of the references to color in this figure legend, the reader is referred to the Web version of this article.)

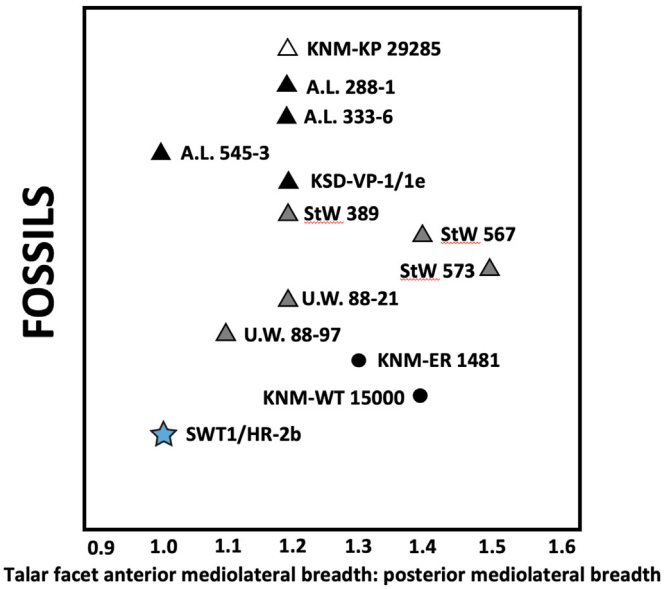

Figure 14. Ratio of the anterior mediolateral and posterior mediolateral breadths of the talar facet of the distal tibia. The relatively low value of SWT1/HR-2c (1.0) might suggest a high degree of ankle joint stability under terrestrial bipedal load. Catalog numbers of individual fossils appear next to the following symbols: open triangle = *Australopithecus anamensis*; black triangle = *Australopithecus afarensis*; gray triangle = South African *Australopithecus*; black circle = presumptive early *Homo*; blue star = *Paranthropus robustus*. Values calculated from data in Carlson et al. (2020: 232–233, Tables 13.1 and 13.2), except for that of SWT1/HR-2c (this study). (For interpretation of the references to color in this figure legend, the reader is referred to the Web version of this article.)

dataset that included the tibiae of mountain gorillas (*Gorilla beringei beringei*). Even though that subspecies does not climb an appreciable amount, the shape of its talar facet is similar to those of all extant, nonhuman African apes. This finding led Carlson et al. (2020) to propose that a relatively expanded anterior margin of the talar facet may not be an indicator of vertical climbing but, instead, might reflect habitual ankle dorsiflexion during the overall positional repertoire. In this view, SWT1/HR-2c's relatively low talar facet anterior mediolateral breath/posterior mediolateral breadth ratio of 1.0 seems to suggest less habitual ankle dorsiflexion and more modern humanlike ankle position in that hominin (Fig. 14). Moreover, Crompton et al. (2021: 263) conjectured that a relatively mediolaterally broader anterior margin of the talar facet "might have given relatively free medial-lateral deviation of the foot on the crus, which would serve arboreal bipedalism better than terrestrial." If the opposite holds true, then its ratio of 1.0 suggests that the SWT1/HR-2 hominin possessed a relatively bipedally stable ankle, allowing for only minimal transverse excursion of the foot.

More relevant to further assessment of SWT1/HR-2's locomotor patterns is the nature of the protuberances and other cortical rugosities that surround its tibial plafond. For instance, the medial malleolus of SWT1/HR-2c is thin mediolaterally, like those of modern human and most other early hominin tibiae (Fig. 15). In contrast, extant nonhuman ape tibiae have medial malleoli that are thick mediolaterally, presumably as a climbing adaptation that protects that bone's distomedial region against shear incurred arboreally. Dorsal to the medial malleolus, the malleolar groove of the STW1/HR-2c tibia is well defined and mediolaterally expansive, suggesting well-developed tendons of the tibialis posterior and flexor digitorium longus, which pass through that sulcus. Both of those muscles contribute to bipedal plantarflexion and foot inversion (the latter important for opposing excessive eversion and thus avoiding valgus deformity in the bipedal foot [Durrant et al., 2011]), and the former is also a contributor to the medial aspect of the pedal longitudinal arch. As discussed earlier, the tibial arch angle of SWT1/HR-2c is also suggestive of the original presence of a longitudinal arch. In addition, the tibial attachment sites for SWT1/HR-2's tibiofibular ligaments are prominent: strong, tightly bound tibiofibular ligaments are important for ankle joint stability.

In summary, the ankle morphology of SWT1/HR-2c, with its nearly perpendicularly directed joint, square-shaped talar facet, thin medial malleolus, and rugged circum-plafond morphology, indicates that the SWT1/HR-2 hominin was adapted to terrestrial bipedalism and thus comports with that of other anatomical segments discussed earlier. Furthermore, it lacks external osteological indications (e.g., squatting facets) of the extreme dorsiflexion capabilities, characteristic of the types and/or frequency of climbing engaged in by nonhuman apes (see e.g., Carlson et al., 2020).

3.5. Taxonomic assignment of the SWT1/HR-2 fossils

Without controversy, the total hominin craniodental sample from Swartkrans comprises at least two genera and two species. Although sometimes considered to belong to a separate species of *Paranthropus* (i.e., *Paranthropus crassidens*) (e.g., Broom, 1949; Howell, 1978; Grine, 1982, 1984, 1985), it is now generally agreed that the bulk of hominin skull and tooth specimens from the site should be placed in the species *P. robustus* (e.g., Tobias, 1967; Fuller, 1996; Keyser et al., 2000; Kaszycka, 2002). The remaining fossils are usually allocated to *H. ergaster* (originally referred to as *Telanthropus capensis* and now sometimes referred to as African *Homo erectus*) and are represented by some well-known specimens, such as SK 45 and SK 847 (Broom and Robinson, 1950; Clarke et al., 1970; Clarke and Howell, 1972; Clarke, 1977a, 1994). In addition to these fairly agreed-upon taxa, Clarke (2012, 2017) has argued that SK 27, a

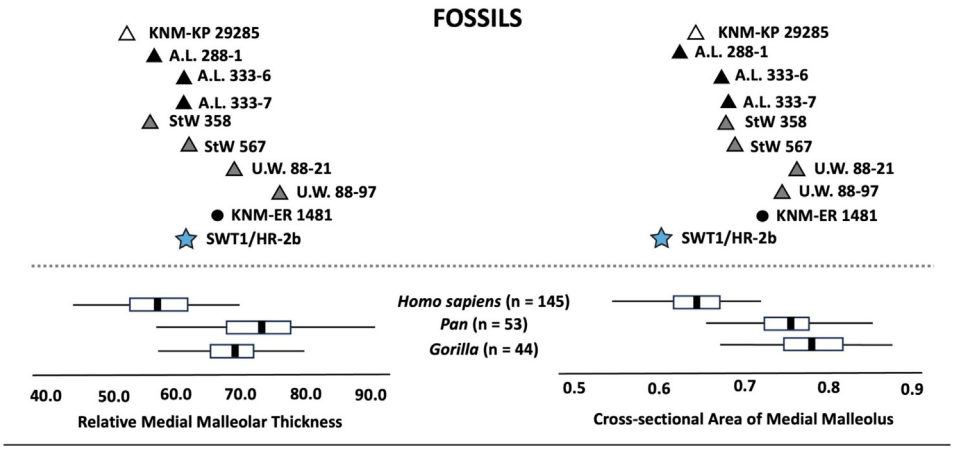

Figure 15. Relative size of the tibia medial malleolus: (malleolus maximum mediolateral thickness/maximum anteroposterior length) * 100 (left); cross-sectional area of the malleolus = (malleolus mediolateral width * anteroposterior length)/(talar facet midpoint anteroposterior width * midpoint mediolateral width) (right). *Pan troglodytes* and *Gorilla gorilla* tibiae have thick malleoli, probably to protect the ankle against shear when it is loaded while inverted, as occurs commonly during climbing (Zipfel et al., 2011). More terrestrial extant hominoids have thinner malleoli; the same is inferred for extinct species, such as *Paranthropus robustus*, represented prominently by SWT1/HR-2c (A = 61.2; B = 0.60). Catalog numbers of individual fossils appear next to the following symbols: open triangle = *Australopithecus anamensis*; black triangle = *Australopithecus afarensis*; gray triangle = South African *Australopithecus*; black circle = presumptive early *Homo*; blue star = *Paranthropus robustus*. All data from Zipfel et al. (2011), except for SWT1/HR-2c (this study), which equals 128.6; means indicated by dark lines, interquartile range by boxes, and range by whiskers. Figure modified from Zipfel et al. (2011, Fig. S6). (For interpretation of the references to color in this figure legend, the reader is referred to the Web version of this article.)

juvenile cranium, variously assigned to *P. crassidens* (e.g., Broom and Robinson, 1952) and *Homo* sp. (Clarke, 1977b), should now be placed in the species *Homo habilis*. Lastly, the SK 15 mandible was originally classified as *T. capensis* (Broom and Robinson, 1949) and then as *H. erectus* (Robinson, 1961), but now, based on detailed comparisons and logic, Clarke (2017) argues it could quite possibly belong to a more recently occurring *Australopithecus africanus* (see also Zanolli et al., 2022).

Of the three skeletal elements that SWT1/HR-2 comprises, it is the femur on which we base our taxonomic allocation of the fossil-set to *P. robustus* (see justification mentioned earlier, subsection 2.2). There is readily discernible variation in the sample of African Late Pliocene and Early Pleistocene hominin femora (e.g., Robinson, 1972; Stern and Susman, 1983; Reed et al., 1993; McHenry, 1994; Partridge et al., 2003; Harmon, 2009a,b; Pickering et al., 2021). However, it is still fair to conclude that *within* the subsample of australopiths, "interspecific femoral variation is low and australopiths are generally morphologically similar" (Harmon, 2009a: 155). Consequently, as enumerated early by Walker (1973), it is possible to differentiate *Australopithecus* and *Paranthropus* femora from those of *Homo* with a high degree of confidence, in that the former group shares relatively smaller heads and proportionally longer and anteroposteriorly compressed necks than is seen in the latter taxon (see also Napier, 1964; Robinson, 1972; Lovejoy and Heiple, 1972; Lovejoy et al., 1973, 2002; Lovejoy, 1975; McHenry and Corruccini, 1978; Jungers, 1988; Harmon, 2009a; Ruff and Higgins, 2013). As described earlier, SWT1/HR-2b conforms to the stereotypical australopith proximal femur morphology. It further, though, distinguishes itself from some other australopith femora—such as those of East African *Australopithecus afarensis*—and, instead, aligns with those of purported *Paranthropus* in its very low neck-shaft angle of 113.0°. Harmon (2009b) argued that South African *Australopithecus* femora display even lower neck-shaft angles than do *Paranthropus* femora, but she based this conclusion largely on the measurements of the proximal femora MLD 46 (Makapansgat) and StW 99 (Sterkfontein). MLD 46 is purportedly an *A. africanus* fossil and has a neck-shaft angle of 120° (Reed et al., 1993). However, in comparative context, this angle is actually not exceptionally low. The mean angle for a large sample of 100 modern human femora is 124.4° ± 3.8 (range = 114.0°–132.0°), and a pooled sample of 14 *Australopithecus* and *Paranthropus* proximal femora has a mean angle of 120.3° ± 5.6 (range = 112.5°–134.0°) (Marchi et al., 2017). As for StW 99, Pickering et al. (2021; see also Partridge et al., 2003) highlighted its morphological similarities with purported *P. robustus* femora from Swartkrans (SK 82, SK 97, SWT1/LB-2). Moreover, StW 99 likely derives from a portion of the Member 5 unit of the Sterkfontein Formation that has yielded other *P. robustus* fossils (Kuman and Clarke, 2000). Together, these observations indicate that this specimen is probably best removed from *A. africanus* and reallocated to *P. robustus* (Partridge et al., 2003; Pickering et al., 2021). In addition, the geological age of SWT1/HR-2 (see above) falls within the previously established temporal range of *P. robustus* (2.22 ± 0.09–0.96 ± 0.09 Ma [Gibbon et al., 2014; Kuman et al., 2021]).

We are currently conducting detailed studies of the cortical and trabecular architectures of the SWT1/HR-2 skeletal elements. However, we provide some preliminary results of those studies here. This is because analyses of internal bone morphology have proved useful in taxonomic assessments of other isolated hominin femora (e.g., Lovejoy et al., 2002; Ruff and Higgins, 2013; Ryan et al., 2018; Cazenave et al., 2019; Pina et al., 2019; Georgiou et al., 2020; Cazenave and Kivell, 2023; but see, Haeusler et al., 2020).

For instance, the ratio of cortical thicknesses in the superior and inferior portions of the femoral neck, as well as the relative superoinferior cortical elongation of the neck base, seem to differentiate the femora of *Homo*, *Australopithecus*, and *Paranthropus* (Ohman et al., 1997; Ruff and Higgins, 2013; Ruff et al., 2016; Cazenave et al., 2019, 2023). Thus, it is unfortunate that the neck of SWT1/HR-2b suffered so much postdepositional damage, disallowing usable observations of cortical bone thickness at its superior extent. Nonetheless, it is intriguing that the cortex of SWT1/HR-2b's neck is relatively thick inferiorly and then thins posteriorly (Fig. 16). This cortical bone distribution pattern is also observed in the necks of StW 479 and StW 522 (Ruff and Higgins, 2013), Sterkfontein femora that are typically assigned to *A. africanus*. In addition, SWT1/HR-2b also resembles StW 522 in that the necks of both femora terminate inferiorly in rather 'sharp' angles—a shape that, it must be emphasized, also characterizes the

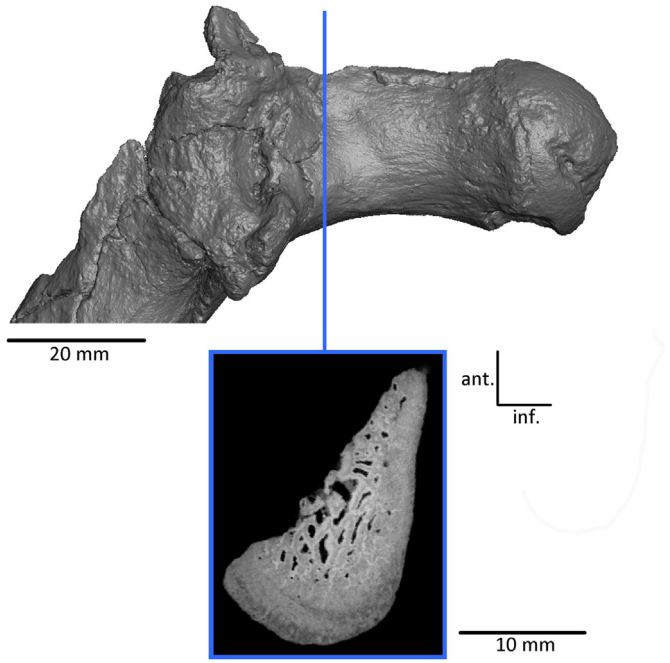

Figure 16. MicroXCT cross section extracted at the base of the SWT1/HR-2b femoral neck (shown in posterior view; superior up, medial to the right), perpendicular to the main neck axis, and showing a thick inferior cortex (6.24 mm) that thins posteriorly but that is missing the anterior and superior aspects. Abbreviations: ant. = anterior; inf. = inferior. (For interpretation of the references to color in this figure, the reader is referred to the Web version of this article).

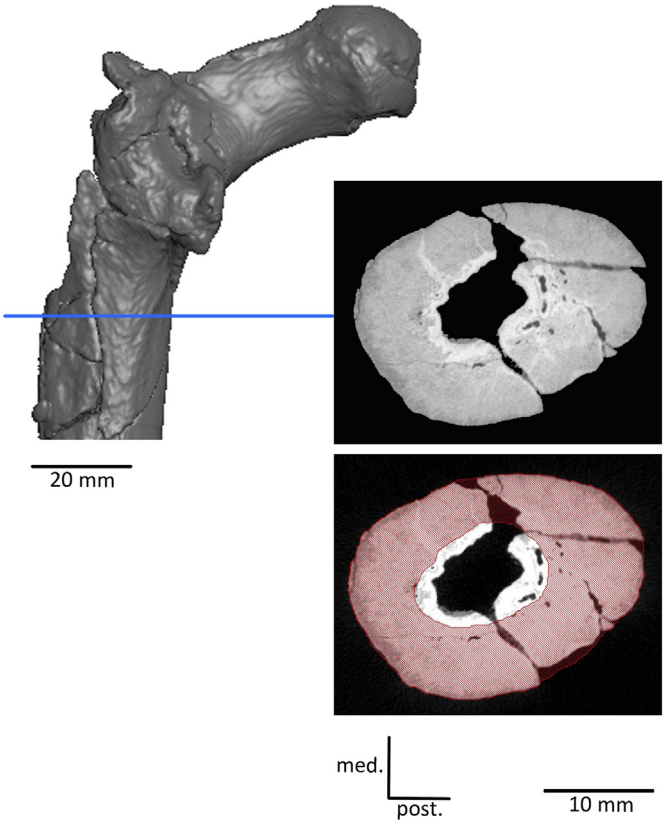

Figure 17. MicroXCT transverse cross section extracted at 1.3 cm inferior to the lesser trochanter of the femur SWT1/HR-2b (shown in posterior view; superior up, medial to the right), showing a cortical bone area (outlined in red in the lower cross section) of 322 mm^2, which is 80% of the total periosteal area of the diaphysis at that position. Among measured hominin femoral diaphyses, this cortical bone proportionality matches most closely those of *Paranthropus* spp. than of other australopiths. Abbreviations: med. = medial; post. = posterior. (For interpretation of the references to color in this figure legend, the reader is referred to the Web version of this article).

Swartkrans presumptive *P. robustus* fossils, SK 87 and SK 92. Lastly, the maximum inferior cortical thickness of SWT1/HR-2b's neck (6.24 mm) falls closer to the mean maximum inferior cortical neck thickness of presumptive *A. africanus* femora (4.73 mm for StW 479 and StW 522) than to that of presumptive *P. robustus* femora (3.46 mm for SK 82 and SK 97) (Ruff and Higgins, 2013; Cazenave et al., 2019). That said, we note that the range of *P. robustus* inferior cortical neck thicknesses is probably quite broad; its high end is pinned currently by the StW 99 femur (see aforementioned discussion and its associated references for justification of this fossil's assignment to *P. robustus*), at 8.20 mm, and thus easily accommodates SWT1/HR-2b.

Moreover, the area of cortical bone inferior to the lesser trochanter of SWT1/HR-2b comprises 80% of total periosteal area in the diaphyseal section at ~80% of femoral length (see above, subsection 2.2, for justification of estimated position of this measurement) (Fig. 17). As summarized in Table 7, in this way, SWT1/HR-2b is much closer to the condition of SK 87 and SK 92 (both presumptive *P. robustus*) and OH 80-12 and OH 84 (presumptive *Paranthropus boisei* from Olduvai, Tanzania) femora than to the femora of modern humans and the femur of the East African *A. afarensis* partial skeleton A.L. 288-1.

SWT1/HR-2b is also allied with SK 82, SK 97, and OH 80-12 in that each shows a relatively platymeric diaphysis (Robinson, 1972; Domínguez-Rodrigo et al., 2013) (Table 6), and although various Early Pleistocene presumptive *Homo* spp. femora also show subtrochanteric platymeria (e.g., Day, 1971; Walker and Leakey, 1993), we have already established earlier that SWT1/HR-2b represents, at a minimum, an australopith, and not *Homo*. Sample sizes are exceedingly small, but data in Table 6 suggest that among South African australopiths, *Australopithecus* tended to exhibit a less platymeric femur than did *P. robustus*.

Table 7
Comparison of some cross-sectional geometric properties of hominin femur diaphyses at approximately 80% of their biomechanical lengths.[a]

Presumed taxon	Specimen	TA (mm^2)	CA (mm^2)	%CA
Australopithecus afarensis	A.L. 288-1[b]	332	198	59.5
Paranthropus boisei	OH 80-12[c]	611	524	85.7
	OH 84[d]	625	545	87.2
Paranthropus robustus	StW 99[e]	634	552	86.9
	SK 82[f]	577	490	84.9
	SK 97[f]	593	457	77.1
	SWT/HR-2b[g]	**403**	**322**	**80.0**
Homo sapiens[h]	$n = 12$	655 (108)	444 (78)	67.8 (9.5)

[a] Abbreviations: TA = total periosteal area; CA = cortical area; %CA = [(CA/TA) * 100]; SD = standard deviation.
[b] Ruff et al. (2016).
[c] Domínguez-Rodrigo et al. (2013).
[d] Aramendi et al. (2024).
[e] Ruff et al. (2020); see discussion in text and in Partridge et al. (2003) and Pickering et al. (2021) for justification of taxonomic assignment.
[f] Ruff et al. (1999).
[g] This study.
[h] Puymerail (2012); for columns 3–5, the first value is the mean, followed by the SD in parentheses.

Thus, on balance, a preponderance of data indicates that, of reasonable taxonomic options, SWT1/HR-2b is, at this time, best assigned to *P. robustus*, and given that SWT1/HR-2b was found in

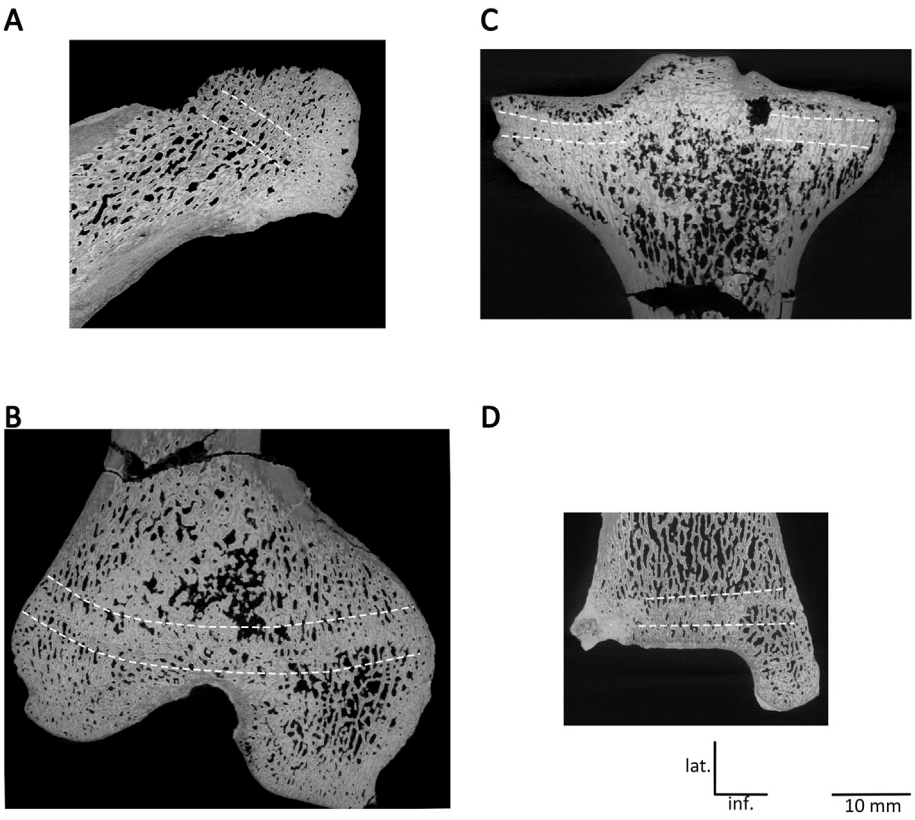

Figure 18. MicroXCT coronal cross sections extracted on the proximal femoral epiphysis (A), the distal femoral epiphysis (B), the proximal tibial epiphysis (C), and the distal tibial epiphysis (D) of the specimens SWT1/HR-2b (femur) and SWT1/HR-2c (tibia), all revealing traces of recently completed epiphyseal fusion (between white dotted lines). These observations indicate that the SWT1/HR-2 hominin was a young adult when it died. Abbreviations: lat. = lateral; inf. = inferior.

intimate spatial and taphonomic association with, and also articulates with, SWT1/HR-2a and SWT1/HR-2c, the whole set of fossils should be assigned currently to this species.

3.6. Developmental age assignment of the SWT1/HR-2 fossils

Selected μXCT coronal cross-sectional slices reveal the inner morphology of the proximal and distal metaphyses and epiphyses of the SWT1/HR-2 femur and tibia (Fig. 18). There is a line of compactly organized trabeculae at the center of the femoral head, perpendicular to the main axis of the femoral neck. We infer that this is a remnant of the femoral proximal epiphyseal plate. Similarly appearing horizontal lines, which course mediolaterally, are also visible in cross sections of the distal femur and distal tibia. Lastly, we identified a faint, horizontal, radio-opaque line in the proximal epiphysis of the tibia, which we interpret as the trace of completed epiphyseal fusion in the proximal tibia (Cameriere et al., 2012; Davies et al., 2013); this epiphyseal scar is positioned in the anterior portion of the medial condyle. On balance, given that epiphyseal scars are present in each of the preserved epiphyses at different degrees of expression, we believe it is most parsimonious to conclude that the SWT1/HR-2 hominin was a young adult at the time of its death. A comprehensive study of modern human limb bones (Davies et al., 2015) demonstrates that (1) not all epiphyses retain scars as adulthood progresses and (2) those that do persist into adulthood rarely span the epiphyses, which, in distinction, is the case for the scars on the distal femur and distal tibia of SWT1/HR-2. These endostructural observations on epiphyseal union agree with those of osteometrics and joint congruities and spatial context and taphonomy to corroborate that the SWT1/HR-2 fossil-set represents a single, young adult hominin individual.

At the same time, compared to modern humans and chimpanzees, these observations of internal bone structure also indicate a unique skeletal developmental schedule for this *P. robustus* individual. For the femur and tibia of modern human individuals, it is the femur proximal epiphysis that first fuses completely (at 12–16 years of age for females and at 14–19 years of age for males), followed by complete fusion of the tibia distal epiphysis (complete fusion at 14–17 years of age for females and 16–18 years of age for males), and then by simultaneous complete fusion of the distal femur and proximal tibia (at 14–18 years of age for females and 16–20 years of age for males) (Cunningham et al., 2016). In wild chimpanzees, the epiphyses of the proximal femur and the proximal and distal tibia fuse simultaneously, with completion at about 12 years of age (e.g., Bolter and Zihlman, 2012). In contrast to those extant hominoids, the SWT1/HR-2 fossil-set indicates a more advanced (i.e., earlier) fusion in the proximal tibia than in the distal tibia and proximal and distal femur.

It is unclear how these results should be evaluated relative to previous research on *P. robustus* ontogeny. For instance, a recent study of the Kromdraai TM 1517 hominin distal humerus, proximal ulna, and hallucal distal phalanx (that are, collectively, associated with teeth and skull portions) indicates that hominin's odonto-postcranial maturational pattern was more like that of an extant African ape than that of a modern human (Cazenave et al., 2020). More specifically, an age seriation of a combined Swartkrans and Drimolen *P. robustus* craniodental sample indicated to its authors

Table 8
Some adult early hominin lower limb bone lengths and crural indices.[a]

Specimen	Geological age (Ma)	Femur (mm)[b]	Tibia (mm)[c]	Total lower limb length (mm)[d]	Crural index[e]	Linear measurements source
ARA-VP-6/500	4.40	(312)	262	(574)	(83.9)	Lovejoy et al. (2009)
StW 573	3.60	335	285	620	85.1	Heaton et al. (2019)
KSD-VP-1/1	3.60	(418)[f]	355	(773)	(84.9)	Haile-Selassie et al. (2010)
A.L. 288-1	3.20	(281)	(241)	(522)	(85.8)	Johanson et al. (1982); Schmid (1983)
MH 1	2.00		266			Berger et al. (2010)
KNM-ER 1472	1.90	401	(340)	(741)	(84.8)	Steudel-Numbers and Tilkens (2004)
KNM-ER 1481	1.90	396	(333)	(729)	(84.1)	Steudel-Numbers and Tilkens (2004)
SWT1/HR-2	**1.80**	**263**	**218**	**481**	**82.9**	**This study**
OH 62	1.80	(280)				Johanson et al. (1987)
Dmanisi 1	1.80	382	306	688	80.1	Lordkipanidze et al. (2007)
KNM-ER 1808	1.60	(485)				Steudel-Numbers and Tilkens (2004)
LB1	0.09	(280)	(235)	(515)	(83.9)	Brown et al. (2004)
U.W. 101-484	0.03		(325)			Garvin et al. (2017)

[a] Values in brackets are estimates.
[b] Bicondylar length (Buikstra and Ubelaker, 1994).
[c] Tibial length (Buikstra and Ubelaker, 1994).
[d] Femoral bicondylar length + tibial length.
[e] Tibial length * 100/bicondylar length (Davenport, 1933).
[f] Lowest published estimate; highest estimate = 438 mm (Haile-Selassie et al., 2010).

that the maturation pattern of the species can be characterized as gorillalike, with bimaturation and extended male growth (Lockwood et al., 2007). Given the relative paucity of detailed osteological developmental data on gorillas, we withhold an opinion on this latter conclusion and its relevance for contextualizing the SWT1/HR-2 maturation results.

3.7. Estimates of the SWT1/HR-2 hominin's lower limb bone lengths and its crural index

The SWT1/HR-2 hominin possesses the shortest femur, tibia, and total lower limb (femoral bicondylar [total] length + tibia

Table 9
Bicondylar length (mm) of the SWT1/HR-2b femur compared to mean bicondylar lengths (mm) of extant hominoid femora.

Specimen or taxon	*n*	Mean	SD	Reference
SWT1/HR-2	**1**	**263.0**		**This study**
Gorilla gorilla	22	342.2	34	Heaton et al. (2019)
Pan troglodytes	70	293.9	15	Heaton et al. (2019)
Pan paniscus	10	297.7		Shea (1984)
Homo sapiens (African small-bodied)	23	376.9	20.4	Jungers et al. (2016)
Homo sapiens (Khoisan)	51	411.7	21	Pearson (1997)
Homo sapiens	548	452.7	32	Heaton et al. (2019)

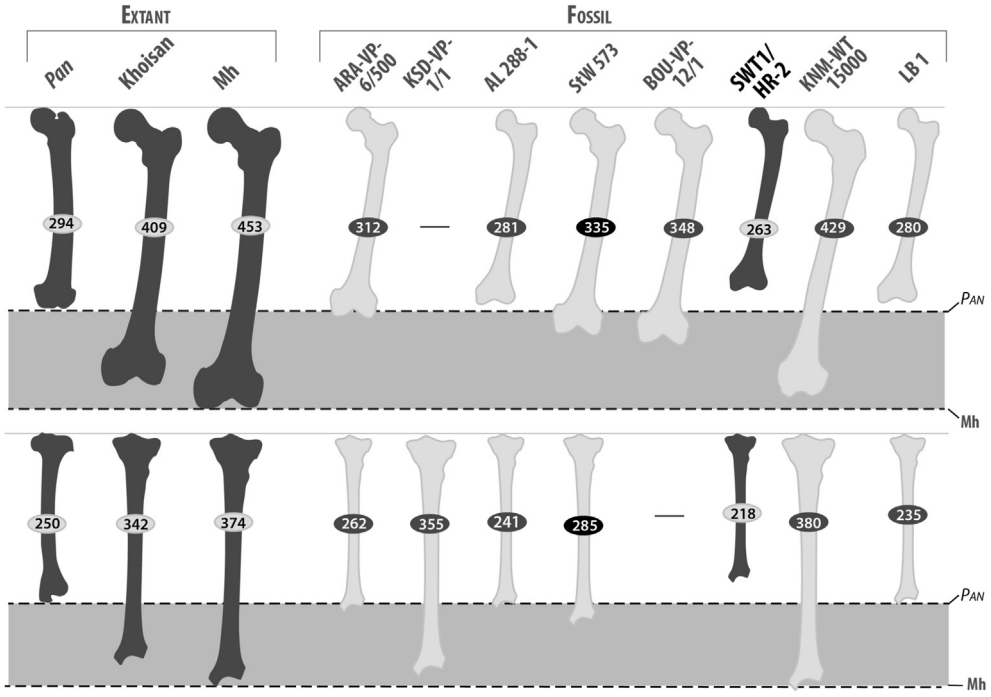

Figure 19. Hominoid comparative femur bicondylar and tibia lengths, presented as means for extant *Pan troglodytes* (*Pan*) (Heaton et al., 2019) and Khoisan (Pearson, 1997) and Western (Mh) *Homo sapiens* (Heaton et al., 2019) and as actual or estimated values for individual fossil specimens. For each element, the shaded horizontal band represents the range between the *Pan* and Mh means. The SWT1/HR-2 femur and tibia are the shortest known adult representatives of those elements in the hominin fossil record and, combined, also represented the shortest, articulated lower limb in that same record. Fossil data: ARA-VP-6/500 (Lovejoy et al., 2009); KSD-VP-1/1 (Haile-Selassie et al., 2010); A.L. 288-1 (Johanson et al., 1982; Schmid, 1983); StW 573 (Heaton et al., 2019); BOU-VP-12/1 (Asfaw et al., 1999); SWT1/HR-2 (this study); KNM-WT 15000 (Pontzer et al., 2010); LB 1 (Brown et al., 2004). Figure adapted from Asfaw et al. (1999) and Heaton et al. (2019).

Table 10
Estimated sizes of some adult small-bodied early hominins.

Specimen	Geological age (Ma)	Mass (kg)	Stature (m)[a]	Body mass index[b]
ARA-VP-6/500	4.40	32.1[c]	1.18	23.1
A.L. 288-1	3.20	26.0[d]	1.10	23.6
SWT1/HR-2	**1.80**	**27.4**	**1.03**	**25.8**
LB1	0.09	27.5[d]	1.09	24.9

[a] Calculated using the formula (0.173 * [femoral bicondylar length (mm) + tibia maximum length (mm)]) + 19.694; r = 0.93, s.e.e. = 2.9 (Baab et al., 2016); see methods section for justification. Femur and tibia lengths: for ARA-VP-6/500 from Lovejoy et al. (2009); for A.L. 288-1 from Johanson et al. (1982) and Schmid (1983); for SWT1/HR-2 from this study; for LB1 from Brown et al. (2004).
[b] Mass/stature^2 (Keys et al., 1972).
[c] Grabowski et al. (2015).
[d] Jungers et al. (2016).

maximum length) of all known adult hominins from 4.4 to c. 0.3 Ma (Table 8; Fig. 19). At 263 mm, the total length of the SWT1/HR-2b femur also falls well below the low end of modern human ranges, including the low end of the range for small-bodied populations and even below the mean values for chimpanzee and bonobo femoral bicondylar length (Table 9). This finding lends support to our decision to estimate the live body mass of SWT1/HR-2 using equations that employ small-bodied modern humans as training models (see below).

The crural index of SWT1/HR-2 is 82.9, which matches exactly the mean crural index of 22 extant gorilla lower limbs (SD = 2.6), as well as those of 548 Western modern human lower limbs (SD = 2.9) (Pontzer et al., 2010; Heaton et al., 2019). This is not surprising. It was confirmed in a recent comparative analysis of the nearly complete lower limb of StW 573 (the 'Little Foot' *A. prometheus* skeleton) (Heaton et al., 2019) that, in terms of mean and variation, the crural index is remarkably stable across extant hominoid taxa and, within the hominins, over time (e.g., Jungers, 1984; Lovejoy et al., 2009).

3.8. Estimates of the SWT1/HR-2 hominin's live stature and body mass

The SWT1/HR-2 individual is estimated to have had a live stature of 103.0 cm, making it among the shortest adults in the Pleistocene hominin fossil record (Table 10). Based on the virtual direct estimate of FHD (using a best-fitted sphere method), we derived a value of 30.6 mm. From that FHD value,[8] we estimate that the live body mass of SWT1/HR-2 hominin was 27.4 kg and that it had a body mass index of 25.8 (Table 10).

3.9. Complications for inferring the sex of the SWT1/HR-2 hominin

As discussed earlier, we assign SWT1/HR-2 to *P. robustus*. The sample of taxonomically diagnostic *P. robustus* skull and tooth fossils includes very large (presumably male) specimens, such as, from Swartkrans, the maxilla and mandible SK 12 and the cranium SK 83, and much smaller (presumably female) specimens, such as the SK 74 mandible (Swartkrans) and the DNH 7 skull, from Drimolen. In that context, it is reasonable to predict that *P. robustus* was characterized by correspondingly relatively large-bodied adult males and small-bodied adult females. Indeed, most quantitative studies conclude a marked degree of body size sexual dimorphism in *P. robustus* (e.g., Lockwood et al., 2007; Grine et al., 2012a; Pickering et al., 2012), with males averaging perhaps ~32 kg and females ~24 kg in estimated live weight (Grabowski et al., 2015). At an estimated live body mass of 27.4 kg, the SWT1/HR-2 hominin falls about midway between those two estimated means. This result counsels against using estimated body size as a determinate of sex for this set of postcranial fossils.

As to morphological approaches to determine sex from bones, the SWT1/HR-2a os coxae presents mixed signals. The bone is extremely robust (with an especially thick acetabulosacral buttress and an extremely large anterior inferior iliac spine), which is male-indicating. However, its greater sciatic notch is wide, shallow, symmetrical, and semicircular, which, for modern humans, is stereotypically female in shape (e.g., Bruzek, 2002; Simpson et al., 2008). At the same time, its preauricular region takes a rather paraglenoid groovelike shape (male-indicating) but also lacks a piriform tubercle (female-indicating). These 'contradictory' signals from a single element are only so when viewing the fossils from the perspective of modern human osteology. It has been demonstrated that os coxae sexing methods used in the modern human context (e.g., Iscan and Derrick, 1984; Bruzek, 2002) are not readily transferable in cases involving australopith fossils (e.g., Arsuaga and Alonso, 1983; Häusler and Schmid, 1995; Haeusler and Ruff, 2020).

As a relevant aside, Gommery and Thackeray (2006, 2008) have posited two anterior inferior iliac spine morphotypes in the small sample of Early Pleistocene South African pelvic fossils. The first group includes specimens from Sterkfontein that are usually attributed to *A. africanus* (Sts 14 and StW 431), as well as specimens usually attributed to *P. robustus* from Swartkrans (SK 50), Kromdraai (TM 1605), and Drimolen (DNH 43A). These specimens are grouped together because the anterior inferior iliac spine of each shows a well-developed lower part that directly adjoins the superior rim of the acetabulum. In contrast, it is argued that pelves in the other group have less robust lower parts, which are separated from their superior acetabular rims by grooves of various dimensions. This second group includes the presumptive *P. robustus* fossils from Swartkrans, SK 3155b (also identified by some as early *Homo*; Brain et al., 1974) and SKW 8012. Gommery and Thackeray (2006: 91) argue that the described difference in anterior inferior iliac spine morphology is an expression of sexual dimorphism. They believe that the first group comprises pelves of males, which have a greater development of their anterior inferior iliac spines than do those of the pelves in the second (female) group. This, they propose, "relates to greater stresses on the superior part of the pelvis in [male] individuals...," which is presumably because the "control of balance of the trunk on the hind limb would probably have been more difficult for large (male) individuals" (Gommery and Thackeray, 2008: 64).

We have, however, arrived at a different conclusion about the relevance of variation in anterior inferior iliac spine morphology within the available sample of South African hominin pelvis fossils. If we take Gommery and Thackeray's analytical approach of dividing the spine into its superior extremity and its lower part, our observations indicate that the specimens fall along a continuum, rather than into two discrete groups. At the 'robust' end are specimens such as StW 431 and Sts 14, which are characterized by

[8] Solving the univariate estimation from femoral head maximum diameter (Grabowski et al., 2015) is (Ln[Mass] = 1.52765485 × Ln(30.6) − 1.9161862), yielding 27.4 kg.

bulbous extremities (i.e., extremities that project strongly over their acetabula and that are also broad internally-externally) and internally-externally broad lower parts that adjoin their acetabula. The other, 'gracile,' end of the continuum includes specimens like SKW 8102 and SK 3155b, which have very narrow, 'bladelike' extremities and very narrow lower parts (but that also adjoin their respective acetabula). Other specimens, such as SK 50, also with a rather 'bladelike' extremity but with a moderately broad lower part, fall between these extremes.

By our reckoning, clusters of specimens that occupy the extremes of this continuum are probably not sexually homogenous. For example, at the 'robust' end of the spectrum, there is no disagreement that StW 431 (part of a partial skeleton) represents a large male individual (e.g., Kibii and Clarke, 2003; Toussaint et al., 2003; Gommery and Thackeray, 2006, 2008; Haeusler and Ruff, 2020), and, contrary to Gommery and Thackeray (2006, 2008), every other analysis of which we are aware concludes that Sts 14 (part of a partial skeleton) is a female specimen (e.g., Robinson, 1972; Arsuaga and Carretero, 1994; Häusler and Schmid, 1995; Kibii and Clarke, 2003; Claxton et al., 2016). We add the unsexed SWT1/HR-2 to this 'robust' grouping.

4. Discussion

4.1. Morphological overview of the SWT1/HR-2 fossil-set and its implications for Paranthropus robustus paleobiology

Seventeen years ago, a comprehensive review of early human evolution concluded that, although *P. robustus* "was most likely capable of bipedal walking . . . most researchers [e.g., Napier, 1964; Day and Napier, 1965; Robinson, 1972] subscribe to the view that it was not an obligate biped" (Wood and Lonergan, 2008: 360). Since then, a significant body of research on the internal bone structure of hominin pedal elements from the *P. robustus*–bearing sites of Swartkrans and Kromdraai has developed (Dowdeswell et al., 2017; Komza and Skinner, 2019; Su and Carlson, 2017). When the results of this work are combined with those from previous studies on external bone morphology (e.g., Susman and Brain, 1988; Susman and deRuiter, 2004), they indicate that at least some hominins from these sites engaged in "habitual [terrestrial] bipedalism, with an indication that the overall structure of the foot was more mobile, allowing for multiaxial movement at the [metatarsophalangeal] and [tarsometatarsal] joints" (Komza and Skinner, 2019: 17). In addition to this general understanding, analysis of the cross-sectional attributes of SKX 33380, a hominin fifth metatarsal from Swartkrans, suggests that the lateral column of the foot was loaded in a manner similar to those of the feet of modern humans (Dowdeswell et al., 2017). Furthermore, the internal structure of the TM 1517 talus from Kromdraai is indicative of a modern humanlike bipedal gait (Su and Carlson, 2017).

These results are, obviously, of great importance. However, despite regular conjecture, it is currently unknown whether the fossils to which these conclusions apply represent *P. robustus* or if they, instead, belong to another (or more) synchronous hominin species. It is in this context that the SWT1/HR-2 fossil-set, with its more secure taxonomic attribution, is a singular and particularly valuable source of information about the locomotor adaptations of *P. robustus*. And, in summary, the external morphology of all joints and limb bone diaphyses of the SWT1/HR-2 fossil-set show morphology well suited for stabilization during orthograde and bipedal loading, and for resistance to torsional and shearing forces that are commonly experienced by primate habitual bipeds. These observations, alone, lead to a fundamental conclusion. The species *P. robustus*, as exemplified by the SWT1/HR-2 fossil-set, was a competent, probably habitual terrestrial biped, *regardless of the precise details of its gait kinematics*. Moreover, the modern humanlike tibial arch angle of SWT1/HR-2c hints that at least some *P. robustus* individuals may have possessed a developed longitudinal arch.

If the SWT1/HR-2 *P. robustus* climbed routinely, there is scant indication in the surface morphology of its lower limb bones that it did so in the ways and/or at the frequencies observed in extant nonhuman apes. For instance, the distal tibia lacks squatting facets and the set of the ankle, along with that joint's surrounding ligamentous attachment sites, seem to suggest a lack of habitual ankle dorsiflexion and a relatively modern humanlike ankle position. In this context, we note that there is a good sample of hominin manual phalanges from Swartkrans. Despite recent suggestions to the contrary (e.g., Wallace et al., 2017), a raft of previous research (e.g., Oxnard, 1973; Stern and Susman, 1983; Susman et al., 1984; Stern et al., 1995; Matarazzo, 1998; Richmond, 2007; Deane and Begun, 2008; Rein, 2011) "suggests a strong functional link between locomotor behaviour and the external morphology of phalanges" (Syeda et al., 2023: 1). The Swartkrans manual proximal phalanges are all described as more like those of modern humans than those of modern, nonhuman hominoids, and only one shows longitudinal curvature within the 95% confidence interval of the chimpanzee and gorilla curvature means, while the others are relatively straight (Susman, 1989). However, we also must stress again that although the Swartkrans phalanges are generally assigned to *P. robustus* (e.g., Susman, 1989), that diagnosis is by no means definitive (e.g., Pickering, 2001).

Moreover, none of these observations, regardless of their associated taxonomic certainty (or uncertainty), can be used to suggest that *P. robustus* never climbed. For example, important behavioral and morphological studies of modern human foragers show them to be quite capable climbers but without betraying that advanced capacity in their external bony ankle morphology (e.g., Venkataraman et al., 2013a, 2013b). Those foragers climb regularly to collect valuable foods, such as honey. Given their small size and arboreal ancestry, there is good reason to assume that early hominins, including *P. robustus*, were also motivated to climb (at least occasionally) to meet various fitness-enhancing goals (e.g., for food, for shelter, and to evade predators). More than the external ankle, the hip of SWT1/HR-2, showing indications of strong flexion abilities, comports with reliable climbing capabilities. Our excavations and preparations of the SWT1/HR-2-bearing breccia continue with the hope of recovering additional hominin fossils, some of which might bear more directly on the issue of arboreal behavior in *P. robustus*. In addition, our ongoing endostructural studies of the SWT1/HR-2 fossil-set hold the potential to alter our (and other) views of *P. robustus* posture and locomotion. This is because both "cortical and trabecular bone model and remodel throughout life to adjust structurally to the local loading environment" (Cazenave and Kivell, 2023: 103304).

In the meantime, one might also predict external osteological indications of strong hip flexion abilities if the SWT1/HR-2 *P. robustus* engaged in habitual squatting activities on the ground. Studies on vertebrate taxonomic uniformitarianism (e.g., Vrba, 1975; Brain, 1981; Watson, 1993; Avery, 1995, 2001; Reed, 1997), cercopithecoid locomotor ecomorphology (Elton, 2001), and stable isotopes of herbivore fossils (e.g., Lee-Thorp et al., 2007; Sponheimer and Lee-Thorp, 2009; Lee-Thorp and Sponheimer, 2013) mostly agree that the mammalian fauna of Swartkrans Member 1 shows a preponderance of grazing and mixed-feeding ungulates. The overall result of these combined efforts is the "reconstruction of a habitat dominated by grassland and edaphic grasslands with nearby perennial water sources to support seasonal flooding and the trees required by the frugivores" (Peterson et al., 2018: 46–47). Within this paleoenvironmental context, some researchers have argued for the

presence of purported bone tools, associated spatially with the fossils of *P. robustus* (and early *Homo*) at Swartkrans (e.g., Brain et al., 1988; Brain and Shipman, 1993) (as well as with both taxa at Sterkfontein [Robinson, 1959], Drimolen [Backwell and d'Errico, 2008], and Kromdraai B [Stammers et al., 2018]). It is conjectured that hominins used these modified bone objects to dig up edible foods, such as underground storage organs of plants and/or termites (e.g., Brain and Shipman, 1993; Backwell and d'Errico, 2001), both of which are found today distributed along the open flanks of Swartkrans Hill and in the open floodplain of the Bloubank River, below the site. If the SWT1/HR *P. robustus* engaged habitually in such extractive activities, it probably involved regular bouts of sitting, kneeling, and/or squatting (all flexed hip postures). From that perspective, this hominin's lack of a steeply retroverted tibial plateau and squatting facets on its distal tibia does not seem congruent with such behavior for *P. robustus*.

4.2. Taphonomic inferences and body size estimates of the SWT1/HR-2 hominin and their implications for Paranthropus robustus paleobiology

The cortices of the SWT1/HR-2a os coxae and SWT1/HR-2b femur are marred by postmortem damage. When compared to bone assemblages of known neotaphonomic origins, some of these modifications—specifically, extensive ragged chewing to specimen edges and associated plastic deformation of the same edges (e.g., Brain, 1981)—can be attributed with high confidence to the masticatory activities of prehistoric mammalian actors.

Furthermore, the anatomical patterning of the biologically derived damage on these specimens leads to the following inferences. First, this damage was most likely imparted on both elements during the same chewing event because there is matching placement of ragged-edge chewing and furrowing on, respectively, the lunate surface of the os coxae and the head of the femur. Second, chewing on the superior border of the os coxae indicates a stereotypic pattern of feeding behavior observed among medium- to large-sized felids, in which, almost invariably, the abdominal viscera of a carcass are consumed in their entirety early in the feeding sequence (e.g., Kruuk and Turner, 1967; Schaller, 1972; Brain, 1981; Blumenschine, 1987; Domínguez-Rodrigo, 1999; Pickering, 2001). In addition, at 27.4 kg, the estimated live body mass of SWT1/HR-2 is just 2 kg heavier than the mean mass of prey preferred by extant leopards (Hayward et al., 2006). Third, most parsimoniously, the entire left lower limb and os coxae of the SWT1/HR-2 *P. robustus* entered the cave as an articulated unit. The left femur and left os coxae fragment were recovered in near-articulation and the left tibia in proximity to the left femur (Fig. 3). Moreover, the left knee joint and the left distal tibia lack any biotically derived damage, which is predicted if there was predator-directed disarticulation of those elements at those articular ends. From these observations and chain of logic, we suggest that the left patella, fibula, and foot of the SWT1/HR-2 *P. robustus* became separated from the rest of the left lower limb only after its deposition on the Swartkrans Member 1 talus slope, when that limb's connective tissues had decayed.

It is improbable that the left lower limb of SWT1/HR-2 experienced any postdepositional scavenging in Swartkrans. For that matter, it is also extremely unlikely that the limb was scavenged in a scenario in which it was abandoned on the landscape outside the cave by a primary consumer and then brought into the cave by a secondary scavenger(s), which could include, for instance, other felids, hyenids, canids, rodents, or birds (e.g., Brain, 1981). Again, it is the lack of tooth marks and any other masticatory damage on the recovered bones (other than that summarized above) upon which these inferences are based. Given these inferences, it is reasonable to suggest, in turn, that the missing elements of the limb (as well as other portions of the skeleton) might still be encased in the unprocessed remnant of the massive SWT1/HR-2 breccia block. It will take time and continued dedication to test this prediction, as is made clear in the aforementioned description of the arduous nature of the mechanical processing of Swartkrans' breccias.

In summary, the pattern of prehistoric, biotically imparted damage on the SWT1/HR-2 fossil-set implicates a medium- or large-sized felid as its agent of deposition; the hominin's estimated live body mass suggests, more specifically, a leopard as that agent. Other common bone-collecting agents, such as those mentioned earlier, impart taxonomically diagnostic tooth damage arrayed across skeletons and even individual bones in patterns specific to them and distinct from those of felids (e.g., Simons, 1966; Brain, 1981; Blumenschine, 1987; Pickering, 2001; Domínguez-Rodrigo and Pickering, 2010; Domínguez-Rodrigo et al., 2012). For instance, unlike meat-slicing cats, durophagous hyenids—whether acting as primary consumers or, instead, as scavengers—would have likely imparted far more catastrophic damage to, if not destroying completely, the diminutive SWT1/HR-2 lower limb bones. In contrast, relatively small-sized ossa coxae, femora, and tibiae—although often-times chewed—are commonly surviving elements in large samples of modern baboon bones that were accumulated and modified by leopards (Simons, 1966; Brain, 1981; Pickering, 2001; Pickering et al., 2011).

Indeed, a leopard-centered model of bone-assemblage formation is particularly salient to our consideration of the depositional circumstances of the SWT1/HR-2 specimens. In order to account for the large number of *P. robustus* fossils recovered previously from Swartkrans—and underpinned by an extensive body of neotaphonomic comparative work—one of us presented long ago the 'Swartkrans leopard hypothesis' (Brain, 1970, 1981, 1993b). Critical to that hypothesis are the following observations. First, the recurrent but sporadic discovery of 'new' fossil taxa—whether they be diatoms or dinosaurs—seems to bear out the truism stated by White (1988: 451) that "the fossil record usually represents a very tiny . . . and very distorted reflection of ancient plant and animal communities . . . " It is reasonable to suggest that the biasing effects of time and taphonomy will be, alternatively, blunted or amplified by the paleoecological position of any particular species. In this framework, hominins are predicted to be rare occupants of the fossil record. This prediction is largely borne out by paleontological results, in which the large vertebrate taxa that are most abundant in modern African food webs, such as ungulates, are also usually much better represented in most fossil assemblages than are, for example, carnivores and primates. With this in mind, Brain (1981) argued that it is simply the very substantial size of the Swartkrans *P. robustus* assemblage, alone, that begs special explanation.

Second, Brain observed that the *P. robustus* sample from Swartkrans comprises specimens that were disarticulated and isolated, as one would predict if their remains entered the cave mostly through the actions of carnivores that consumed them. Additionally, in one of the most striking taphonomic anecdotes in all of vertebrate paleontology, Brain (1970) demonstrated that the spacing of two punctures in the Swartkrans Member 1 (HR) *P. robustus* juvenile calotte, SK 54, match the spacing of the tips of the canines of a fossilized leopard jaw (SK 349), also from the HR.[9]

[9] We disagree with the recent suggestion that SK 54 more likely represents *Homo erectus* than it does *Paranthropus robustus* (Braga et al., 2023). The overall morphology of the fossil, and especially its incipient supraglabella hollow and its thin, flattened supraorbital margin, which are unique to *Paranthropus*, are consistent with that taxon (Clarke, 1990).

Figure 20. The SWT1/HR-3 fossil leopard (*Panthera pardus*) skull in right lateral view. Bar scale = 1 cm. (For interpretation of the references to color in this figure, the reader is referred to the Web version of this article).

Third, Brain (1981) observed that the *P. robustus* sample from Swartkrans contains a large proportion of subadults, whose estimated live body masses would have been well within the body-size range of prey upon which leopards focus (e.g., Hayward et al., 2006). Fourth, Brain (1981) observed that, in open habitats, modern leopards often consume their prey in trees, out of the reach of food competitors, such as nonclimbing hyenids. Add to this observation that trees—in otherwise open, highveld landscapes—grow preferentially around the well-watered and wind-sheltered shafts leading to underground caverns, and Brain was able to argue that residues from arboreal feeding platforms of prehistoric leopards could have easily dropped into such shafts and become incorporated into cave bone assemblages. Current reconstructions of the Swartkrans Member 1 paleoenvironment (as discussed earlier) suggest much the same relatively open conditions as those summarized in Brain's observations of leopard behavior in modern karstic landscapes.

Brain (1981, 1993b) later elaborated the 'Swartkrans leopard hypothesis' by referring to observations of extant baboons. Some of those that reside in temperate climates aggregate in large numbers during the cold winter months to sleep in the relative warmth of the mouths of caves (e.g., Gow, 1973; McGrew et al., 2003; Barrett et al., 2004; Nel et al., 2021). A similar nocturnal roosting situation also characterized baboons living around the sinkholes of Mount Suswa (Kenya) (see Table 2), where leopards apparently exploited the situation by launching predatory attacks from deeper recesses of the caves on the primates sleeping higher up (Simons, 1966). Brain postulated that part of, or the entireties of, the primate (i.e., monkey plus hominin) fossil assemblages from Swartkrans could have formed in a similar fashion.

Regardless of its specifics, Brain was ever cognizant that the 'Swartkrans leopard hypothesis' was just that—a hypothesis. As such, he subjected it to relentless scrutiny and revision over the intervening years since its formulation. Most importantly, Brain—based on his long career of neotaphonomic research—never wavered from the view that the accumulation of any large fossil assemblage was almost invariably multifactorial. The preponderance of taphonomic evidence certainly bears this out for the faunas of Swartkrans Cave (Brain, 1981, 1993b; Watson, 1993; Pickering et al., 2008). With this appreciation, that of all possible felid culprits, it is most parsimonious to infer that a leopard was the predator, sole consumer, and depositor of the SWT1/HR-2 hominin.

We conclude on a note of coincidence by mentioning the discovery of SWT1/HR-3, a complete leopard skull found in the very same breccia block from which SWT1/HR-2 was excavated (Fig. 20). This uncanny spatial association of a leopard-modified *P. robustus* fossil (SWT1/HR-2) and a remarkable leopard fossil (SWT1/HR-3) corresponds fittingly with Brain's (1970) discovery of the spatially associated SK 54 carnivore-modified hominin calotte and SK 349 leopard mandible 55 years ago.

5. Conclusions

Since 1948, paleontological work at Swartkrans has produced a great number of hominin craniodental fossils but relatively few hominin postcranials. For instance, there were only four partial ossa coxae, six partial femora, and no tibiae. Now, with the SWT1/HR-2 fossil-set, not only do we have the first known virtually complete Swartkrans femur and complete tibia, but those elements also belong together and articulate with a partial os coxae. Our comparative morphological studies indicate that these associated fossils derive from a very small, young adult *P. robustus*. As such, they can be used as species-diagnostic templates against which other isolated hominin pelvic, femur, and tibia fossils can be compared for taxonomic identification.

Moreover, analyses of the external morphology of the SWT1/HR-2 *P. robustus* fossils have allowed for an interpretation of that species' locomotor behavior. It appears that *P. robustus*, as exemplified by SWT1/HR-2, was a capable, and probably habitual, terrestrial biped. The SWT1/HR-2 fossil-set shows various traits that are linked in modern humans to the regular use of terrestrial bipedal gaits, including, at the knee, a high bicondylar angle, a sustrochlear hollow, and a well-developed lateral patellar lip. The hip of SWT1/HR-2 was fully adapted for habitual extension and orthograde and bipedal load-bearing. Its external ankle was constructed for terrestrial bipedal stability, is directed roughly perpendicularly to the tibial diaphysis, and lacks signs of extreme dorsiflexion capabilities. There is even indication that SWT1/HR-2 may have possessed a pedal longitudinal arch.

Association of the SWT1/HR-2 fossils also made it possible to calculate total lower limb length and to estimate live stature and body mass for a young adult of this species. Unsurprisingly, SWT1/HR-2 shows a crural index that aligns precisely with that of modern humans and gorillas, confirming the previous finding that the proportional relationship between the thigh and crus is conservative within the hominoids. The estimated small live body size of SWT1/HR-2 (103.0 m, 27.4 kg) confirms earlier conclusions that *P. robustus* individuals were diminutive (e.g., McHenry, 1991; Grabowski et al., 2015). As suggested by the tooth-marked state of its os coxae and femur, the small size of the SWT1/HR-2 *P. robustus* may have made it vulnerable to carnivores, such as leopards, which prefer to hunt prey of its projected live bodyweight.

Continuing studies of the SWT1/HR-2 fossil-set, including especially those on internal bone structure, promise to refine the interpretations of its positional and locomotor behaviors discussed here. Moreover, ongoing preparation of the HRM breccia blocks from which that set derives might well yield additional fossils of the same individual, providing the opportunity to further expand our understanding of *P. robustus* paleobiology.

Acknowledgments

The surviving coauthors dedicate this paper to Bob Brain (1931–2023), our colleague, friend, and a paleoanthropological

inspiration. Very special thanks to Gordon Getty, Paddy Moore, and the L.S.B. Leakey Foundation (USA) and to Rob Blumenschine and Andrea Leenan and the Palaeontological Scientific Trust (PAST, South Africa) for their generous support of this project through grants awarded to T.R.P. and to Oppenheimer Generations for funding awarded to K.K. and R.J.C. Other funding for the Swartkrans Paleoanthropology Research Project (SPRP) includes the following grants to T.R.P.: the National Science Foundation (USA) and the Vilas Associates, Kellet Mid-Career Award, and Graduate School Research programs (University of Wisconsin-Madison); the following grants to K.K.: PAST, the National Research Foundation (NRF, South Africa) African Origins Platform (grant number = 98830), the NRF Rated Researcher Incentive Fund, the NRF Competitive Programme for Rated Researchers (grant number = 81782), the Centre of Excellence in Palaeosciences at the University of the Witwatersrand, and the University of the Witwatersrand Research Incentive Fund; and the following grant to D.S.: African Origins Platform (NRF) (grant number = 136508). In addition, the University of the Witwatersrand Faculty of Science provided salary support for Swartkrans technician, Abel Molepolle. Additional profound thanks to our SPRP colleagues, Barry Jacoby, Sipho Makhele, Itulemeleng Molefe, Abel Molepolle, Andrew Phaswana, and Lucas Sekowe and to Marion Bamford, Bernhard Zipfel, and Sifelani Jirah at the Evolutionary Studies Institute (University of the Witwatersrand) for their various permissions and support. Thanks to Lunga Bam and Jakobus Hoffman for X-ray microtomographic scanning of the SWT1/HR-2 fossils at the South African Nuclear Energy Corporation SOC Ltd. (Necsa), Pelindaba. We also acknowledge the NRF (Department of Science and Technology) for financial support (grant #UID23456) to establish the MIXRAD microfocus X-ray tomography facility at Necsa. Many thanks to Kristian Carlson, Manuel Domínguez-Rodrigo, Ashley Hammond, and Annalisa Pietrobelli for helpful discussions and technical advice, as well as to an anonymous reviewer and the Editor (Mark Grabowski) and Associate Editor (Gabrielle Russo) of the *Journal of Human Evolution* for manifold suggestions that improved this work. We have no competing interests. This is paper no. 10 in the SPRP publication series.

Author contributions

Travis Rayne Pickering: Writing – review & editing, Writing – original draft, Validation, Supervision, Resources, Project administration, Methodology, Investigation, Funding acquisition, Formal analysis, Data curation, Conceptualization. **Marine Cazenave:** Writing – review & editing, Writing – original draft, Methodology, Investigation, Formal analysis, Data curation, Conceptualization. **R.J. Clarke:** Writing – review & editing, Validation, Project administration, Methodology, Formal analysis, Conceptualization. **A.J. Heile:** Investigation, Formal analysis, Data curation. **Matthew V. Caruana:** Writing – review & editing, Supervision, Project administration, Methodology, Investigation, Formal analysis, Data curation, Conceptualization. **Kathleen Kuman:** Writing – review & editing, Validation, Funding acquisition. **Dominic Stratford:** Writing – review & editing, Writing – original draft, Supervision, Resources, Funding acquisition, Formal analysis. **C.K. Brain:** Resources, Conceptualization. **Jason L. Heaton:** Writing – review & editing, Validation, Methodology, Investigation, Formal analysis, Data curation, Conceptualization.

References

3D Systems, 2023. Geomagic Design X (Software). Version 2023.20.0.
Adams, D.C., Collyer, M.L., Kaliontzopoulou, A., Baken, E., 2021. Geomorph: Software for geometric morphometric analyses. R package version 3.3.2.
Aramendi, J., Mabulla, A., Baquedano, E., Domínguez-Rodrigo, M., 2024. Biomechanical and taxonomic diversity in the early Pleistocene in East Africa: Structural analysis of a recently discovered femur shaft from Olduvai Gorge (Bed I). J. Hum. Evol. 186, 103469.
Arsuaga, J., 1981. Iliac angular measurements in *Australopithecus*. J. Hum. Evol. 10, 293–294.
Arsuaga, J., Alonso, J., 1983. Sexual variability and taxonomical variability in the innominate bone of *Australopithecus*. Z. Morph. Anthropol. 73, 297–308.
Arsuaga, J., Carretero, J.M., 1994. Multivariate analysis of the sexual dimorphism of the hip bone in a modern human population and in early hominids. Am. J. Phys. Anthropol. 93, 241–257.
Asfaw, B., White, T., Lovejoy, C.O., Latimer, B., Simpson, S., Suwa, G., 1999. *Australopithecus garhi*: A new species of early hominid from Ethiopia. Science 284, 629–635.
Auerbach, B., Ruff, C., 2004. Human body mass estimation: A comparison of 'morphometric' and 'mechanical' methods. Am. J. Phys. Anthropol. 125, 331–342.
Avery, M., 1995. Southern savannas and Pleistocene hominid adaptations: The micromammalian perspective. In: Vrba, E., Denton, G., Partridge, T., Burckle, L. (Eds.), Paleoclimate and Evolution with Emphasis on Human Origins. Yale University Press, New Haven, pp. 459–478.
Avery, M., 2001. The Plio-Pleistocene vegetation and climate of Sterkfontein and Swartkrans, South Africa, based on micromammals. J. Hum. Evol. 41, 113–132.
Baab, K., Brown, P., Falk, D., Richtsmeier, J., Hildebolt, C., Smith, K., Jungers, W., 2016. A critical evaluation of the Down Syndrome diagnosis for LB1, type specimen of *Homo floresiensis*. PLoS One 11, e0155731.
Backwell, L., d'Errico, F., 2001. Evidence of termite foraging by Swartkrans early hominids. S. Afr. J. Sci. 98, 1358–1363.
Backwell, L., d'Errico, F., 2008. Early hominid bone tools from Drimolen, South Africa. J. Archaeol. Sci. 35, 2880–2894.
Barrett, L., Gaynor, D., Rendall, D., Mitchell, D., Henzi, S., 2004. Habitual cave use and thermoregulation in chacma baboons (*Papio hamadryas ursinus*). J. Hum. Evol. 46, 215–222.
Behrensmeyer, A.K., 1978. Taphonomic and ecologic information from bone weathering. Paleobiology 1978, 150–162.
Berger, L., Tobias, P., 1996. A chimpanzee-like tibia from Sterkfontein, South Africa and its implications for the interpretation of bipedalism in *Australopithecus africanus*. J. Hum. Evol. 30, 343–348.
Berger, L., de Ruiter, D., Churchill, S., Schmid, P., Carlson, K., Dirks, P., Kibii, J., 2010. *Australopithecus sediba*: A new species of *Homo*-like australopith from South Africa. Science 328, 195–204.
Blumenschine, R.J., 1987. Characteristics of an early hominid scavenging niche. Curr. Anthropol. 28, 383–406.
Blumenschine, R.J., Marean, C.W., Capaldo, S., 1996. Blind tests of inter-analyst correspondence and accuracy in the identification of cut marks, percussion marks, and carnivore tooth marks on bone surfaces. J. Archaeol. Sci. 23, 493–507.
Bolter, D., Zihlman, A., 2012. Skeletal development in *Pan paniscus* with comparisons to *Pan troglodytes*. Am. J. Phys. Anthropol. 147, 629–636.
Boulle, E.-L., 2001. Evolution of two human skeletal markers of the squatting position: A diachronic study from Antiquity to the Modern Age. Am. J. Phys. Anthropol. 115, 50–56.
Braga, J., Thackeray, J., 2003. Early *Homo* at Kromdraai B: Probabilistic and morphological analysis of the lower dentition. C. R. Palevol 2, 269–279.
Braga, J., Wood, B., Zimmer, V., Moreno, B., Miller, C., Thackeray, J.F., Zipfel, B., Grine, F., 2023. Hominin fossils from Kromdraai and Drimolen inform *Paranthropus robustus* craniofacial morphology. Sci. Adv. 9.
Brain, C.K., 1970. New finds at the Swartkrans australopithecine site. Nature 225, 1112–1119.
Brain, C.K., 1981. The Hunters or the Hunted? An Introduction to African Cave Taphonomy. University of Chicago Press, Chicago.
Brain, C.K., 1993a. Structure and stratigraphy of the Swartkrans Cave in light of the new excavations. In: Brain, C.K. (Ed.), Swartkrans: A Cave's Chronicle of Early Man. Transvaal Museum, Pretoria, pp. 23–33.
Brain, C.K., 1993b. A taphonomic overview of the Swartkrans fossil assemblages. In: Brain, C.K. (Ed.), Swartkrans: A Cave's Chronicle of Early Man. Transvaal Museum, Pretoria, pp. 257–264.
Brain, C.K., Shipman, P., 1993. The Swartkrans bone tools. In: Brain, C.K. (Ed.), Swartkrans: A Cave's Chronicle of Early Man. Transvaal Museum, Pretoria, pp. 195–217.
Brain, C.K., Churcher, C., Clark, J., Grine, F., Shipman, P., Susman, R., Turner, A., Watson, V., 1988. New evidence of early hominids, their culture and environment from the Swartkrans Cave. S. Afr. J. Sci. 84, 828–835.
Brain, C.K., Vrba, E., Robinson, J., 1974. A new hominid innominate bone from Swartkrans. Ann. Transvaal Mus. 29, 55–63.
Broom, R., 1938. The Pleistocene anthropoid apes of South Africa. Nature 142, 377–379.
Broom, R., Robinson, J.T., 1949. A new type of fossil man. Nature 164, 322–323.
Broom, R., Robinson, J.T., 1950. Man contemporaneous with the Swartkrans apeman. Am. J. Phys. Anthropol. 8, 151–155.
Broom, R., Robinson, J.T., 1952. Swartkrans Ape-Man, *Paranthropus crassidens*. Transvaal Museum, Pretoria.
Brown, P., Sutikna, T., Morwood, M., Soejono, R., Jatmiko, Saptomo, E., Due, R., 2004. A new small-bodied hominin from the Late Pleistocene of Flores, Indonesia. Nature 431, 1055–1061.
Bruzek, J., 2002. A method for visual determination of sex, using the human hip bone. Am. J. Phys. Anthropol. 117, 157–168.

Buikstra, J., Ubelaker, D., 1994. Standards for Data Collection from Human Skeletal Remains. Research Series No. 44. Arkansas Archaeological Survey Research Series, Fayetteville.
Cameriere, R., Cingolani, M., Giuliodori, A., Ferrante, L., 2012. Radiographic analysis of epiphyseal fusion at knee joint to assess likelihood of having attained 18 years of age. Int. J. Leg. Med. 126, 889–899.
Carlson, K., Zipfel, B., Jungers, W., 2020. Tibia and fibula. In: Zipfel, B., Richmond, B., Ward, C. (Eds.), Hominin Postcranial Remains from Sterkfontein, South Africa, 1936–1995. Oxford University Press, New York.
Cazenave, M., Kivell, T., 2023. Challenges and perspectives on functional interpretations of australopith postcrania and the reconstruction of hominin locomotion. J. Hum. Evol. 175, 103304.
Cazenave, M., Braga, J., Oettlé, A., Pickering, T.R., Heaton, J., Nakatsukasa, M., Thackeray, J.F., de Beer, F., Hoffman, J., Dumoncel, J., Macchiarrelli, 2019. Cortical bone distribution in the femoral neck of *Paranthropus robustus*. J. Hum. Evol. 135, 102666.
Cazenave, M., Dean, C., Zanolli, C., Oettlé, A., Hoffman, J., Tawane, M., Thackeray, J.F., Macchierelli, R., 2020. Reassessment of the TM 1517 odonto-postcranial assemblage from Kromdraai B, South Africa, and the maturational pattern of *Paranthropus robustus*. Am. J. Phys. Anthropol. 172, 714–722.
Cazenave, M., Oettlé, A., Pickering, T.R., Heaton, J., Nakatsukasa, M., Thackeray, J.F., Hoffman, J., Macchiarelli, R., 2021. Trabecular organization of the proximal femur in *Paranthropus robustus*: Implications for the assessment if its hip loading conditions. J. Hum. Evol. 153, 102964.
Cazenave, M., Kivell, T., Dunmore, C., Skinner, M., 2023. Signals of early hominin postural and locomotor diversity in the structural arrangement of the femoral neck. Am. J. Biol. Anthropol. 189, 29.
Cazenave, M., m Pina, M., Hammond, A., Böhme, M., Begun, D., Spassov, N., Vecino Gazabón, A., Zanolli, C., Bergeret-Medina, A., Marchi, D., Macchiarelli, R., Wood, B., 2024. Postcranial evidence does not support habitual bipedalism in *Sahelanthropus tchadensis*: A reply to Daver et al. (2022). J. Hum. Evol. In press.
Cibulka, M., 2004. Determination and significance of femoral neck anteversion. Phys. Ther. 84, 550–558.
Clarke, R., 1977a. The Cranium of the Swartkrans hominid, SK 847, and its relationship to human origins (Dissertation). University of the Witwatersrand.
Clarke, R., 1977b. A juvenile cranium and some adult teeth of early *Homo* from Swartkrans, Transvaal. S. Afr. J. Sci. 3, 46–49.
Clarke, R., 1990. Observations on some restored hominid specimens in the Transvaal Museum, Pretoria. In: Sperber, G.H. (Ed.), From Apes to Angels: Essays in Anthropology in Honor of Phillip V. Tobias. Wiley-Liss, New York, pp. 131–151.
Clarke, R., 1994. Advances in understanding the craniofacial anatomy of South African early hominids. In: Corruccini, R., Ciochon, R. (Eds.), Integrative Paths to the Past: Essays in Honor of F. Clark Howell. Prentice Hall, Upper Saddle River (NJ), pp. 205–222.
Clarke, R., 2012. The history of research in human evolution in Africa and what lessons have been learned. In: Sanz, N. (Ed.), Human Origins Sites and the World Heritage Convention in Africa. UNESCO, New York, pp. 44–67.
Clarke, R., 2017. *Homo habilis*: The inside story. In: Sahnouni, M., Semaw, S., Garaizar, J. (Eds.), Proceedings of the II Meeting of African Prehistory. National Center for Investigation of Human Evolution, Burgos, pp. 25–51.
Clarke, R., Howell, F.C., 1972. Affinities of the Swartkrans 847 cranium. Am. J. Phys. Anthropol. 37, 319–335.
Clarke, R., Howell, F.C., Brain, C.K., 1970. More evidence of an advanced hominid at Swartkrans. Nature 225, 1219–1222.
Clarke, R., Pickering, T.R., Heaton, J., Kuman, K., 2021. The earliest South African hominids. A. Rev. Anthropol. 50, 125–143.
Claxton, A., Hammond, A., Oleinik, E., DeSilva, J., 2016. Virtual reconstruction of the *Australopithecus africanus* pelvis Sts 65 with implications for obstetrics and locomotion. J. Hum. Evol. 99, 10–24.
Coryndon, S., 1964. Bone remains in the cave. In: Glover, P., Glover, E., Trump, E., Wateridge, L. (Eds.), The Lave Caves of Mount Suswa, Kenya, with Particular Reference to Their Ecological Role, pp. 60–63. Studies in Speleology 1, pp. 51–66.
Crompton, R., McClymont, J., Elton, S., Thorpe, S., Sellers, W., Heaton, J., Pickering, T.R., Pataky, T., Carlson, K., Jashashvili, T., Beaudet, A., Bruxelles, L., Goh, E., Kuman, Clarke, R., 2021. StW 573 *Australopithecus prometheus*: Its significance for an australopith bauplan. Folia Primatol. 92, 243–275.
Cunningham, C., Scheuer, L., Black, S., 2016. Developmental Juvenile Osteology. Academic Press, London.
Dalstra, M., Huiskes, R., 1995. Load transfer across the pelvic bone. J. Biomech. 28, 715–724.
Davenport, C., 1933. The crural index. Am. J. Phys. Anthropol. 17, 333–353.
Daver, G., Mackaye, H., Likius, A., Moussa, A., Pallas, L., Vignaud, P., Clarisse, N., 2022. Postcranial evidence of late Miocene hominin bipedalism in Chad. Nature 609, 94–100.
Davies, D., Chen, L., Young, S., 2013. Evaluation of epiphyses in the skeletally immature knee using magnetic resonance imaging: A pilot study to analyze parameters for anterior cruciate ligament reconstruction. Am. J. Sports Med. 41, 1579–1585.
Davies, C., Hackman, L., Black, S., 2015. The epiphyseal scar: Changing perceptions in relation to skeletal age estimation. Ann. Hum. Biol. 42, 348–357.
Day, M., 1971. Postcranial remains of *Homo erectus* from Bed IV, Olduvai Gorge, Tanzania. Nature 232, 383–387.
Day, M., Napier, J., 1965. Fossil foot bones. Curr. Anthropol. 6, 419–420.
Deane, A., Begun, D., 2008. Broken fingers: Retesting locomotor hypotheses for fossil hominoids using fragmentary proximal phalanges and high-resolution polynomial curve fitting (HR-PCF). J. Hum. Evol. 55, 691–701.
DeSilva, J., 2009. Functional morphology of the ankle and the likelihood of climbing in early hominins. Proc. Natl. Acad. Sci. U.S.A. 106, 6567–6572.
DeSilva, J., Throckmorton, Z., 2010. Lucy's flat feet: The relationship between the ankle and rearfoot arching in early hominins. PLoS One 5, e14432.
DeSilva, J., Holt, K., Churchill, S., Carlson, K., Walker, C., Zipfel, B., Berger, L., 2013. The lower limb and mechanics of walking in *Australopithecus sediba*. Science 340, 1232999.
DeSilva, J., Carlson, K., Claxton, A., Harcourt-Smith, W., McNutt, E., Sylvester, A., Walker, C., Zipfel, B., Churchill, S., Berger, L., 2018. The anatomy of the lower limb skeleton of *Australopithecus sediba*. Paleoanthropology 2018, 357–405.
Domínguez-Rodrigo, M., 1999. Flesh availability and bone modification in carcasses consumed by lions. Palaeogeogr. Palaeoclimatol. Palaeoecol. 149, 373–388.
Domínguez-Rodrigo, M., Pickering, T.R., 2010. A multivariate approach for discriminating bone accumulations created by spotted hyenas and leopards: Harnessing actualistic data from East and southern Africa. J. Taphon. 8, 155–179.
Domínguez-Rodrigo, M., Piqueras, A., 2003. The use of tooth pits to identify carnivore taxa in tooth-marked archaeofaunas and their relevance to reconstruct hominid carcass processing behaviours. J. Archaeol. Sci. 30, 1385–1391.
Domínguez-Rodrigo, M., Gidna, A., Yravedra, J., Musiba, C., 2012. A comparative neo-taphonomic study of felids, hyaenids and canids: An analogical framework based on long bone modification patterns. J. Taphon. 10, 151–170.
Domínguez-Rodrigo, M., Pickering, T.R., Baquedano, E., Mabulla, A., Mark, D., Musiba, C., Bunn, H., Smith, V., Diez-Martin, F., Pérez-Gonzalez, A., Sánchez, P., Barboni, D., Gidna, A., Heaton, J., Arriaza, M., 2013. First partial skeleton of a 1.34-million-year-old *Paranthropus boisei* from bed II, Olduvai Gorge, Tanzania. PLoS One 8, e80347.
Dowdeswell, M., Jashashvili, T., Patel, B., Lebrun, R., Susman, R., Lordkipanidze, D., Carlson, K., 2017. Adaptation to bipedal gait and fifth metatarsal structural properties in *Australopithecus, Paranthropus*, and *Homo*. Comptes Rendus Palevol 16, 585–599.
Durrant, B., Chockalingam, N., Hashmi, F., 2011. Posterior tibial tendon dysfunction. J. Am. Podiatr. Med. Assoc. 101, 176–186.
Elton, S., 2001. Locomotor and habitat classification of cercopithecoid postcranial material from Sterkfontein Member 4, Bolt's Farm and Swartkrans Members 1 and 2, South Africa. Palaeontol. Afr. 37, 115–126.
Fabry, G., MacEwen, G., Shands, A., 1973. Torsion of the femur: A follow-up study in normal and abnormal conditions. J. Bone Joint Surg. 55, 1726–1738.
Frankel, V., Burstein, A., 1965. Load capacity of tubular bone. In: Biomechanics and Related Bio-Engineering Topics. Pergamon, London.
Fukushima, K., Miyagi, M., Inoue, G., Shirasawa, E., Uchiyama, K., Takashira, N., Takaso, M., 2018. Relationship between spinal sagittal alignment and acetabular coverage: A patient-matched control study. Arch. Orthop. Trauma Surg. 138, 1495–1499.
Fuller, K., 1996. Analysis of the probability of multiple taxa in a combined sample of Swartkrans and Kromdraai dental material. Am. J. Phys. Anthropol. 101, 429–439.
Garvin, H., Elliott, M., Delezene, L., Hawks, J., Churchill, S., Berger, L., Holliday, T., 2017. Body size, brain size, and sexual dimorphism in *Homo naledi* from the Dinaledi Chamber. J. Hum. Evol. 111, 119–138.
Georgiou, L., Dunmore, C., Bardo, A., Buck, L., Hublin, J.-J., Skinner, M., 2020. Evidence for habitual climbing in a Pleistocene hominin in South Africa. Proc. Natl. Acad. Sci. U.S.A. 117, 8416–8423.
Gibbon, R.J., Pickering, T.R., Sutton, M.B., Heaton, J.L., Kuman, K., Clarke, R.J., Brain, C.K., Granger, D.E., 2014. Cosmogenic nuclide burial dating of hominin-bearing Pleistocene cave deposits at Swartkrans, South Africa. Quatern. Geochronol. 24, 10–15.
Gommery, D., Thackeray, J.F., 2006. Sts 14, a male subadult partial skeleton of *Australopithecus africanus*? S. Afr. J. Sci. 102, 91–92.
Gommery, D., Thackeray, J.F., 2008. A new hominid hip bone from Swartkrans (SKW 8012) in relation to the anatomy of the anterior inferior iliac spine. Annls. Transv. Mus. 45, 55–66.
Gommery, D., Senut, B., Keyser, A., 2002. A fragmentary pelvis of *Paranthropus robustus* of the Plio-Pleistocene site of Drimolen (Republic of South Africa). Geobios 35, 265–281.
Gow, C., 1973. Habitual sheltering in an extensive cave system by baboons near Bredasdorp, South Africa. S. Afr. J. Sci. 69, 182.
Grabowski, M., Hatala, K., Jungers, W., Richmond, B., 2015. Body mass estimates of hominin fossils and the evolution of human body size. J. Hum. Evol. 85, 75–91.
Grine, F., 1982. A new juvenile hominid (Mammalia: Primates) from Member 3, Kromdraai Formation, Transvaal, South Africa. Annls. Transv. Mus. 33, 163–239.
Grine, F., 1984. Deciduous molar microwear of South African australopithecines. In: Chivers, D., Wood, B., Bilsborough, A. (Eds.), Food Acquisition and Processing in Primates. Plenum, New York.
Grine, F., 1985. Australopithecine evolution: The deciduous dental evidence. In: Delson, E. (Ed.), Ancestors: The Hard Evidence. Liss, New York, pp. 153–167.
Grine, F., Jungers, W., Tobias, P., Pearson, O., 1995. Fossil *Homo* femur from Berg Aukas, northern Namibia. Am. J. Phys. Anthropol. 97, 151–186.
Grine, F., Jacobs, R., Reed, K., Plavcan, J., 2012a. The enigmatic molar from Gondolin, South Africa: Implications for *Paranthropus* paleobiology. J. Hum. Evol. 63, 597–609.

Gruss, L., Schmitt, D., 2015. The evolution of the human pelvis: Changing adaptations to bipedalism, obstetrics and thermoregulation. Phil. Trans. R. Soc. B 370, 20140063.
Haeusler, M., Ruff, C., 2020. Pelves. In: Zipfel, B., Richmond, B., Ward, C. (Eds.), Hominin Postcranial Remains from Sterkfontein, South Africa, 1936–1995. Oxford University Press, New York, pp. 181–201.
Haeusler, M., Webb, N., Krenn, V., Fornai, C., 2020. Locomotor and taxonomic diversity of Sterkfontein hominins not supported by current trabecular evidence of the femoral head. Proc. Natl. Acad. Sci. U.S.A. 117, 28568–28569.
Haile-Selassie, Y., Latimer, B.M., Alene, M., Deino, A.L., Gibert, L., Melillo, S.M., Saylor, B.Z., Scott, G.R., Lovejoy, C.O., 2010. An early *Australopithecus afarensis* postcranium from Woranso-Mille, Ethiopia. Proc. Natl. Acad. Sci. U.S.A. 107, 12121–12126.
Hammond, A., Plavcan, J., Ward, C., 2013. Precision and accuracy of acetabular size measures in fragmentary hominin pelves obtained using sphere-fitting techniques. J. Hum. Evol. 150, 565–578.
Harmon, E., 2006. Size and shape variation in *Australopithecus afarensis* proximal femora. J. Hum. Evol. 51, 217–226.
Harmon, E., 2009a. The shape of the early hominin proximal femur. Am. J. Phys. Anthropol. 139, 154–171.
Harmon, E., 2009b. Size and shape variation in the proximal femur of *Australopithecus africanus*. J. Hum. Evol. 56, 551–559.
Harris, E., 2010. The natural history and pathophysiology of flexible flatfoot. Clin. Podiatr. Med. Surg. 27, 1–23.
Häusler, M., Schmid, P., 1995. Comparison of the pelves of Sts 14 and A.L. 288-1: Implications for birth and sexual dimorphism in australopithecines. J. Hum. Evol. 29, 363–383.
Hayward, M., Henschel, P., O'Brien, J., Hofmeyr, M., Balmes, G., Kerley, G., 2006. Prey preferences of the leopard (*Panthera pardus*). J. Zool. 270, 298–313.
Heaton, J., Pickering, T.R., Carlson, K., Crompton, R., Jashashvili, T., Beaudet, A., Bruxelles, L., Kuman, K., Heile, A.J., Stratford, D., Clarke, R., 2019. The long limb bones of the StW 573 *Australopithecus* skeleton from Sterkfontein Member 2: Descriptions and proportions. J. Hum. Evol. 133, 167–197.
Heiple, K., Lovejoy, C.O., 1971. The distal femoral anatomy of *Australopithecus*. Am. J. Phys. Anthropol. 35, 75–84.
Howell, F.C., 1978. Hominidae. In: Maglio, V.J., Cooke, H.B.S. (Eds.), Evolution of African Mammals. Harvard University Press, Cambridge, pp. 154–248.
Huard, P., Montagné, M., 1950. Le squelette humain et l'attitude accroupie. Bull. Soc. Etud. Indochin. 25, 401–426.
Hunt, K., Dunevant, S., Yohler, R., Carlson, K., 2021. Femoral bicondylar angles among dry-habitat chimpanzees (*Pan troglodytes schweinfurthii*) resemble those of humans: Implications for knee function, australopith sexual dimorphism, and the evolution of bipedalism. J. Anthropol. Res. 77, 303–337.
Iscan, M., Derrick, K., 1984. Determination of sex from the sacroiliac joint: A visual assessment technique. Florida Scientist 47, 94–98.
Johanson, D., Lovejoy, C.O., Kimbel, W., White, T., Ward, S., Bush, M., Latimer, B., Coppens, Y., 1982. Morphology of the Pliocene partial hominid skeleton (A.L. 288-1) from the Hadar Formation. Am. J. Phys. Anthropol. 57, 403–451.
Johanson, D., Masao, F., Eck, G., White, T., Walter, R., Kimbel, W., Asfaw, B., Manega, P., Ndessokia, P., Suwa, G., 1987. New partial skeleton of *Homo habilis* from Olduvai Gorge, Tanzania. Nature 327, 205–209.
Jungers, W., 1984. Body size and scaling of limb properties in primates. In: Jungers, W. (Ed.), Size and Scaling in Primate Biology. Plenum, New York, pp. 345–381.
Jungers, W., 1988. Relative joint size and hominoid locomotor adaptations with implications for the evolution of hominid bipedalism. J. Hum. Evol. 17, 247–265.
Jungers, W., 1991. Scaling of postcranial joint size in hominoid primates. J. Hum. Evol. 6, 391–399.
Jungers, W., Grabowski, M., Hatala, K., Richmond, B., 2016. The evolution of body size and shape in the human career. Phil. Trans. R. Soc. B 371, 20150247.
Kaszycka, K., 2002. Status of Kromdraai: Cranial, Mandibular and Dental Morphology, Systematic Relationships, and Significance of the Kromdraai Hominids. Cahiers de Paléoanthropologie. CNRS Editions, Paris.
Kaya, D., Doral, M., 2012. Is there any relationship between Q-angle and lower extremity malalignment? Acta Orthop. Traumatol. Turcica 46, 416–419.
Ker, R., Bennett, M., Bibby, S., Kester, R., Alexander, R., 1987. The spring in the arch of the human foot. Nature 325, 147–149.
Keys, A., Karvonen, N., Kimura, N., Taylor, H., 1972. Indices of relative weight and obesity. J. Chron. Dis. 25, 329–343.
Keyser, A.W., 2000. The Drimolen skull: The most complete australopithecine cranium and mandible to date. S. Afr. J. Sci. 96, 189–193.
Keyser, A.W., Menter, C., Moggi-Cecchi, J., Pickering, T.R., Berger, L.R., 2000. Dimolen: A new hominid-bearing site in Gauteng, South Africa. S. Afr. J. Sci. 96, 193–197.
Kibii, J., Clarke, R., 2003. A reconstruction of the StW 431 *Australopithecus* pelvis based on newly discovered fragments. S. Afr. J. Sci. 99, 225–226.
Kibii, J., Churchill, S., Schmid, P., Carlson, K., Reed, N., de Ruiter, D., Berger, L., 2011. A partial pelvis of *Australopithecus sediba*. Science 333, 1407–1411.
Komza, K., Skinner, M., 2019. First metatarsal trabecular bone structure in extant hominoids and Swartkrans hominins. J. Hum. Evol. 131, 1–21.
Kruuk, H., Turner, M., 1967. Comparative notes on predation by lion, leopard, cheetah and wild dog in the Serengeti area, East Africa. Mammalia 31, 1–27.
Kuman, K., Clarke, R.J., 2000. Stratigraphy, artefact industries and hominid associations for Sterkfontein, Member 5. J. Hum. Evol. 38, 827–847.
Kuman, K., Granger, D., Gibbon, R., Pickering, T.R., Caruana, M., Bruxelles, L., Clarke, R., Heaton, J., Stratford, D., Brain, C.K., 2021. A new absolute date from Swartkrans Cave for the oldest occurrences of *Paranthropus robustus* and Oldowan stone tools in South Africa. J. Hum. Evol. 156, 103000.
Kunos, C., Latimer, B., 2000. Cross-sectional geometric properties of the distal tibia metaphysis in humans and apes. Am. J. Phys. Anthropol. 30, 202–203.
Lague, M., 2002. Another look at shape variation in the distal femur of *Australopithecus afarensis*: Implications for taxonomic and functional diversity at Hadar. J. Hum. Evol. 42, 609–626.
Latimer, B., Ohman, J., Lovejoy, C.O., 1987. Talocrural joint in African hominoids: Implications for *Australopithecus afarensis*. Am. J. Phys. Anthropol. 74, 155–175.
Lazennec, J., Brusson, A., Rousseau, M., 2013. Lumbar-pelvic-femoral balance on sitting and standing lateral radiographs. J. Orthop. Traumatol. Surg. Res. 99, S87–S103.
Lee-Thorp, J., Sponheimer, M., 2013. Hominin ecology from hard tissue biogeochemistry. In: Sponheimer, M., Lee-Thorp, J., Reed, K., Ungar, P. (Eds.), Early Hominin Paleoecology. University of Colorado Press, Boulder, pp. 281–324.
Lee-Thorp, J., Sponheimer, M., Luyt, J.C., 2007. Tracking changing environments using stable carbon isotopes in fossil tooth enamel: An example from the South African hominin sites. J. Hum. Evol. 53, 595–601.
Lockwood, C.A., Menter, C., Moggi-Cecchi, J., Keyser, A.W., 2007. Extended male growth in a fossil hominin species. Science 318, 1443–1446.
Lordkipanidze, D., Jashashvili, T., Vekua, A., Ponce de León, M., Zollikofer, C., Rightmire, G., Pontzer, H., Ferring, R., Oms, O., Tappne, M., Bukhsianidze, M., Agusti, J., Kahlke, R., Kiladze, G., Martinez-Navarro, B., Mouskhelishvili, A., Nioradze, M., Rook, L., 2007. Postcranial evidence from early *Homo* from Dmanisi, Georgia. Nature 449, 305–310.
Lovejoy, C.O., 1975. Biomechanical perspectives on the lower limb of early hominids. In: Tuttle, R. (Ed.), Primate Functional Morphology and Evolution. Mouton, The Hague, pp. 291–327.
Lovejoy, C.O., 2007. The natural history of human gait and posture: Part 3, the knee. Gait Posture 25, 325–341.
Lovejoy, C.O., Heiple, K., 1972. Proximal femur anatomy of *Australopithecus*. Nature 235, 175–176.
Lovejoy, C.O., Heiple, K., Burstein, A., 1973. The gait of *Australopithecus*. Am. J. Phys. Anthropol. 38, 757–779.
Lovejoy, C.O., Burstein, A., Heiple, K., 1976. Biomechanical analysis of bone strength: A method and its application to platycnemia. Am. J. Phys. Anthropol. 44, 489–506.
Lovejoy, C.O., Johanson, D., Coppens, Y., 1982. Hominid lower limb bones recovered from the Hadar Formation: 1974–1977 collections. Am. J. Phys. Anthropol. 57, 679–700.
Lovejoy, C.O., Meindl, R., Ohman, J., Heiple, K., White, T., 2002. The Maka femur and its bearing on the antiquity of human walking: Applying contemporary concepts of morphogenesis to the human fossil record. Am. J. Phys. Anthropol. 119, 97–133.
Lovejoy, C.O., Suwa, G., Spurlock, L., White, T., 2009. The pelvis and femur of *Ardipithecus ramidus*: The emergence of upright walking. Science 326, 71e1–71e6.
Lyman, R.L., 1994. Vertebrate Taphonomy. Cambridge University, Cambridge.
Macchiarelli, R., Bondioli, L., Galichon, V., Tobias, P.V., 1999. Hip bone trabecular architecture shows uniquely distinctive behaviour in South African australopithecines. J. Hum. Evol. 36, 211–232.
Macchiarelli, R., Bergeret, A., Marchi, D., Wood, B., 2020. Nature and relationships of *Sahelanthropus tchadensis*. J. Hum. Evol. 149, 10289.
Marchi, D., Walker, C., Wei, P., Holliday, T., Churchill, S., Berger, L., DeSilva, J., 2017. The thigh and leg of *Homo naledi*. J. Hum. Evol. 104, 174–204.
Martin, R., 1928. Lehrbuch der Anthropologie in Systematischer Darstellung mit Besonderer Berücksichtigung der Anthropologischen Methoden für Studierende, Ärzte und Forschungsreisend, Vol. 2. Gustav Fischer Verlag, Stuttgart.
Martin, R., Saller, K., 1957. Lehrbuch der Anthropologie in Systematischer Darstellung mit Besonderer Berücksichtigung der Anthropologischen Methoden für Studierende, Ärzte und Forschungsreisend, Vol. 1. Gustav Fischer Verlag, Stuttgart.
Matarazzo, S., 1998. Knuckle walking signal in the manual digits of *Pan* and *Gorilla*. J. Hum. Evol. 135, 27–33.
McGrew, W., McKee, J., Tutin, C., 2003. Primates in caves: Two reports of *Papio* spp. J. Hum. Evol. 44, 521–526.
McHenry, H.M., 1978. Fore- and hindlimb proportions in Plio-Pleisticene hominids. Am. J. Phys. Anthropol. 49, 15–22.
McHenry, H.M., 1991. Petite bodies of the 'robust' australopithecines. Am. J. Phys. Anthropol. 86, 445–454.
McHenry, H.M., 1992. Body size and proportion in early hominids. Am. J. Phys. Anthropol. 87, 407–431.
McHenry, H.M., 1994. Behavioral ecological implications of early hominid body size. J. Hum. Evol. 27, 77–87.
McHenry, H.M., Corruccini, R.S., 1978. The femur in early human evolution. Am. J. Phys. Anthropol. 49, 473–488.
Menter, C., Kuykendal, K., Keyser, A.W., Conroy, G., 1999. First record of hominid teeth from the Plio-Pleistocene site of Gondolin, South Africa. J. Hum. Evol. 37, 299–307.
Moffett, E., 2017. Dimorphism in the size and shape of the birth canal across anthropoid primates. Anat. Rec. 300, 870–889.
Myatt, J., Crompton, R., Thorpe, S., 2011. Hindlimb muscle architecture in non-human great apes and a comparison of methods for analysing inter-species variation. J. Anat. 219, 150–166.
Napier, J.R., 1964. The evolution of bipedal walking in the hominids. Arch. Biol. 75, 673–708.
Nel, C., Bradfield, J., Lombard, M., Val, A., 2021. Taphonomic study of a modern baboon sleeping site at Misgrot, South Africa: Implications for large-bodied primate taphonomy in karstic deposits. J. Paleolithic Archaeol. 4, 4.

Ohman, J., Krochta, T., Lovejoy, C.O., Mensforth, R., Latimer, B., 1997. Cortical bone distribution in the femoral neck of hominoids: Implications for the locomotion of *Australopithecus afarensis*. Am. J. Phys. Anthropol. 104, 117–131.
Oxnard, C., 1973. Functional inferences from morphometrics: Problems posed by uniqueness and diversity among the primates. Syst. Biol. 22, 409–424.
Partridge, T., Granger, D.E., Caffee, M.W., Clarke, R.J., 2003. Lower Pliocene hominid remains from Sterkfontein. Science 300, 607–612.
Pearson, O.M., 1997. Postcranial morphology and the origin of modern humans. Ph.D. Dissertation, State University of New York at Stony Brook.
Peterson, A., Abella, E., Grine, F., Teaford, M., Ungar, P., 2018. Microwear textures of *Australopithecus africanus* and *Paranthropus robustus* molars in relation to paleoenvironment and diet. J. Hum. Evol. 119, 42–63.
Pickering, T.R., 2001. Taphonomy of the Swartkrans hominid postcrania and its bearing on issues of meat-eating and fire management. In: Stanford, C., Bunn, H. (Eds.), Meat-Eating and Human Evolution. Oxford University Press, Oxford, pp. 33–51.
Pickering, T.R., Egeland, C., Domínguez-Rodrigo, M., Brain, C.K., Schnell, A., 2008. Testing the 'shift in the balance of power' hypothesis at Swartkrans, South Africa: Hominid cave use and subsistence behavior in the early Pleistocene. J. Anthropol. Archaeol. 27, 30–45.
Pickering, R., Kramers, J.D., Hancox, P.J., de Ruiter, D., Woodhead, J., 2011. Contemporary flowstone development links early hominin bearing cave deposits in South Africa. Earth Planet Sci. Lett. 306, 23–32.
Pickering, T.R., Heaton, J., Zwodeski, S., Kuman, K., 2011. Taphonomy of bones from baboons killed and eaten by leopards in Mapungubwe National Park, South Africa. J. Taphon. 9, 117–159.
Pickering, T.R., Heaton, J.L., Clarke, R.J., Sutton, M.B., Brain, C.K., Kuman, K., 2012. New hominid fossils from member 1 of the Swartkrans Formation, South Africa. J. Hum. Evol. 62, 618–628.
Pickering, T.R., Heaton, J.L., Sutton, M.B., Clarke, R.J., Kuman, K., Senjem, J., Brain, C.K., 2016. New early Pleistocene hominin teeth from the Swartkrans Formation, South Africa. J. Hum. Evol. 100, 1–15.
Pickering, T.R., Heaton, J., Clarke, R., Stratford, D., Heile, A.J., 2021. Hominin lower limb bones from Sterkfontein Caves, South Africa (1998–2003 excavations). S. Afr. J. Sci. 117, 1–10.
Pina, M., Alba, D.M., Moya-Sola, S., Almecija, S., 2019. Femoral neck cortical bone distribution in dryopithecine apes and the evolution of hominid locomotion. J. Hum. Evol. 136, 102651.
Plavcan, J., Hammond, A., Ward, C., 2013. Calculating hominin and nonhuman anthropoid femoral head diameter from acetabular size. Am. J. Phys. Anthropol. 155, 469–475.
Pontzer, H., Rolian, C., Rightmire, G., Jashashvili, T., Ponce de León, M., Lordkipanidze, D., Zollikofer, C.P., 2010. Locomotor anatomy and biomechanics of the Dmanisi hominins. J. Hum. Evol. 58, 492–504.
Preuschoft, H., Tardieu, C., 1996. Biomechanical reasons for the divergent morphology of the knee joint and the distal epiphyseal suture in hominoids. Folia Primatol. 66, 82–91.
Purkait, R., Chandra, H., 2004. A study of sexual variation in Indian femur. Forensic Sci. Int. 146, 25–33.
Puymerail, L., 2012. The functionally-related signatures characterizing the endostructural organization of the femoral shaft in modern humans and chimpanzees. C. R. Palevol 12, 223–231.
Rafferty, K., Ruff, C., 1994. Articular structure and function in *Hylobates, Colobus*, and *Papio*. Am. J. Phys. Anthropol. 94, 95–408.
Reed, K., Kitching, J., Grine, F., Jungers, W., Sokoloff, L., 1993. Proximal femur of *Australopithecus africanus* from Member 4, Makapansgat, South Africa. Am. J. Phys. Anthropol. 92, 1–15.
Reed, K., 1997. Early hominid evolution and ecological change through the African Plio-Pleistocene. J. Hum. Evol. 32, 289–322.
Rein, T., 2011. The correspondence between proximal phalanx morphology and locomotion: Implications for inferring the locomotor behavior of fossil catarrhines. Am. J. Phys. Anthropol. 146, 435–445.
Reynolds, D., Lucas, J., Klaue, K., 1999. Retroversion of the acetabulum: A cause of hip pain. J. Bone Joint Surg. Br. 81, 281–288.
Richmond, B., 2007. Biomechanics of phalangeal curvature. J. Hum. Evol. 53, 678–690.
Robinson, J., 1952. The australopithecine-bearing deposits of the Sterkfontein area. Annls. Transv. Mus. 22, 1–19.
Robinson, J., 1959. A bone implement from Sterkfontein. Nature 184, 583–585.
Robinson, J., 1961. The australopithecines and their bearing on the origin of man and of stone tool making. S. Afr. J. Sci. 57, 3–12.
Robinson, J., 1972. Early Hominid Posture and Locomotion. University of Chicago, Chicago.
Rose, M., 1984. A hominine hip bone, KNM-ER 3228, from East Lake Turkana, Kenya. Am. J. Phys. Anthropol. 63, 371–378.
Ruff, C., 1988. Hindlimb articular surface allometry in Hominoidea and *Macaca*, with comparisons to diaphyseal scaling. J. Hum. Evol. 17, 687–713.
Ruff, C., 1995. Biomechanics of the hip and birth in early *Homo*. Am. J. Phys. Anthropol. 98, 527–574.
Ruff, C., 1998. Evolution of the hominid hip. In: Strasser, E., Fleagle, J., McHenry, H., Rosenberger, A. (Eds.), Primate Locomotion: Recent Advances. Plenum Press, New York, pp. 449–469.
Ruff, C., 2003. Long bone articular and diaphyseal structure in Old World monkeys and apes, II: Estimation of body mass. Am. J. Phys. Anthropol. 120, 16–37.
Ruff, C., 2010. Body size and body shape in early hominins—implications of the Gona pelvis. J. Hum. Evol. 58, 166–178.
Ruff, C., Hayes, W., 1983a. Cross-sectional geometry of Pecos Pueblo femora and tibiae—a biomechanical investigation: I, method and general patterns of variations. Am. J. Phys. Anthropol. 60, 359–381.
Ruff, C., Hayes, W., 1983b. Cross-sectional geometry of Pecos Pueblo femora and tibiae—a biomechanical investigation: II, sex, age, and side differences. Am. J. Phys. Anthropol. 60, 383–400.
Ruff, C., Higgins, R., 2013. Femoral neck structure and function in early hominins. Am. J. Phys. Anthropol. 150, 512–525.
Ruff, C., Walker, A., Teaford, M., 1988. Body mass, sexual dimorphism and femoral proportions of *Proconsul* from Rusinga and Mfangano Islands, Kenya. J. Hum. Evol. 18, 515–536.
Ruff, C., Scott, W., Liu, A., 1991. Articular and diaphyseal remodeling of the proximal femur with changes in body mass in adults. Am. J. Phys. Anthropol. 86, 397–413.
Ruff, C., Higgins, R., Carlson, K., 2020. Long bone cross-sectional geometry. In: Zipfel, B., Richmond, B., Ward, C. (Eds.), Hominin Postcranial Remains from Sterkfontein, South Africa, 1936–1995. Oxford University Press, New York.
Ruff, C., McHenry, H., Thackeray, J., 1999. Cross-sectional morphology of the SK 82 and SK 97 proximal femora. Am. J. Phys. Anthropol. 109, 509–520.
Ruff, C., Burgess, M., Ketcham, R., Kappelman, J., 2016. Limb bone structural properties and locomotor behavior in A.L. 288-1 ("Lucy"). PLoS One 11, e0166095.
Ryan, T., Carlson, K., Gordon, A., Jablonski, N., Shaw, C., Stock, J., 2018. Human-like hip joint loading in *Australopithecus africanus* and *Paranthropus robustus*. J. Hum. Evol. 121, 12–23.
Schaller, G., 1972. The Serengeti Lion. University of Chicago Press, Chicago.
Schmid, P., 1983. Eine Rekonstruktion des Skelettes von A.L. 288-1 (Hadar) und deren Konsequenzen. Folia Primatol. 40, 283–306.
Schneider, C., Rasband, W., Eliceiri, K., 2012. NIH Image to ImageJ: 25 years of image analysis. Nature 9, 671–675.
Schultz, A., 1937. Proportions, variability and asymmetries of the long bones of the limbs and the clavicles in man and apes. Hum. Biol. 9, 281–328.
Shea, B., 1984. An allometric perspective on the morphological and evolutionary relationships between pygmy (*Pan paniscus*) and common (*Pan trogylodytes*) chimpanzees. In: Susman, R. (Ed.), The Pygmy Chimpanzee. Springer, Boston, pp. 89–130.
Shefelbine, S., Tardieu, C., Carter, D., 2002. Development of the femoral bicondylar angle in hominid bipedalism. Bone 30, 765–770.
Sigmon, B., 1986. Evolution of the hominid pelvis. Palaeontol. Afr. 26, 25–32.
Simons, J.W., 1966. The presence of leopard and a study of food debris in the leopard lairs of the Mount Suswa Caves, Kenya. Bull. Cave Explor. Group East Afr. 1, 51–69.
Simpson, S., Quade, J., Levin, N., Butler, R., Dupont-Nivet, G., Everett, M., Semaw, S., 2008. A female *Homo erectus* pelvis from Gona, Ethiopia. Science 322, 1089–1091.
Sponheimer, M., Lee-Thorp, 2009. Biogeochemical evidence for the environments of early *Homo* in South Africa. In: Grine, F., Fleagle, J., Leakey, R. (Eds.), The First Humans: Origin and Early Evolution of the Genus *Homo*. Springer, Dordrecht, pp. 185–194.
Stammers, R., Caruana, M., Herries, A., 2018. The first bone tools from Kromdraai and stone tools from Drimolen, and the place of bone tools in South African Earlier Stone Age. Quatern. Int. 495, 87–101.
Steininger, C., Berger, L., Kuhn, B., 2008. A partial *Paranthropus robustus* skull from Cooper's Cave, South Africa. S. Afr. J. Sci. 104, 143–146.
Stern, J.T., Susman, R., 1983. The locomotor anatomy of *Australopithecus afarensis*. Am. J. Phys. Anthropol. 60, 279–317.
Stern, J.T., Jungers, W., Susman, R., 1995. Quantifying phalangeal curvature: An empirical comparison of alternative methods. Am. J. Phys. Anthropol. 97, 1–10.
Steudel-Numbers, K.L., Tilkens, M., 2004. The effect of lower limb length on the energetic cost of locomotion: Implications for fossil hominins. J. Hum. Evol. 47, 95–109.
Stratovan Corporation, 2022. Stratovan Checkpoint (Software). Version 2022.07.21.
Su, A., Carlson, K., 2017. Comparative analysis of trabecular bone structure and orientation in South African hominin tali. J. Hum. Evol. 106, 1–18.
Susman, R., 1988. Hand of *Paranthropus robustus* from Member 1, Swartkrans: Fossil evidence for tool behavior. Science 240, 781–784.
Susman, R., 1989. New hominid fossil from the Swartkrans Formation (1979–1986 excavations): Postcranial specimens. Am. J. Phys. Anthropol. 79, 451–474.
Susman, R., Brain, T., 1988. New first metatarsal (SKX 5017) from Swartkrans and the gait of *Paranthropus robustus*. Am. J. Phys. Anthropol. 77, 7–15.
Susman, R., deRuiter, D., 2004. New hominin first metatarsal (SK 1813) from Swartkrans. J. Hum. Evol. 47, 171–181.
Susman, R., Stern, J., Jungers, W., 1984. Arboreality and bipedality in the Hadar hominids. Folia Primatol. 43, 113–156.
Swartz, S., 1989. The functional morphology of weight bearing: Limb joint surface area allometry in anthropoid primates. J. Zool. 218, 441–460.
Syeda, S., Tsegai, Z., Cazenave, M., Skinner, M., Kivell, T., 2023. Cortical bone distribution of the proximal phalanges in great apes: Implications for reconstructing manual behaviours. J. Anat. 243, 707–728.
Tardieu, C., 1981. Morpho-functional analysis of the articular surfaces of the knee joint in primates. In: Chiarelli, S.B., Corruccini, R.S. (Eds.), Primate Evolutionary Biology. Springer-Verlag, Berlin, pp. 68–80.
Tardieu, C., 1999. Ontogeny and phylogeny of femoro-tibial characters in humans and hominid fossils: Functional influence and genetic determinism. Am. J. Phys. Anthropol. 110, 365–377.
Tardieu, C., 2010. Development of the human hind limb and its importance for the evolution of bipedalism. Evol. Anthropol. 19, 174–186.

Tardieu, C., Trinkaus, E., 1994. Early ontogeny of the human femoral bicondylar angle. Am. J. Phys. Anthropol. 92, 183–195.
Tardieu, C., Glard, Y., Garron, E., Boulay, C., Jouve, J.-L., Dutour, O., Boetsch, G., Bollini, G., 2006. Relationship between formation of the femoral bicondylar angle and trochlear shape: Independence of diaphyseal and epiphyseal growth. Am. J. Phys. Anthropol. 130, 491–500.
Tobias, P.V., 1967. Olduvai Gorge, Volume 2: The Cranium of *Australopithecus (Zinjanthropus) boisei*. Cambridge University Press, Cambridge.
Toussaint, M., Macho, G., Tobias, P., Partridge, T., Hughes, A.R., 2003. The third partial skeleton of a late Pliocene hominin (StW 431) from Sterkfontein, South Africa. S. Afr. J. Sci. 99, 215–223.
Trinkaus, E., 1975. Squatting among Neandertals: A problem in the behavioral interpretation of skeletal morphology. J. Archaeol. Sci. 2, 327–351.
Trinkaus, E., Long, J., 1990. Species attribution of the Swartkrans Member 1 first metacarpals: SK 84 and SKX 5020. Am. J. Phys. Anthropol. 83, 419–424.
Trinkaus, E., Churchill, S., Ruff, C., Vandermeersch, B., 1999. Long bone shaft robusticity and body proportions of the Saint-Césaire 1 Châtelperronian Neandetal. J. Archaeol. Sci. 26, 753–773.
Venkataraman, V., Kraft, T., Dominy, N., 2013a. Tree climbing and human evolution. Proc. Natl. Acad. Sci. U.S.A. 110, 1237–1242.
Venkataraman, V., Kraft, T., DeSilva, J., Dominy, N., 2013b. Phenotypic plasticity of climbing-related traits in the ankle joint of great apes and rainforest hunter-gatherers. Hum. Biol. 85, 14.
Vrba, E.S., 1975. Some evidence of chronology and palaeoecology of Sterkfontein, Swartkrans and Kromdraai from the fossil Bovidae. Nature 254, 301–304.
Walker, A.C., 1973. New *Australopithecus* femora from East Rudolf, Kenya. J. Hum. Evol. 2, 545–555.
Walker, A.C., Leakey, R.E.F. (Eds.), 1993. The Nariokotome *Homo erectus* Skeleton. Harvard University Press, Cambridge.
Walker, A.C., Ruff, C., 1993. The reconstruction of the pelvis. In: Walker, A.C., Leakey, R.E.F. (Eds.), The Nariokotome *Homo erectus* Skeleton. Harvard University Press, Cambridge, pp. 221–233.
Wallace, I., Burgess, M., Patel, B., 2017. Phalangeal curvature in a chimpanzee raised like a human: Implications for inferring arboreality in fossil hominins. Proc. Natl. Acad. Sci. U.S.A. 117, 11223–11225.
Ward, C., Leakey, M., Walker, A.C., 1999. The new hominid species *Australopithecus anamensis*. Evol. Anthropol. 7, 197–205.
Ward, C., Leakey, M., Walker, A.C., 2001. Morphology of *Australopithecus anamensis* from Kanapoi and Allia Bay, Kenya. J. Hum. Evol. 41, 255–368.
Ward, C., Kimbel, W., Harmon, E., Johanson, D., 2012. New postcranial fossil of *Australopithecus afarensis* from Hadar, Ethiopia (1990 – 2007). J. Hum. Evol. 63, 1–51.
Watson, V., 1993. Composition of the Swartkrans bone accumulations, in terms of skeletal parts and animals represented. In: Brain, C.K. (Ed.), Swartkrans: A Cave's Chronicle of Early Man. Transvaal Museum, Pretoria, pp. 35–74.
Westcott, D., 2006. Effect of mobility on femur midshaft shape and robusticity. Am. J. Phys. Anthropol. 130, 201–213.
White, T., 1988. The comparative biology of 'robust' *Australopithecus*: Clues from context. In: Grine, F. (Ed.), Evolutionary History of the 'Robust' Australopithecines. Aldine de Gruyter, New York, pp. 449–497.
Wilkinson, J., 1962. Femoral anteversion in the rabbit. J. Bone Joint Surg. 44, 386–397.
Wood, W., 1920. The tibia of the Australian aborigine. J. Anat. 54, 232–257.
Wood, B., Lonergan, N., 2008. The hominin fossil record: Taxa, grades and clades. J. Anat. 21, 354–376.
Wood, B., Richmond, B., 2000. Human evolution: Taxonomy and paleobiology. J. Anat. 197, 19–60.
Wood, B., Schroer, K., 2013. Paranthropus. In: Begun, D. (Ed.), A Companion to Paleoanthropology. Blackwell, New York, pp. 457–478.
Zahn, R., Grotjohann, S., Pumberger, M., Ramm, H., Zachow, S., Putzier, M., Perka, C., Tohtz, S., 2017. Influence of pelvic tilt on functional acetabular orientation. Technol. Health Care 22, 557–565.
Zanolli, C., Davies, T., Skinner, M., 2022. Dental Data challenge the ubiquitous presence of homo in the cradle of humankind. Proc. Natl. Acad. Sci. U.S.A. 119, e2111212119.
Zihlman, A., 1971. The question of locomotor differences in *Australopithecus*. In: Proceedings of the Third International Congress on Primatology (Zurich), 1970, pp. 54–66.
Zipfel, B., DeSilva, J., Kidd, R., Carlson, K., Churchill, S., Berger, L., 2011. The foot and ankle of *Australopithecus sediba*. Science 333, 1417–1420.